THE ROLE OF THE SVZ IN ISCHEMIC CONDITION

CANDIDATE:

Miss TIZIANA ROSSETTI, BSc, MSc

This thesis is submitted for the degree of Doctor of Philosophy at Royal Holloway, University of London

Acknowledgement

To my parents and friends,

They are my strength and my happiness,

Without which no dream would have ever been achieved.

SUPERVISORS:

•Dr. Rafael J. Yáñez-Muñoz, *Senior Lecturer in Genetics,* School of Biological Sciences, Royal Holloway-University of London, UK

•Dr. Atticus Hainsworth, *Senior Lecturer in cerebrovascular disease, St George's University of London. UK*

EXAMINERS:

•Dr Simon Waddington, *Reader in Gene Transfer Technology*, UCL, London. UK

•Dr. Lorraine Work, Lecturer at the Institute of Cardiovascular and Medical Sciences. University of Glasgow, Glasgow. UK

Declaration of Authorship

I Tiziana Rossetti hereby declare that this thesis and the work presented in it is entirely my own. Where I have consulted the work of others, this is always clearly stated.

Signed: Tiziana Rossetti

Date: 24 November 2012

ABSTRACT

The occlusion of a cerebral artery or stroke often results in neuronal deficit and/or patient death. A partial recovery often follows non-fatal stroke and this may be due to the activation of the progenitor cells in the Sub-Ventricular Zone (SVZ) naturally occurring after ischemia. In order to clarify the role of the SVZ neurogenesis in animal recovery, the effect of neurogenesis inhibition and boosting were studied in the mouse Middle Cerebral Artery occlusion model (MCAo). 6 to 10-week-old male mice were pre-treated with intracranial injections of lentiviral vector (LV) or integration deficient lentiviral vectors (IDLV), in order to target the SVZ. The IDLV carried an expression cassette encoding for a precursor Glial cell-derived neurotrophic factor (GDNF) or the tetanus toxin fragment C (TTC), which recently has been demonstrated to have growth factor like behaviour. Another group of animals received the LV carrying a double promoter expression cassette encoding for an eGFP, and in order to inhibit the cell cycle in targeted cells the shRNA_Cyclin D1. All vectors were co-injected with the LV_ pHR'SIN-cPPT-SEW, which contains an eGFP cassette. Two weeks later the animals received the MCAo, and for three weeks the sensorimotor behaviour was tested. Neurological assessment showed the sensory-motor debilitation was significant increased after the treatment with the LV_shRNA_CyclinD1 (* $p<0.05$); the IDLV_GDNF and IDLV_TTC groups showed a trend to improve neurological deficit in the subjects alive until day 5. In the IDLV_GDNF, the SVZ's derived green cells were positively correlated with the ischemic volume, *$p<0.05$ $R=0.68$, and the neurodegeneration, ***$p<0.001$ $R=0.92$. Moreover, while the SVZ neurogenesis inhibition reduced life expectancy, the boosting significantly improved it. Immunofluorescence analysis showed a migration extended to the striatum and cortex with a max distance of 1.87 mm from the SVZ.

TABLE OF CONTENTS

TABLE OF FIGURE and TABLES

TABLE OF THE NAMES AND ABBREVIATIONS

AIDS, Acquired immune deficiency syndrome

Ang-1, angioprotein 1

Ang-1, Angioprotein 1

AP, anterior-posterior

CA, Capsid protein

CCND1, Cyclin D1

CD4, cluster of differentiation 4

Cdk4, Cyclin-dependent kinase 4

CMV, cytomegalovirus promoter

CNS, Central Nervous System

CSF, cerebrospinal fluid

CSF, cerebrospinal fluid

CXCR4, chemokine CXC Motif Receptor 4

CXCR4, C-X-C chemokine receptor type 4

DG, dentate gyrus

DG, dentate gyrus

dnCyclin D1, dominant negative Cyclin D1

dNTPs, deoxynucleosides triphosphate

dsDNA, double-stranded DNA

dsRNA, double stranded RNA

DV, dorso-ventral

E2F, transcription factor

E2F, Transcription Factor Element 2

EGF, Epidermal Growth Factor

FGF, Fibroblast Growth Factor

GDNF, Glial cell-line derived growth factor

HDAC, histone deacetylase complex

HIV-1, human immunodeficiency virus type 1

IDLV, Integration Deficient Lentiviral Vector

IDLV_pRRLcC_pGDNF_IRESeW, Integration deficient

IDLV_pRRLcC_TTC_IRESeW,

IDLVs, integration deficient lentivectors

IGF-1, Insulin Growth Factor 1

IN, Integrase

Integration deficient Lentiviral vector_ pRRLcC_TTC_IRESeW

IU/ml, Infection Units per millilitre

LB Amp, LB medium enriched with Ampicillin

Lentivial vector_pGIPZs_shRNA_Cyclin_D1_640492

Lentiviral vector_ pGIPZs_ shRNA_Cyclin_D1_640495

Lentiviral vector_ pRRLcC_pGDNF_IRESeW

Lentiviral vector_pGIPZs_shRNA_Cyclin_D1_Empty

LV_ dnCyclinD1, Lentiviral vector_ pRRLsc_Segfp_CdnCND1W

LV_pHR'SIN-cPPT-SEW, Lentiviral vector_ pHR'SIN-cPPT-SEW

LV_shRNA_Cyclin_D1_92,

LV_shRNA_Cyclin_D1_95,

LV_shRNA_Cyclin_D1_Empty,

LVs, lentivectors

M1, Motor cortex 1

M2, Motor cortex 2

MA, Matrix protein

MCAo, Middle Cerebral artery occlusion

ML, medio-lateral

MOI , multiplicity of infection

MOI, Multiplicity of Infection

MTT, 3 – (4,5-dimethylthiazol-2-yl) 2,5-diphenyltetrazoliumbromide

mV, milliVolt

Naf, Neutrophil/activating factor

NC, Nucleocapsid protein

NCS1, Neuronal calcium sensor-1

NPCs, Neural progenitor cells

NS, nervous system

OB, Olfactory bulb

PI, Propidium Iodide

PIC, preintegration complex

PIC, Pre-Integration complex

pMCAo, permanent Middle Cerebral Artery occlusion

pMCAo, permanent_MCAo

PR, Protease

R, correlation coefficient in linear regression analysis

Rb, retinoblastoma protein

RISC, RNA-induced silencing complex

RMS, Rostral Migratory Stream

RNAi, RNA interference

rpm, rotation per minute

RT, Retrotranscriptase

RT, reverse transcriptase

RTC, reverse transcription complex

S1, Somato-sensory cortex 1

SDF-1, Stromal Derived Growth Factor

SDF-1, stromal-derived factor-1

SFFV, spleen focus-forming virus promoter

SGZ, Sub-Granular Zone

shRNA, short hairpin RNA

ssDNA, single stranded DNA

SU, Surface protein or gp120

SVZ, Sub-Ventricular Zone

Swi/Snf1, SWItch/Sucrose Non-Fermentable

TGFβ1, Transforming growth factor β

TGFβ1, Transforming Growth Factor β1

Tie2, endothelium-specific receptor tyrosine kinase 2

Tie2, Tyrosine-protein kinase receptor 2

TM, Transmembrane protein or gp41

tMCAo, temporary Middle Cerebral Artery occlusion

TTC, Tetanus toxin fragment C

Vif, Viral infectivity factor

Vpr, Viral protein r

VSV-G, glycoprotein G of the vesicular stomatitis virus

VSV-G, Glycoproteins G of the Vesicular Stomatitis Virus

ρ, correlation coefficient in Spearman's rank correlation coefficient analysis

PART 1

CHAPTER 1

BACKGROUND AND GENERAL INTRODUCTION

1.1 GENERAL INTRODUCTION

Every year in the UK 53,000 people die because of stroke, a major cause of mortality (9% of all total deaths). Stroke is also responsible for over 9,500 premature deaths every year (data from the Stroke Foundation, published on http://www.scribd.com).

Therapeutic treatments currently in use are very limited and only a small fraction of survivors is able to have a complete recovery. Recovery depends on the damage severity and only therapies based on rehabilitation seem to significantly improve patient conditions; in any case neuronal degeneration resulting from stroke, can be rescued by rehabilitation. Rehabilitation improves network functionality by enhancing plasticity in surviving neurons.

Although a complete understanding of the disease's outcome is not clarified yet, new strategies to improve patients' conditions and to increase survivors are currently studied by numerous laboratories. On this view, the understanding of the brain's ability to respond to ischemia could help development of new strategies, and could offer a significant contribution in the war against this disease.

1.2 STROKE AND NEUROGENESIS

Ischemic brain damage occurs in two different ways:

• Ischemic stroke, occurring by an occlusion of a cerebral artery or stroke, that gives rise to neurodegeneration and/or neural damage, both in the

core[1] region and in surrounding penumbral[2] areas (Bederson, Pitts et al. 1986)

• Haemorrhagic stroke, occurring when a weakened blood vessels ruptures, causing a more localized and reduced neuronal damage.

There are several animal models that emulate some of the clinical features of stroke damage. One of the most common in use is the focal ischemia animal model by the occlusion (permanent or temporary) of the Middle Cerebral Artery (MCAo) (Figure 1.f1). The MCAo produces a reduction of cerebral blood flow within the striatum and the cerebral cortex, resulting in loss of cells. The damage depends on the duration of the occlusion; initial damage is localised in the striatum, while over 30 minutes of occlusion can produce extensive damage across the brain (motor cortex, hippocampus and somatosensory cortex) (Menzies, Hoff et al. 1992; Traystman 2003; Adcock, Ford et al. 2006 Menzies, et al., 1992, Traystman, 2003).

Numerous studies have reported that the MCAo produces an increase in proliferation of progenitors in the rodent Sub-Ventricular Zone (SVZ) and Sub-Granular Zone (SGZ). This was first described in 2001 (Jin, Minami et al. 2001) demonstrating an increase in the number of the Neural progenitor cells (NPCs) born in the SVZ and SGZ after ischemia[3] (Jin, Minami et al. 2001; Zhang, Zhang et al. 2001; Arvidsson, Collin et al. 2002; Parent, Vexler et al. 2002).

In an experiment performed by Parent et al. (2002), the increase in the number of NPCs was detected as the increase of the BrdU labelled cells in the perinfarct regions ten days after MCAo (Parent, Vexler et al. 2002).

[1] The core region is where the highest damage occurs due to neurodegeneration resulting in a 75-90% reduction in blood flow.

[2] The penumbra area is the area surrounding the core, where neurodegeneration is reduced but cellular damage is still significant.

[3] Ischemia, the reduction of blood supply responsible for neurodegeneration and severe cellular damage, is synonymous with stroke

Moreover, Thirty-five days after MCAo, many of the "new born cells" expressed DARPP-32 or Calbindin[4] (Arvidsson, Collin et al. 2002; Parent, Vexler et al. 2002).

Gu et al. in 2000 administrated the cell proliferation marker 5-bromodeoxyuridine (BrdU) to Wistar rats, which thereafter underwent MCAo. The immunofluorescence proved a majority of glia, microglia and endothelial cells labelled with the BrdU, moreover 3% to 6% of this cells expressed the neuronal specific marker Map-2. These cells were randomly distributed on the neocortical layer II and IV (Gu, Brannstrom et al. 2000). Many laboratories in analogue projects confirm these studies (Zhang, Zhang et al. 2001; Arvidsson, Collin et al. 2002; Parent, Vexler et al. 2002; Gotts and Chesselet 2005). Concordant with our observations, these data demonstrated that the multiplication of progenitors is naturally stimulated by neurodegeneration.

Besides, 18 days after MCAo Yamashita and colleagues were able to detect, 98% of progenitors in the striatum (n = 1108 cells) and they were co-expressing Dcx and βIII-tubulin[5] (Yamashita, Ninomiya et al. 2006). In the experiment reported by Yamashita et al. (2006) the post ischemic detection of NPCs was obtained by an Ax-CAN-Cre plasmid injection into the lateral ventricle of CAG-CAT-Cre transgenic mice. This technique allowed long lasting expression and detection of eGFP in NPCs migrated from the SVZ to the ischemic regions. The analysis after death demonstrated a 29% (n = 5 cells) of eGFP-positive cells co-expressing NeuN (Yamashita, Ninomiya et al. 2006). Immunoelectron microscopy proved that the eGFP-positive axons contained presynaptic vesicles and formed synapses with the neurons located in the surrounding area (Yamashita, Ninomiya et al. 2006).

[4] DARPP-32 and calbindin are Medium-sized spiny neuronal markers

[5] Neuronal marker

More recently Ohira et al. (2010) reported a new neurogenic area in rat neocortical layer one which is activated after ischemia (Ohira, Furuta et al.; Ohira, Furuta et al. 2010).

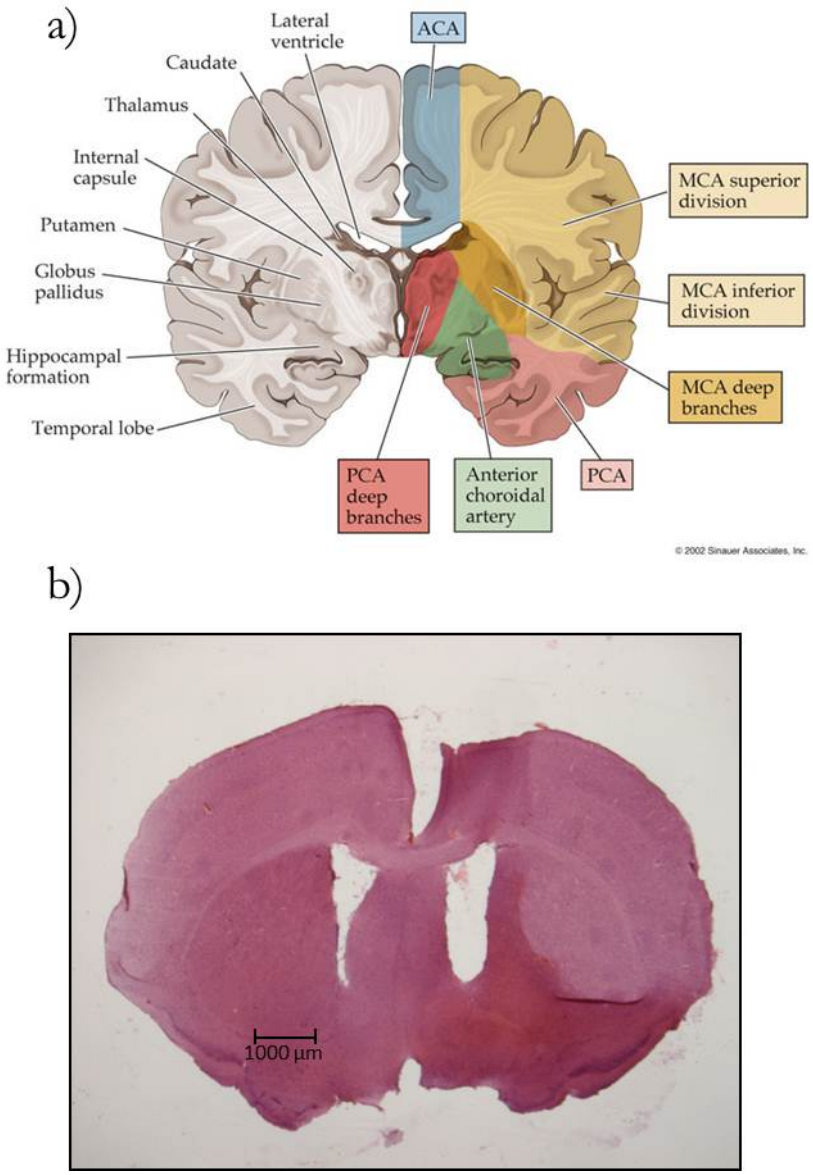

Figure 1.f1 Middle cerebral artery occlusion.
a) Map of the regions that receive blood supply delivered by the Middle Cerebral Artery, recognizable by the yellow areas,Sinauer Associates, 2002. b) C57/Bl/6, six week-old male, received 1 h MCAo and two weeks later was killed by transcardial perfusion; the staining was performed by Haematoxylin and Eosin.

1.2.1 NEUROGENESIS IN RODENT BRAIN

NPCs are self-renewing, multipotent cells able to differentiate into ependymal cells, neurons, astrocytes and oligodendrocytes (Taupin and Gage 2002). The existence of active or quiescent NPCs in the adult mammalian nervous system was demonstrated within the neocortical layer one, SGZ and SVZ (Ohira, Furuta et al.; Altman and Das 1965; Corotto, Henegar et al. 1993; Luskin 1993). In physiological conditions activation of NPC divisions in the SVZ produces new-born cells able to migrate through the Rostral Migratory Stream (RMS), reaching the Olfactory Bulbs (OBs). Toward the migratory pathway and in the OBs, migrating neuroblasts differentiate in interneurons, glomerular and periglomerular cells (Figure 1.f2 and 1.1.f3) (Doetsch, Garcia-Verdugo et al. 1997).

In some circumstances, for example after stroke, NPCs deviate from their "physiological pathway" and migrate toward the damage regions (Gotts and Chesselet, 2005). Once they reach the ischemic areas, NPCs associate with reactive astrocyte and blood vessels to produce neurovascular niche like structures (Ohab, Fleming et al. 2006; Thored, Arvidsson et al. 2006; Yamashita, Ninomiya et al. 2006).

The NPCs dissected from SVZ can be cultured *in vitro* with the use of mitogens (EGF or FGF2), and they grow as free-floating spheres (neurospheres). Upon mitogens removal, neurospheres can differentiate into adult neurons, astrocytes or oligodendrocytes (Lennington, Yang et al. 2003).

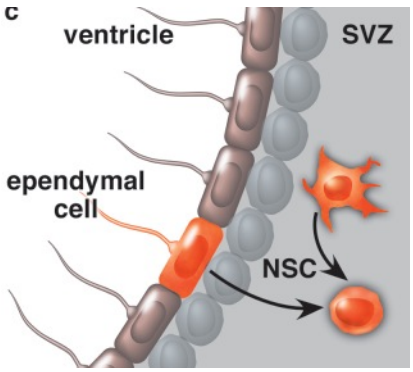

Figure 1.f2. Sub-Ventricular Zone (SVZ) (Taupin and Gage, 2002).

The SVZ is a neurogenetic area located on the wall of the third cerebral ventricle. NSCs here are maintained in a quiescent state until appropriate stimuli occur to affect their division, migration and differentiation.

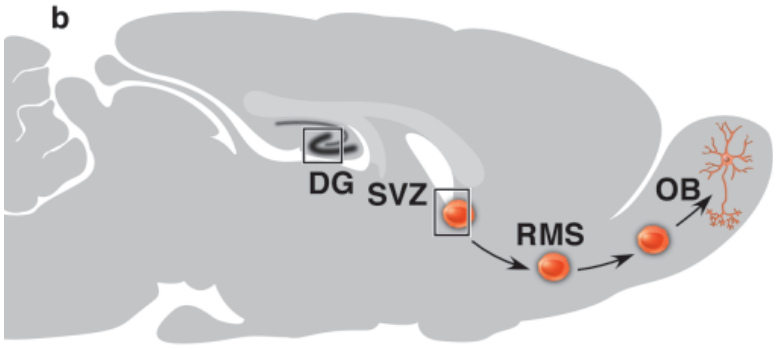

Figure 1.f.3. Rostroal-mygratory stream and SVZ (Taupin and Gage, 2002)

The picture shows a sagittal section of a rodent brain; highlighted the SVZ from which the neuroblasts migrate toward the OBs. The neuroblasts travel in a chain-like structure that transient on a specialized route called RMS; the route terminates at OBs level.

1.2.2 REGULATION AND MAINTENANCE OF THE BRAIN NEUROGENIC AREAS: THE GROWTH FACTORS FAMILY

The Nerve Growth Factor (NGF) was discovered in the late forty by Rita Levi Montalcini and Stanley Cohen; since then, the interest for this compound and its big family had seen an increasing attention and wide therapeutics application (Orts Llorca 1988; Hamburger 1993; Aloe 2004). The NGF comprises a big family of proteins that are involved in neuronal survival as well as stimulate dendritic branching and plasticity. In the Nervous System (NS) the Growth Factor (GF) family is highly expressed during development, as well as in the adult is an important factor for neuronal survival and plasticity (Pardon 2010). The GF family is currently applied in brain research with particular interest for the regulation and survival of NPCs.

1.2.2.1 EGF AND FGF2

Self-renewal and long-term survival of NPCs is stable when maintained in culture by two well known GF: the Epidermal Growth Factor (EGF), and Fibroblast Growth Factor 2 (FGF2) (Reynolds and Weiss 1992; Kuhn, Winkler et al. 1997). Some studies investigating the effects of EGF and FGF2 on telencephalon development, have demonstrated the closely regulated control of such molecules: FGF2 is produced early and during E 8.5[6], whilst EGF is expressed only at E14.4[7] (Tropepe, Sibilia et al. 1999; Maric, Maric et al. 2003). In the adult NS SVZ's NPCs express both EGF receptor and the FGF receptor 1, and hence respond to either EGF or FGF2 (Gritti, Frolichsthal-Schoeller et al. 1999).

1.2.2.2 IGF-1

[6] Embryonic day 8,5.

[7] Embryonic 14,4. Between eighteenth and nineteenth days of embryo life time

Yan et al. (2006) demonstrated that Insulin Growth Factor 1 (IGF1) is produced by astrocytes in the rat penumbral cortex. This is one of the post-ischemic up-regulated diffusible factors detectable after focal ischemia, and acts to promote progenitor cell proliferation. Interestingly, no IGF-1 positive cells were observed in the post-ischemic dentate gyrus (DG) and SVZ (Yan, Sailor et al. 2006). IGF-1 is an endogenous mitogen which acts widely during development including in neurogenic areas. The action of IGF-1 is closely related to the concomitant occurrence of mitogens like EGF or FGF-2, and promotes differentiation after its withdrawal (Kalluri, Vemuganti et al. 2007).

1.2.2.3 CYCLIN D1

Cell cycle activation is strictly regulated by a number of factors known as cyclins. Cyclin D1 is a limiting molecule that promotes the progression from G1 to S phases of mitosis. Many factors controls Cyclin D1 gene transcription; for example, the interaction of many growth factors like EGF with the specific membrane receptor, can induce activation of the ERK and PI3/Akt pathways, in turn responsible to increase Cyclin D1 transcription and the protein accumulation in the cytoplasmic region (Burch and Heintz 2005). The cytoplasmic accumulation of Cyclin D1 leads to Cdk4 association, in turn responsible for the complex activation. As kinase-complex, it starts to interact with different cellular pathways by protein phosphorylation; for instance, the phosphorylation of the Retinoblastoma protein (Rb) determines the reduction of affinity with the E2F and in turn this is responsible for the cell cycle progression (Burch and Heintz 2005). Rb is a repressor factor that binds[8] the Transcription Factor Element 2 (E2F). The kinase activity of CyclinD1/Cdk4 complex phosphorylates Rb/E2F, which is in turn responsible for the release of Rb

[8] E2F is able to activate many genes involve in S phase progression, particularly cyclin E gene

and E2F activation (Dowdy, Hinds et al. 1993; Ewen, Sluss et al. 1993) (Figure 1.f4).

When the cell cycle is blocked in G1, the E2F is inactive by the binding to the Rb protein. In these circumstances, Rb recruits the histone deacetylase (HDAC) and methyltransferase (HMT) making the DNA inaccessible for E2F (Brehm, Miska et al. 1998; Luo, Postigo et al. 1998; Magnaghi-Jaulin, Groisman et al. 1998; Nielsen, Schneider et al. 2001). At DNA level, the modification of histone tails by HDAC and HMT, causes them a variation in charge by deacetylation and methylation of its lysine and arginine aminoacids. This results in an alteration of chromatin structure, and is in turn responsible for gene silencing (Figure 1.f5). The close association between the histone complex and DNA prevents any access for enzymes and factors necessary for transcription (Figure 1.f5) (Coqueret 2002).

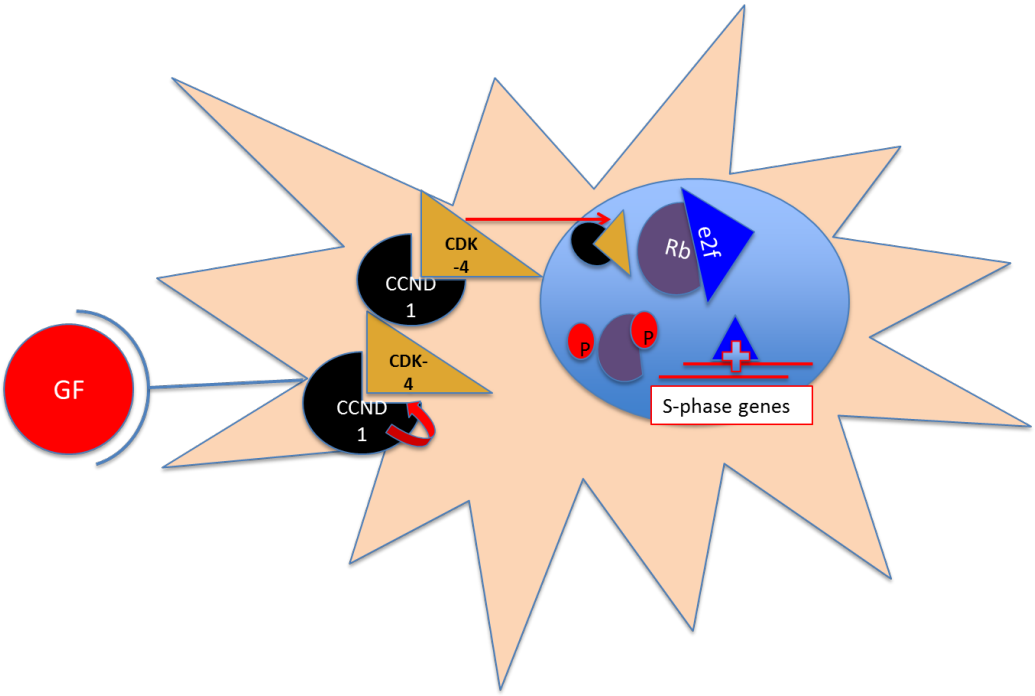

Figure 1.f4. Cyclin D1 pathway.

Extracellular stimuli, such the binding of growth factors (GF) to the receptor can increase the amount of the cytoplasmic Cyclin D1, which becomes active by interaction with Cdk4. As a complex CyclinD1-cdk4 migrates in the nucleus where the Kinase activity of CDK4 phosphorylate the Rb-E2F complex and is responsible for the release of the transcription factor E2F. E2F as last is involved in DNA ultra-structure modifications and S-phase genes activation.

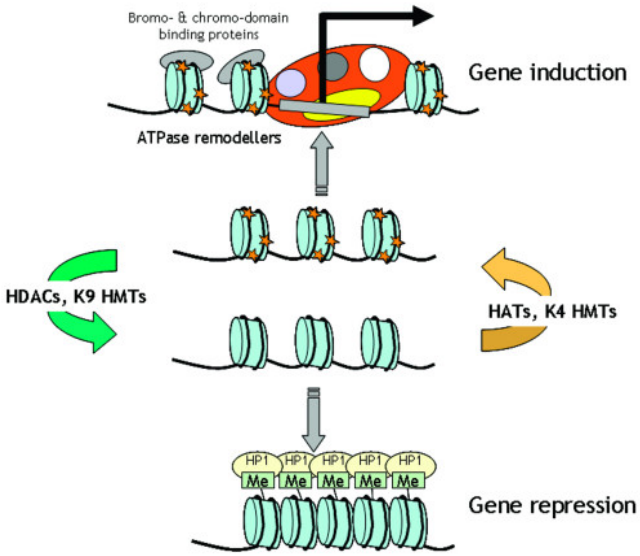

Figure 1.f5. Chromatin remodelling by HDACs, HATs and histone methylase (Adcock, Ford et al. 2006).

Chromatin remodelling systems: histone acetyltransferase complex (HAT) adds the acetyl group to the histone tails; this modification reduces DNA condensation, thus increasing enzyme accessibility. The inverse action is performed by HDAC for a reduced DNA accessibility and gene silencing. The methylation by HMT often follows deacetylation creating a stronger gene silencing.

1.2.2.4 GDNF

The glial cell-line derived growth factor (GDNF), acting through the glycosylphosphatidylinositol- (GPI) receptor c-Ret, a transmembrane tyrosine kinase receptor, and the glial cell line-derived neurotrophic factor family receptor α 1, 2, 3 and 4, GFR α1, α2, α3 and α4, is able to promote cell survival and in vitro neuron differentiation. Moreover, it was demonstrated that GFR α1 mRNA is up-regulated in SVZ and Cortex after 2 hours MCAo (Figure 1.f6) (Arvidsson, Kokaia et al. 2001).

Stroke induces widespread changes in gene expression for glial cell line-derived neurotrophic factor family receptors in the adult rat brain. Dempsey et al. (2003) proved a direct effect of GDNF on SVZ expansion. Prior to the ischemia being induced by MCAo, the animals were subjected to 24 hours intracerebroventricular infusion of GDNF, and one week after a significant increase in NPCs was noted in the SVZ (Dempsey and Kalluri 2007). The newly-formed NPCs survived for three weeks post MCAo (Dempsey, Sailor et al. 2003).

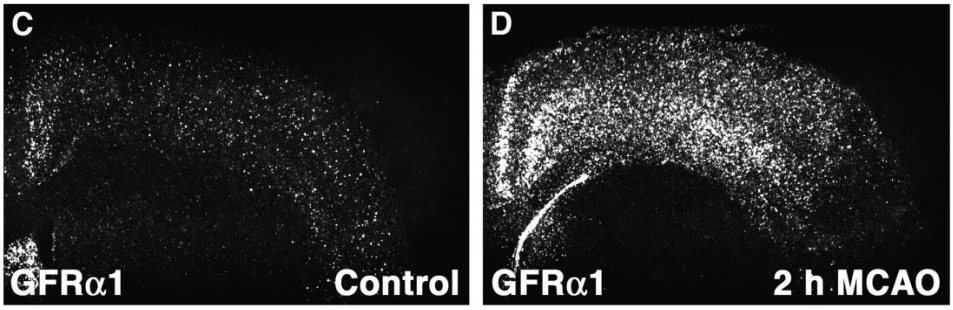

Figure 1.f6. Stroke induces up regulation of GFR α1 receptor (Arvidsson, Kokaia et al. 2001).

Effect of 2h_MCAo and 24h of reperfusion in a rat brain: the ischemia increased GFR α1 mRNA in the SVZ and Cortex.

1.2.2.5 TTC

The tetanus toxin is a neurotoxin secreted from the *Clostridium tetani* bacteria. The toxin comprises two polypeptide chains connected by a disulfide bond. The heavy chain can be divided into two different regions: the binding domain and the translocation domain. The binding domain is able to bind the gangliosides onto the nerve terminals and to be up taken by neurons. The neurotoxin, once in neurons, can be transported along the axon and across synapses and it can act at several sites within the Central Nervous System (CNS) and sympathetic NS. The translocation domain allows the neurotoxin to access cytosol. The light chain is a zinc endopeptidase that once activated by cytoplasmic enzymes, is able to cut the disulphide bond between the two chains. Moreover, it cuts Synaptobrevin 2 and determines the block of the release of GABA and Glycine to motor neurons, in turn causing the persistent muscle contraction symptomatic of tetanus (Roux, Saint Cloment et al. 2005; Caleo and Schiavo 2009).
The tetanus toxin fragment C (TTC) is the C terminal portion of the heavy chain that is considered non-toxic, and in research is used as a neuronal tract tracer.

Many studies have demonstrated the effect of TTC on improving compound delivery, such as that of mature GDNF in the CNS to provide neuro-protection to axotomized motor neurons (Larsen, Benn et al. 2006). Moreover, its neurotrophic-like effect was quite recently demonstrated in the ALS mouse model. In this experiment conducted by Moreno-Igoa et al. in 2009, naked DNA encoding for the TTC was intramuscularly injected in the transgenic $SOD1^{G93A}$ mouse model; the treatment improved hindlimb muscle innervation, delayed the ALS onset through improved motor neuron survival, and mediated lifespan elongation (Moreno-Igoa, Calvo et al. 2010).

1.2.3 INCREASE OF GROWTH FACTOR PRODUCTION AFTER ISCHEMIA

After ischemia many growth factors and related receptors are up-regulated within the damaged tissue (Lippoldt, Reichel et al. 2005). Some published studies pointed out possible relationships between post MCAo neurogenesis and growth factors (Dempsey and Kalluri 2007). The action of these stimulating factors is not always closely related to the proliferation of neural progenitors, some of which can induce mitosis, like EGF and FGF2, while others block cell self-renewal. Transforming Growth Factor β1 (TGFβ1) is an example of a factor which blocks self-renewal; its action directly interrupts cell division through up-regulation of mitosis inhibitors (Yamashita, Ninomiya et al. 2006).

1.3 NEUROGENIC ENVIRONMENT

1.3.1 THE NICHES

Stem cells are distinguished from other cell types by two specific characteristics: they can generate identical daughter cells from division or self-renewal and they can produce different cell types after differentiation. In order to control and regulate self-renewal and multipotency, the specific environment of the neuronal niche is required. This niche provides paracrine and autocrine signals, in turn responsible for stem cell activation, differentiation and finally, niche support cells. Within the neuronal niche, stem cells are anchored to the basal lamina or stromal cells; the organization of this micro-environment provides a specific substrate which is pivotal to cells' orientation and division, and to modulate regulatory factors and metabolites accessibility (Riquelme, Drapeau et al. 2008; Imayoshi, Sakamoto et al. 2009; Ming and Song 2011; Yao, Mu et al. 2012).

1.3.2 NEUROGENIC AREAS

1.3.2.1 SVZ IN PHYSIOLOGICAL AND PATHOLOGICAL CONDITIONS

The SVZ is located along the lateral wall of the third ventricle, and consists of a layer of quiescent cells separated from cerebrospinal fluid (CSF) by multi-ciliate ependymal cells. The newly-born cells originate from the SVZ migrate in a chain-like structure toward the RMS pathway by which they reach the OBs. Within the OBs the newly-formed inhibitory interneurons, granules and periglomerular cells are integrated into the neuronal network (Belluzzi, Benedusi et al. 2003).

In pathological conditions, for example, post MCAo, SVZ progenitors respond to the damage through reactivation of the cell cycle and migration toward the ischemic areas (Wurmser, Palmer et al. 2004). The migration occurs via chain like structures closely associated with endothelial cells. Once they reach the ischemic area, they associate with astrocytes and express Dcx (Yamashita, Ninomiya et al. 2006). This cluster organization resembles the neuronal niches located in the neurogenic areas (Louissaint, Rao et al. 2002; Alvarez-Buylla and Lim 2004; Wurmser, Palmer et al. 2004; Yamashita, Ninomiya et al. 2006). Migrating neuroblasts use chemoattractant molecules to reach the infarct area. Stromal Derived Growth Factor (SDF-1) and Angioprotein 1 (Ang-1) are proteins secreted by endothelial cells and are up-regulated in hypoxic conditions. These proteins regulate stem cell differentiation and migration through the receptors Tie2 and CXCR4 (Ohab, Fleming et al. 2006). Angiogenesis is associated with neurogenesis in the niche environment (Leventhal, Rafii et al. 1999; Alvarez-Buylla and Lim 2004; Wurmser, Palmer et al. 2004). Moreover Ohab et al. (2006) demonstrated a functional link between the formation of new blood vessels and neuroblast migration occurring post MCAo. In this study they inhibited angiogenesis via endostatin treatment,

and demonstrated a 10-fold Dcx-positive cell reduction in the perinfarct area (Ohab, Fleming et al. 2006).

1.3.2.2 SGZ IN PHYSIOLOGICAL AND PATHOLOGICAL CONDITIONS

The SGZ is located within the hippocampus, between the granule cell layer of the dentate gyrus (DG) and the hilus. This neurogenic area has been demonstrated to be present in mammals, especially in superior primate brain. The granular zone forms relatively late during development (around one week before birth) and produces neurons over the whole lifetime. Numerous factors regulate the SGZ. For instance, the SGZ is negatively regulated by age and stress hormones (corticosterone and cortisol), and positively regulated by estrogen, progesterone and antidepressants (Galea, Spritzer et al. 2006; Brinton, Thompson et al. 2008; Schoenfeld and Gould 2012)

The SGZ produces and integrates in the hippocampus circuit around ten thousand newborn neurons in a life time. The hippocampus is a limbic structure involved in learning and memory. Learning increases neurogenesis in SGZ and promotes survival of newly generated cells (Gould, Beylin et al. 1999). Once new NPCs have been generated, they migrate for a short distance in the granular layer, extending dendrites to the molecular layer and starting to pull out the growth cone along the mossy fibre path. These cells are completely able to be reinserted into the neuronal network and to become actively functional.

The SGZ seems to have at least two different astrocyte populations: radial and horizontal astrocytes. The radial astrocytes express Nestin and extend basal processes into the granule cell layer. The horizontal astrocytes which are in turn generated by the radial astrocytes do not express nestin and express S100; they extend basal processes under the granule cell layer (Riquelme, Drapeau et al. 2008).

Although SGZ and SVZ are well established areas of neurogenesis in many animal models, in humans the notion of existence of an SVZ-like region is still controversial (Curtis, Kam et al. 2007; Sanai, Berger et al. 2007).

1.4 LENTIVIRAL VECTORS

1.4.1 BRIEF HISTORY AND GENERAL BACKGROUND

The idea of using viral vectors to deliver genes into eukaryotes was first conceived in the late 1970s, from the meeting of molecular virology and the first characterization studies of genetic diseases with Mendelian inheritance. Among the multiple types of viral vectors available, lentiviral vectors have relatively high coding capacity (around 7.5 kb), low immunogenicity and the ability to transduce non-dividing cells. The most commonly used lentiviral vectors are derived from HIV-1 (Cockrell and Kafri 2003; Cockrell and Kafri 2007).

In 1991 and 1992 the ability of the Human Immunodeficiency Virus type 1(HIV-1) to infect non-dividing macrophages and non-proliferating cells was demonstrated in vitro (Weinberg, Matthews et al. 1991; Lewis, Hensel et al. 1992). The aptitude to infect non-dividing cells depends on the preintegration complex (PIC). This complex contains diverse viral proteins (Viral protein r, Vpr; Viral matrix protein; integrase), some host proteins (including the Barrier-to-autointegration factor) and the viral dsDNA or provirus. The main role of the complex is to mediate the active transport of the dsDNA through the nuclear pores, and to allow the integration into the host chromatin (Fouchier and Malim 1999). The integrase is the protein responsible for the viral DNA integration and, as discussed below, a single substitution in its amino acid chain sequence can reduce or prevent the catalytic activity. In this case, the non-integrated vector DNA can remain

in an episomal state, and be efficiently transcribed, particularly in quiescent cells (Yanez-Munoz, Balaggan et al. 2006).

The initial lentiviral vectors produced did not have a wide tropism, but were limited to transduction of CD4-producing target cells, and with high probability of producing replication competent particles (Poznansky, Lever et al. 1991; Buchschacher and Panganiban 1992). A real improvement followed the introduction of pseudotyping, by which the wt HIV envelope protein is substituted with that from other virus having wider tropism, particularly the Vesicular Stomatitis Virus envelope glycoprotein G (VSV-G). Crucial was also the introduction of new strategies to reduce the likelihood of recombination events between vector components (Naldini, Blomer et al. 1996). These pseudotyped LV were able to efficiently transduce human cells in culture and rat neurons in vivo (Naldini, Blomer et al. 1996; Naldini, Blomer et al. 1996).

The most important limitation of these first viral systems was the biosafety: the probability to produce replication-competent elements in the host organism was a big obstacle for possible therapeutic applications. From 1997 many genes involved in the viral replication were eliminated, and the viral genome was first split into 3 different plasmids (second generation LV) then into four (third generation LV) (Sakuma, Barry et al. 2012). This not just reduced the probability of recombination between viral vector plasmids, improving the biosafety, but also increased vector genes delivering capability. In order increased biosafety, LVs were developed from non-primate Lentiviruses (Naldini 1998).

1.4.2 HIV LIFE CYCLE

The human immunodeficiency virus (HIV) is the virus responsible for the Acquired Immune Deficiency Syndrome (AIDS) (Janssen, St Louis et al.

1992; Maeda and Mitsuya 2007; Sullivan, Patel et al. 2011; Owen 2012). HIVs belong to the lentivirus genus, within the retrovirus family. Lentiviruses are complex retroviruses which in addition to *gag, pol and env* contain accessory genes. The HIV life cycle can be divided into early and late stages. The early stage starts with the interaction of the viral envelope protein gp120 with the macrophages receptor CD4, also located on the surface of T-helper lymphocytes; both of them are important cells of the immune system. After the first interaction between pg120 and CD4, a third protein; the trans-membrane chemokine receptor CCR5 is recruited. The co-receptor CCR5, together with the CD4, determines the site where the viral envelope fuses with the host cellular membrane and the viral nucleocapsid accesses the cytoplasm. After the macrophages infection, a pg120 modified protein is expressed on the cellular membrane, in turn responsible for the interaction with a different receptor located on the T-cells membrane, the CXCR4 (Nguyen and Taub 2002). The result of this infection is a severe reduction of both macrophages and T-cells, in turn responsible for the development of AIDS (Figure 1.f7).

The viral genome consists of ~9-kb RNA encoding for 15 different proteins (Table 1.1.t1) (Frankel and Young 1998). Once in the host cytoplasm the viral nucleocapsid is disassembled (uncoating), and a pre-integration complex (PIC) is formed. Once built, the PICs are able to mediate the nuclear transport and the provirus integration (Figure 1.f7) (Nisole and Saib 2004).

The late stage begins when the double strand cDNA is integrated into the host genome, and gene transcription starts. The first transcripts to be translated are Tat, Rev and Nef: Tat controls the rate the proviral transcription is activated, Rev is involved in the proviral mRNA splicing before the nuclear export, while, Nef is responsible for the particles released by endocytosis. The proviral mRNA is retained in the nucleus until it is spliced as an effect of the Rev binding to the RRE. The nuclear

accumulation of Rev determines the shift between highly spliced mRNA, single spliced and un-spliced, and it is responsible for the viral life cycle phases. The structural proteins are produced by the Gag and Env transcripts, and the viral genome packed into the capsid. The capsid is built by a protein-protein interaction of the Gag and Pol polyproteins with the Capsid protein (CA). The ssRNA is packed into the capsid as a result of the interaction between the Ψ sequences and the NC protein. Additionally, the package contains Vif, Vpr, Nef and some cellular tRNA (Figure 1.f7) (Frankel and Young 1998; Nielsen, Pedersen et al. 2005).

Budding of the nucleocapsid complex through the plasma membrane produces the envelope coating; the envelope in turn contains the extracellular gp120 and transmembrane protein gp41, both necessary to start the successive interaction with T-helper and macrophages cells (Figure 1.f7) (Frankel and Young 1998; Nielsen, Pedersen et al. 2005).

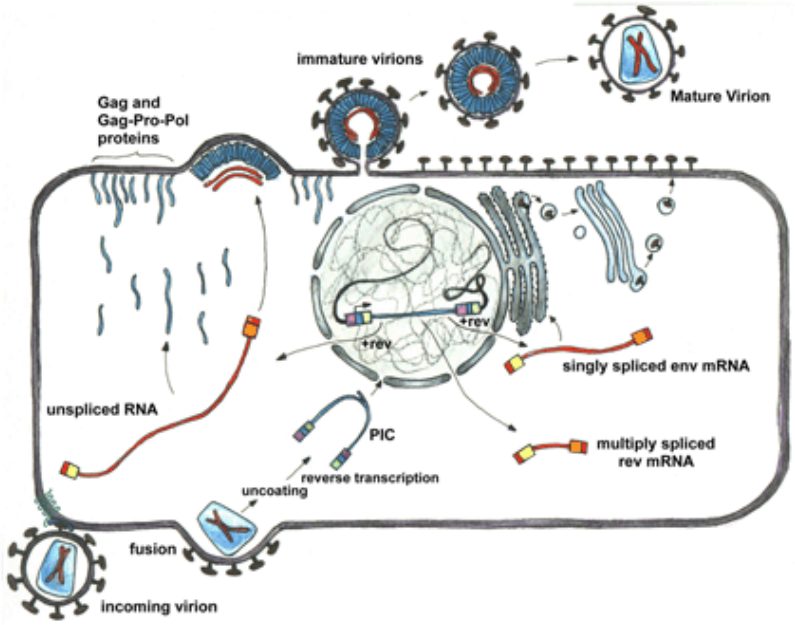

Figure 1.f7. Lentivirus life cycle.

The picture describes the HIV virus life cycle: interaction and integration with the host, transcription, viral particles assembly and as last endocytosis mediated release. The picture was made by Dyana Terry Soenz from Poeschla's lab and it was downloaded online at http://mayoresearch.mayo.edu/mayo/research/poeschla/index.cfm

Name of protein	Function	Transcript
MA, matrix	Viral assembly, facilitates infection in non-dividing cell types	Gag
CA, capsid	Structural protein	Gag
NC, nucleocapsid	Structural protein	Gag
p6,	Mediate the release of particles	Gag
SU, surface protein or gp120	Surface receptor	Env
TM, transmembrane protein or gp41	Surface receptor	Env
PR, Protease	Protein cleavage	Pol
RT, Reverse transcriptase	reverse transcription	Pol
IN, Integrase	Viral genome integration	Pol
Vif	Found in the viral particle	Vif
Vpr	Found in the viral particle	Vpr
Nef	Found in the viral particle	Nef
Tat	Gene regulatory function	Part of Vpr-Vpu-Env
Rev	Gene regulatory function	Vpu-Env
Vpu	Indirectly assist the virion assembly	Env

Table 1.1.t1. Table of the HIV proteins (Frankel and Young 1998).

1.4.3 LENTIVECTOR SYSTEMS

The production of lentiviral vectors relies on splitting the necessary components into several plasmids, called packaging (encoding viral genes required for vector production but not incorporated into the vector genome), envelope (encoding a heterologous envelope protein for pseudotyping, commonly VSV-G) and transfer (encoding the transgene cassette and *cis*-acting sequences required for vector production, reverse

transcription and integration) plasmids. In this study second- and third-generation LV were used. Lentiviral generations refer to the genes encoded by the packaging plasmids. A second-generation system includes *gag, pol, tat and rev*, while a third-generation system uses only *gag, pol and rev*, with the latter one being present on a separate plasmid (Vigna and Naldini, 2000). The production on LV particles requires the packaging, *rev*, envelope and transfer plasmids to be co-transfected into producer cells. The host cells mainly in use for LV production and used in this specific project were the human embryonic kidney HEK293T cell line, due to their highly efficient transfection. These plasmids were transfected into the HEK 293T cells using a Calcium Phosphate transfection.

1.4.4 IDLVs

The integration process is a pivotal step of the Lentivirus' life cycle, after which the provirus becomes part of the host genome. The Integrase protein contained in the PIC complex mediates this step. The integration starts with the cleavage of both dinucleotides at the 3' ends, then the host genome is cut and the proviral cDNA is transferred into the gap. Finally the gaps are repaired and the ligation occurs.

The catalytic activity of integrase can be disrupted by mutations, the most commonly used leading to a change from aspartic acid 64 to valine on the polypeptide chain. This change causes a significant reduction in proviral integration, and an increase in the formation of episomal DNA vector circles, which can be efficiently transcribed and are metabolically stable in non-dividing cells (Leavitt, Robles et al. 1996; Yanez-Munoz, Balaggan et al. 2006). Such Integration Deficient Lentiviral Vector (IDLVs) can transduce target cells and allow transgenic expression. Dividing cells, as the NPCs, can be efficiently transduced by IDLV; in this case the episomal vector as well as the encoded transgene are expected to be progressively

diluted through cell division (Yanez-Munoz, Balaggan et al. 2006; Wanisch and Yanez-Munoz 2009).

1.5 RNAi and shRNA

RNA interference or RNAi is a post-transcriptional regulatory system, occurring from nematodes to fungi, and is a very important mechanism by which organisms can temporarily interrupt mRNA translation and protect themselves from viral attack. It was first described in 1990 by Napoli et al. and then by Guo and Kemphues in 1995, both of whom did not have a real understanding of the biological significance behind the event they were looking at. In the experiment accomplished by Guo and Kemphues, the C. elegance par-1 gene expression silencing was attempted and achieved by injection of an anti-sense or a sense strand RNA. To have a clarification about the mechanism behind the RNA mediated "gene silencing", we had to wait for a 1998 publication in Nature by Fire et al. In this paper they reported a strong "gene silencing" mediated by double-stranded RNA. At most a modest effect was found when a single-stranded RNA (sense or anti-sense) was injected. They coined the term RNAi to describe the event, and Fire and Mello were awarded with a Nobel Prize in 2006.

The interference system acts through small pieces of RNA (21-23 nt), obtained from a double strand RNA (dsRNA), cleavage by the endoribonuclease DICER. The short RNA is recruited by the RNA-induced silencing complex (RISC), which once assembled with the siRNA, is able to recruit the complementary or partially complementary mRNA, and produces respectively degradation or silencing (Figure 1.f8) (Kim and Rossi 2007).

Using the RNAi pathway, the shRNA can silence or degrade mRNA and can be a powerful tool for gene therapy. The shRNA is a small sequence of RNA that can shape as hairpin and is widely in use for gene silencing by

blocking mRNA translation. It can be delivered by viral (for example LVs) and non-viral vectors, (McIntyre and Fanning 2006; Mahmood ur, Ali et al. 2008).

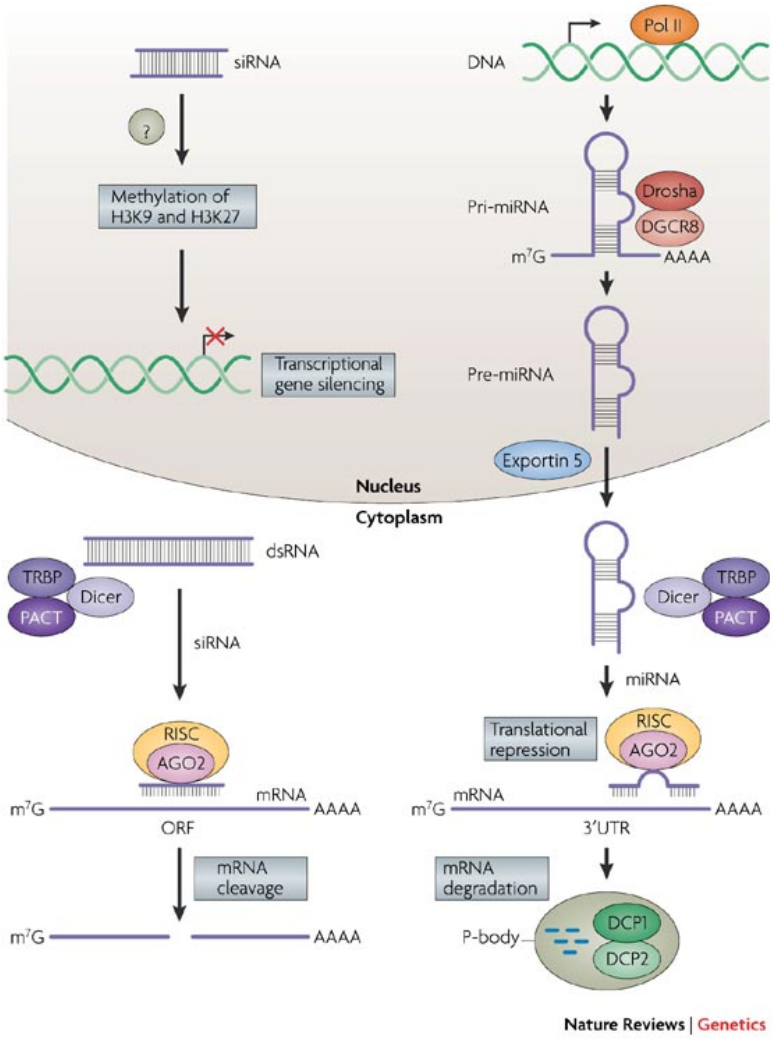

Figure 1.f8. iRNA by Kim and Rossi 2007 (Strategies for silencing human disease using RNA interference).

RNAi is a mechanism by which organisms can block mRNA translation and self-protect against some recognized viruses. The mechanism is mediated by a double strand RNA and is in turn recognized and cleaved by the ribonuclease DICER, once the siRNA is produced, and can interact with the RISC complex. Once the RISC is bound, it recognizes and activates mRNA cleavage.

AIMS OF THE PROJECT

As the growing body of evidence suggests, neurogenesis occurs in pathological conditions such as stroke, neurodegenerative diseases and severe brain damage. The exact role of this event is not completely understood and has not yet been clarified. In order to better understand SVZ neurogenesis in ischemic conditions, this project aims to boost and inhibit neurogenesis and assess the effect of the treatments in a long-term study.

The project can be divided in four separate aims:

1. To set up a neurogenesis inhibition system based on LVs
2. To set up and validate an MCAo model for long-term study
3. To set up an LV-based system to detect and quantify neurogenesis in vivo in the presence or absence of stroke
4. To study the effect of SVZ neurogenesis modulation on post-ischemic recovery.

CHAPTER 2

MATERIALS AND METHODS

2.1 CLONING

2.1.1 STANDARD CLONING TECHNIQUE

The plasmids used for this project were designed using Vector NTI software from Invitrogen, and the production was achieved through techniques of molecular biology.

The plasmid DNA was first amplified by heat shock transformation in Top 10 *E. coli* cells. Bacteria that incorporated the exogenous DNA or transformed bacteria, acquired one or more antibiotic resistance that was encoded in the plasmid; these resistance was then used to select the desired colony. In this case an ampicillin resistance was encoded in the plasmid DNA sequence. Once the plasmid was incorporated in the bacteria the cells acquired the resistance and there were selected by growing in an Ampicillin enriched medium (both techniques are described below).

After the colony was amplified, the DNA was extracted and enzymatic digestions were used to excise the undesired sequences from the original plasmids; compatible ends were bounded by Ligase T4 reaction.

To ensure the correct sequence on the selected plasmid, enzymatic digestions were used as well as the plasmid was entirely sequenced as below reported.

2.1.1.1 RESTRICTION ENZYME DIGESTS

The DNA extracted from Top ten E. Coli cells was cut by digestion with restriction enzymes, selected in order to obtain compatible strand ends to be successively ligated by the T4 Ligase reaction.

20 µl of total digestion reagents, contained 2 µl of enzyme's buffer, 1 µl of the selected restriction enzyme and 1 µg of plasmid DNA, was mixed and incubated over night at 37°C. The reaction efficiency was estimated by gel electrophoresis, from which the correct size band was assessed and purified.

2.1.1.2 GEL ELECTROPHORESIS AND DNA EXTRACTION

MATERIALS

Loading buffer, Sigma
Agarose, Sigma
Ethidium bromide, Sigma
GeneRuler 1 kb, Fermentas
QIAgen gel extraction kit, QIAgen

SOLUTIONS AND BUFFERS

10X TAE

48.4 g of Tris base [tris(hydroxymethyl)aminomethane]
11.4 ml of glacial acetic acid (17.4 M)
3.7 g of EDTA, disodium salt
Deionized water

The 1X TAE was obtained in a 1:10 dilution.

Digested DNA was re-suspended in loading buffer, and loaded in 0.8% agarose gel containing 0.5 µg/ml of ethidium bromide; as a DNA reference the GeneRuler ladder 1 kb was used. DNA was run in 1% TAE buffer at 50 V for 30-45 minutes.

After electrophoresis, DNA fragments were detected by illumination under UV light, and the correct size band was excised from the gel and purified with the QIAgen extraction kit, following manufacturer's instructions. Briefly, the cut band was first weighted; 3 volumes of buffer QG (w/v) were added per unit of gel slice and incubated at 50°C for 10 minutes. 1 gel unit of isopropanol was added to the solution and applied to a QIAquick spin column, then centrifuged for 1 minute. The flow-through was discarded and 0.5 ml of buffer QG was added to the column and centrifuged for one more minute. 0.75 ml of PE buffer was added to the column and washed out by centrifugation. The column was placed in a clean tube and the DNA eluted with 30 µl of EB.

2.1.1.3 KLENOW POLYMERASE REACTION

Klenow Polymerase, Promega
Klenow Polymerase Buffer, Promega
BSA, Promega

Klenow Polymerase allows filling 5' ends obtained by specific enzymatic digestion.
The reaction mixture contained 2.5 µl of DNA (0.1-1 µg), 1 µl of Klenow Polymerase buffer, 2 µl of dNTPs 2 mM, 1 µl of BSA and 2.5 µl of water; the solution was incubated for 1 hour at room temperature, and successively the enzyme activity was stopped in a 75°C thermostat for 10 minutes.

2.1.1.4 LIGATION

MATERIALS

T4 Ligase, Promega
T4 ligase Buffer, Promega
BSA 10%, Promega

DNA fragments were ligated together with a T4 Ligase reaction; a starting amount of 100 ng of Backbone DNA was used. The insert concentration was calculated with the following formula:

(1) $ng\ insert \div bp\ insert = ng\ backbone \div bp\ backbone$

(2) $ng\ insert = ngbackbone \times \frac{bp\ insert}{bp\ backbone}$

Depending on the structure of the ends of the molecules (two sticky ends, two blunt ends or one sticky and one blunt end) the equation in (1) becomes:

To join two sticky ends

(3) $(ng\ insert \div bp\ insert) \times 3 = (ng\ backbone \div bp\ backbone) \times 1$

To join one sticky end and one blunt

(4) $(ng\ insert \div bp\ insert) \times 5 = (ng\ backbone \div bp\ backbone) \times 1$

To join two blunt ends

(5) $(ng\ insert \div bp\ insert) \times 10 = (ng\ backbone \div bp\ backbone) \times 1$

10 µl of the ligation mix contained 1% of BSA 1 µl, 10% of ligase buffer 1 µl, DNA as calculated above, 1 µl of T4 Ligase, and water. The reaction was incubated over night at 18ºC. The day after, the ligated DNA was introduced into the bacteria by heat shock transformation, clones selected with ampicillin, amplified and DNA extracted (see below).

2.1.1.5 BACTERIAL TRANSFORMATION and CLONE AMPLIFICATION

MATERIALS

LB Broth, Sigma
Bacteriological Agar for Molecular Biology, Sigma
Ampicillin, Sigma

1-1.5 µl of plasmid DNA was introduced in Top ten competent cells by heat shock transformation. E. Coli Top ten cells stored at -80°C were slowly defrosted on ice and the DNA added to the tube. DNA incorporation was heat induced; the bacteria-DNA solution was placed at 42ºC for 45 seconds, then quickly the tube was put back on ice. Transformed bacteria were incubated for 1 hour in an antibiotic free LB medium at 37°C, then spread onto ampicillin plates and incubated over night at 37°C. The day after, the positive clones were selected and amplified in the conditional LB medium.

2.1.1.6 PLASMID DNA EXTRACTION

MATERIALS

Miniprep and Maxiprep kit, QIAgen

Plasmid DNA extraction from bacteria was achieved by QIAgen Miniprep and Maxiprep. For 1 to 5 ml (150 to 500 ml for Maxiprep) of inoculated bacteria 250 µl of P1 buffer was added (10 ml for Maxiprep), followed by 250 µl of P2 buffer and 350 µl of P3 buffer (10 ml of each buffer for Maxiprep), each time gently inverting the tube 4-6 times (Maxiprep were incubated on ice for 30 minutes). The tube was centrifuged at 13,000 rpm for 10 minutes (Maxiprep were centrifuged at 3500 rpm for 30 minutes),

and the supernatant added to the QIAprep spin column. The tube was centrifuged at maximum speed and the flow-through discharged (Maxiprep were filtered by gravity and the flow-through collected in a 50 ml falcon tube). After washing with 500 µl of PB buffer and 750 µl of PE buffer the DNA was eluted with 50 µl of EB buffer. In the case of Maxiprep, 10 ml of QBT buffer was used to equilibrate the Quiagen-tip 500, and then the flow-through was applied to the column, as well as 2 x 30 ml of buffer QC. The DNA was eluted by adding 15 ml of buffer QF; it was then precipitated with 10.5 ml of isopropanol and centrifuged at max speed for 30 minutes. After discharging the liquid and let the DNA air dry, the pellet was re-suspended in a suitable volume of TE buffer.

2.2 LENTIVIRAL VECTOR PRODUCTION

2.2.1 CELL LINES

MATERIALS

DMEM, PAA
FBS, PAA
Penicillin and Streptomycin , PAA
Trypsin/EDTA solution , PAA
PBS, PAA

All cell lines used were maintained in a Dulbecco's modified medium enriched with 10% foetal bovine serum and antibiotics (streptomycin/penicillin), under 5% CO_2 and controlled humidity. The cellular confluence was tightly controlled, and was not allowed to expand for more than 80% of the total free surface.
Cells used in the project:

• HEK 293T is the human kidney epithelial cell line engineered to constitutively express the SV40 large T antigen. The HEK 293T cell line was used to produce LV.

• HeLa cells are human fibroblasts isolated from a patient who had cervix cancer in 1951. These cells respond very well to LV transduction and were used for titration.

• NIH3t3 cells are mouse fibroblasts. These cells have an overexpression of the v-H-Ras protein, in turn responsible for an increase level of Cyclin D1 (Liu, Chao et al. 1995). The increased amount of Cyclin D1 produces a shorter G_1 and it is responsible for the tumorigenic phenotype. This cell line was used to assess variation of CyclinD1 protein content and the cell cycle blocking, as effect of the LVs_dnCyclinD1 and LVs_shRNA_CyclinD1 transduction.

2.2.2 VECTOR PREPARATION

MATERIALS

Water, Sigma-Aldrich
2.5 M $CaCl_2$, Sigma-Aldrich
HEPES, Sigma-Aldrich
NaCl, Sigma-Aldrich
Na_2HPO_4, Sigma-Aldrich
Polybrene, Sigma-Aldrich
DNAse I, Promega
TE endotoxin free, Quiagen
Filter 0,22-µm-pore-size, Nalgene

Third or second generation HIV-based LVs was obtained via transfection of respectively four and three plasmids into HEK 293T cells (Yanez-Munoz, Balaggan et al. 2006).

CALCIUM PHOSPHATE TRANSFECTION

2-2.5 x10^6 cells were plated two days before transfection in a 15 cm plate; this cellular concentration produces two days later a transfection optimum confluence (60-70%).

LVs were produced by Calcium Phosphate transfection. On the transfection day, between 1 and 4 hours before starting the procedure, the medium was replaced with 18 ml of fresh DMEM,.
To optimize vector packaging the following molar DNA ratios were used:

1. For a third generation LV

   Env (pMD2.VSV-G): rev (pRSV-REV***): packaging (***pCMVΔR8.74***): transfer plasmid = 1:1:1:2***

2. For a second generation LV

   Env (pMD2.VSV-G***): Packaging (***pMDLg/pRRE***): transfer plasmid = 1:1:2***

The plasmid DNA mixture was re-suspended in TE buffer and water; the final concentration for the TE solution was 0.1 %.

DNA complexes were induced by adding 125 µl of $CaCl_2$ drop-by-drop while vortexing for 1 minute, then 1'250 µl of 2xHBS were added.

The solution contained the DNA complexes were added to the cells and left 14-16 hours in the incubators. At 16 hours, the medium was replaced with a fresh one.

The vectors were harvested at 48 and 72 hours post-transfection.

HARVESTING

The medium was collected and centrifuged at 2,500 rpm for 10 minutes, and then the supernatant filtered via a 0.22 µm pore size. Vector concentration was achieved by overnight centrifugation at 4,000 rpm and 4°C. The day after, the supernatant was discarded and the pellet re-

suspended in 50 µl of DMEM with no supplements. To remove debris, LVs were centrifuged for 10 minutes at 4,000 rpm and 4°C; finally DNAse 5 u/ml and $MgCl_2$ 10 mM was added to the collected supernatant.

2.2.3 TITRATION

MATERIALS

Polybrene, Sigma-Aldrich
PFA, Sigma-Aldrich

HeLa cells were used to titrate LVs. We used two titration systems; one was based on *eGFP* expression estimated by Flow Cytometry, while for all vectors without an *eGFP* cassette, the titre was estimated by qPCR.

2.2.3.1 FLOW CYTOMETRY

TRANSDUCTION

At day zero 10^5 cells were plated out per six well plate well. The day after, the cells were transduced by replacing the medium with 2 ml of fresh DMEM containing Lentivector particles. To titrate each batch, ten-fold vector dilutions were prepared in complete DMEM; the range used for the transductions was from 10^{-3} to 10^{-6}. 8 µg/ml of polybrene was added to the plates to improve transduction efficiency. 3 days later cells were harvested and fixed in 1% PFA.

ESTIMATION OF INFECTION UNITS

The number of eGFP positive cells per sample was estimated by Flow Cytometry. Transduction occurs by multiple or single infection events per cell; in order to estimate the number of vectors based on the number of green cells, it is important to exclude samples for which the possibility of

multiple infection events is high. Based on the assumption that with less than 10% of green cells, the transduction event occurs only by a single infection, the number of green cells could be used as a good estimation for the number of vectors originally present during the transduction. The titre was expressed in Transducing Units per millilitre (TU/ml) and was calculated using the following formula:

(6) $$eGFP\ Infection\ Unit/ml(IU/ml) = [\frac{F \times C}{V}] \times D$$

F = frequency of green cells
C = total number of cells at day zero
V = volume of inoculum
D = Lentiviral vector dilution

2.2.3.2 qPCR

MATERIALS
DNeasy blood & tissue kit, QIAgen
TaqMan, Applied Biosystems
SensiMix Syber No Rox Kit, Bioline
Ethanol 99-100%, Sigma-Aldrich

Vectors without a functional eGFP cassette were titrated by qPCR.

TRANSDUCTION
The day before transduction 10^5 cells were placed in a six well plate; 24 hours later the transduction was performed. For each batch two serial dilutions were prepared: 1:2,000 and 1:20,000 that for a 10^8IU/ml vector correspond to MOIs 0.5 and 0.05. One day after the cells were harvested; the DNA was extracted using the DNeasy blood and tissue kit from QIAgen, and eluted in 400 µl of PBS.

DNA EXTRACTION

For the DNA extraction 20 µl of Proteinase K and 200 µl of AL buffer were added together, placed in a 56°C bath and incubated for 10 minutes. After adding 200 µl of Ethanol 99-100% the samples were loaded onto a DNeasy Mini spin column and centrifuged at 800 rpm for 1 minute. After discharging the collecting tube and the flow-through within, the buffers AW1 and AW2 were added to the column. Each buffer was centrifuged at 800 rpm for 1 minute and consequently flow-through discharged. The DNA was eluted from the column with 200 µl of AE buffer.

qPCR REACTION

Two different reactions were conducted separately for the titration of the lentivectors: the LRT reaction quantified the number of copies of the lenti_backbone, while the Actin reaction quantified the number of Actin gene copies in the sample.

LRT reaction, LVs copies number:

Sample volume = 6.25 µl

Primer concentration= 300mM

Standards=10^2-10^7 copies of pHR'SIN-cPPT-SEW/reaction

Starting cycle: 50°C 2 minutes, 95°C 10 minutes, 50x (95°C 15 sec, 60°C 1 minute)

Actin reaction, internal standard:

Sample volume= 5 µl

Primer concentration= 300mM

Probe concentration=200 mM

Standards=10-10^6 copies Hela cell equivalents (genomic DNA)

Starting cycle: 50°C 2 minutes, 95°C 10 minutes, 50x (95°C 15 sec, 60°C 1 minute).

The number of LRT copies normalized to cell number using the Actin gene is a very sensitive estimation of the vector genome copies that have completed reverse transcription per transduced cell, and it can be used for the estimation of vector titre.
Formula to estimate the vector titre:

(7) $$IU/ml = \left[\frac{(\#of\ copies\ for\ LRT\times 64)}{(\#of\ copies\ for\ Actin\times 80)}\times D\times C\right]$$

D = dilution factor
C = total number of cells at day zero
$(\#of\ copies\ for\ LRT\times 64)$= *total number of LRT copies in the transduced sample*
$(\#of\ copies\ for\ Actin\times 80)$= *total number of actin copies in the transduced sample*

2.3 IN VITRO TRANSDUCTION FOR CyclinD1 DOWN-REGULATION

MATERIAL

Polybrene, Sigma-Aldrich

After packaging, LVs_dn_Cyclin D1 and LVs_shRNA were tested for their *in vitro* effect on the NIH3t3 cell line by using a viability assay and Western blot.

2.3.1 TRANSDUCTION

At day zero, 2.5 x 10^5 cells were plated in a serum enriched medium; the transduction was performed the day after with 8µg/ml of Polybrene.

The multiplicity of infection (MOI) is a parameter used to standardize the amount of virus or vector added per cell for *in vitro* treatments; in the case of vectors:

MOI = Transducing Units / cell

2.4 VIABILITY ASSAY

2.4.1 MTT

MATERIAL

Thyazolyl Blue Tetrazolium Blue (MTT), Sigma-Aldrich
DMSO, Sigma Aldrich

The viability assay was used to diagnose the effect of dnCyclin D1 and shRNA_Cyclin D1 on the NIH3t3 cell cycle.

At day zero 0.5 x 10^5 cells were placed in a 6 well plate and were transduced the day after. The viability assay was performed by adding 100 µl of MTT for 4'000 cells and incubating for 3 hours at 37°C. After incubation the medium containing MTT (5 µg/ml) was discharged and the plates were left to dry overnight at room temperature. 250 µl of DMSO was used per well to dissolve the crystals formed from the reaction between MTT and the mitochondrial enzyme Reductase. The samples were analysed by spectrophotometer at λ = 570 nm. Because the Reductase is directly proportional to the number of cells metabolically active, the

absorbance produced by the reaction with MTT is directly proportional to the live cells number and can be used to estimate their concentration.

2.5 PROTEIN ANALYSIS

2.5.1 WESTERN BLOT

MATERIALS

Complete EDTA free lysis buffer, Roche
Protein quantification, Bio-Rad
Immobilon P transfer membrane, Millipore
Sodium dodecyl sulphate, Sigma-Aldrich
2-mercaptoethanol, Sigma-Aldrich
TRIZMA, Sigma-Aldrich
Glycine, Sigma-Aldrich
NaCl, Sigma-Aldrich
Tween 20, Sigma-Aldrich
Glycerol, Sigma-Aldrich
Dried milk, Tesco

SOLUTIONS AND BUFFERS

1. Laemmli Buffer 2X

4% SDS
10% 2-mercaptoethanol
20% Glycerol
0.125 M TRIZMA
pH 6.8

2. Migration Buffer 10X

0.25 M TRIZMA
1.9 M Glycine
1% SDS
pH 8.3

3. Transfer Buffer 10X

48 mM TRIZMA
39 mM Glycine
0.375% SDS (37.5 ml of 10% SDS)

Cells were transduced with the method previously described, harvested by adding 50 µl of complete EDTA-free lysis buffer and scraped from the plate using a cell scraper. The lysate was spun at high speed, and the supernatant collected and stored at -80°C.

PROTEIN CONTENT ASSAY

Protein concentration, expressed in µg/µl, was estimated by Bio-Rad protein assay. Briefly, after obtaining a dilution of 1-5 times for each protein sample, 160 µl of the standard or the sample was added to the well in a 96 well plate; 40 µl of the dye reagent was added soon after. Because the protein interaction with the dye causes a colour change in a concentration dependent manner, using the BSA standard samples is possible to build a standard curve that matches absorbance with protein concentration. The standard curve allows the estimation of the protein content in the unknown samples (protocol available through Thermo Scientific web site, *TECH TIP #57)*.

SDS-PAGE GEL

The samples were denatured by incubation with Laemmli buffer at 95°C for 10 minutes. Denatured proteins were loaded in a 12% SDS-Page gel by which they were separated according to size. Gels were placed in a Bio-Rad apparatus and covered by 1x migration buffer. Introducing a potential difference of 200 V for 1-1.5 hours in the apparatus, subsequently induced migration.

The electro-transfer technique allowed protein mobilization from a gel to an Immobilon P membrane. For the electro-transfer, a sandwich like structure was built using sponges with some Whitman paper and in the middle the membrane facing the gel.

The blotting was loaded in a transfer buffer with the same Bio-Rad apparatus used for protein separation. For the electro-transfer 100 V was applied for 1 hour.

2.5.2 IMMUNO REACTION

MATERIALS

Tween 20, Sigma-Aldrich

Milk, Tesco

PBS tablets, Sigma-Aldrich

Mouse anti Cyclin D1, # C7464, Sigma Aldrich

Rabbit anti alpha tubulin, # T8660, Sigma Aldrich

Goat anti mouse 800, # 926-31066, Odyssey®

Rabbit anti goat Alexa fluor 680, #A20984, Invitrogen

SOLUTIONS AND BUFFERS

PBS_T
Phosphate buffer saline 1 M
Tween 20 0.025%

BLOCKING SOLUTION
PBS_T
Milk 5%

After the electro-transfer the membrane was incubated for 1 hour at room temperature in blocking solution, then overnight at 4°C with the antibody of interest diluted in the PBS-T buffer. The day after the membrane was washed twice in PBS-T, and incubated for 1.5 hours at room temperature with the secondary antibody. The antibodies' concentration used is described in Table 2.1.t1

After incubation the membrane was washed twice in PBS_T and analysed by Odyssey technology.

Antibody	company	concentration
Anti-mouse Cyclin D1	Invitrogen	1:1000
Anti-rabbit alpha tubulin	Invitrogen	1:1000
Alexa Fluor, Goat anti rabbit 680	Invitrogen	1:30,000
Alexa Fluor Donkey anti mouse 700	Invitrogen	1:30,000

Table 2.1.t1. Antibodies concentrations used in the western blot assay.

2.6 IN VIVO STUDY

2.6.1 ANIMALS

All procedures in live animals conformed with Animals (Scientific Experimentation) Act 1986, were carried out under the appropriate UK Home Office licences, and had LREC approval.

Six-ten week old male C57BL/6 mice were used to perform MCAo; this strain has a reduced Willis Circle's posterior communicating artery, in turn responsible for a high sensitivity to ischemia. These are widely used to produce the Middle Cerebral Artery occlusion model or MCAo (Fujii, Hara et al. 1997; Small and Buchan 2000).

All experiments were conducted blind; the animals were randomized and injected with a coded viral batch. A colleague, who was neither familiar nor involved in this study, prepared the coded vials and prepared a sealed envelope with the key to the batches used. The envelope was opened only after terminating the histological cell quantification.

Females were excluded from the project as the oestrus cycle hormones (estradiol and estrogens) produce arterial vasodilatation and improve endothelial functions; this is reflected in a reduction of cardiovascular disease risk factor, and provides an active protection from ischemia (Etgen, Jover-Mengual et al.). In addition, female hormones have a protective effect that might interfere with the results and data analysis.

2.6.2 ANIMAL MODELS

An animal model is a powerful tool to investigate diseases; the main idea is to reproduce a specific human condition in order to examine it and develop possible therapies.
There are a number of ways to validate an animal model:

- Predictive validity, the ability to respond to drugs, already in use to treat the disease the model is meant to reproduce.
- Construct validity, refers to the theoretical clarification of how and why an animal model would mimic a human disease.
- Etiological validity, the etiology of the model and the disease of the model is meant to emulate must have points in common.
- Face validity, refers to the phenomenological similarity between the behaviour shown by the model and symptoms related to the disease.

It is very unlikely that a model has all of these qualities simultaneously, but a good model could only have one or two of them.
The MCAo produces severe neuronal damage and death within the striatum cortex and the hippocampal formation, and is therefore widely used as focal ischemia model.

2.6.3 MCAo MODEL

MATERIALS:

Isofluorane, Baxter

The MCAo is performed under general anaesthesia using a mix of isoflurane, oxygen and nitrous oxide. The anaesthesia effectiveness was assessed by paw pinching and constantly monitored during the surgery.

The procedure was performed through a midline incision of the neck and the subsequent isolation of the right common carotid artery at the level of its bifurcation, from which the internal and the external carotid originate (Figure 2.f1). The blood flow was interrupted through the use of four knots, two located in the common carotid at different levels and one in each branch of the upper bifurcation. The protocol used in this project to induce permanent and temporary MCA occlusion is currently in use, and it was previously described by Gibson and Murphy 2004 (Gibson and Murphy 2004).

Once the blood flow was interrupted, and a small hole was produced on the artery's wall, a 6-0 monofilament nylon suture, coated with clear silicon was inserted and advanced up the ICA to the level of the Middle Cerebral Artery. This model produces major neurodegeneration and cellular damage in the ipsilateral hemisphere, although minor effects are visible also in the contralateral.

Different variations of the model based on the occlusion time were investigated in this project. For the permanent_MCAo, pMCAo, the filament was permanently left in place, while for the temporary_MCAo, tMCAo, it was alternately left for either one hour (1h_MCAo) or thirty minutes (30'_MCAo). The temporary occlusion of the MCA is associated with reperfusion that occurs with the blood flux restoration. The reperfusion is responsible for oxidative stress and a mechanical increase of the blood pressure; both factors are responsible to increase cellular damage and neuronal degeneration.

Some negative control animals were included, that underwent “sham” surgery. The sham animals were produced in two different ways; for the pMCAo, the sham received only the carotid dissection and its exposure. In the tMCAo model, after the cerebral occlusion, the normal flow was not completely restored, because a small piece of filament was left in the main carotid. For this reason, in the sham animals produced in the experiments involving the tMCAo, the main carotid was exposed and a small piece of the filament was left in the main branch.

After the surgery the animals were placed on a heat pad and wet pellet was administrated in a petri-dish at least for one week after the ischemic event.

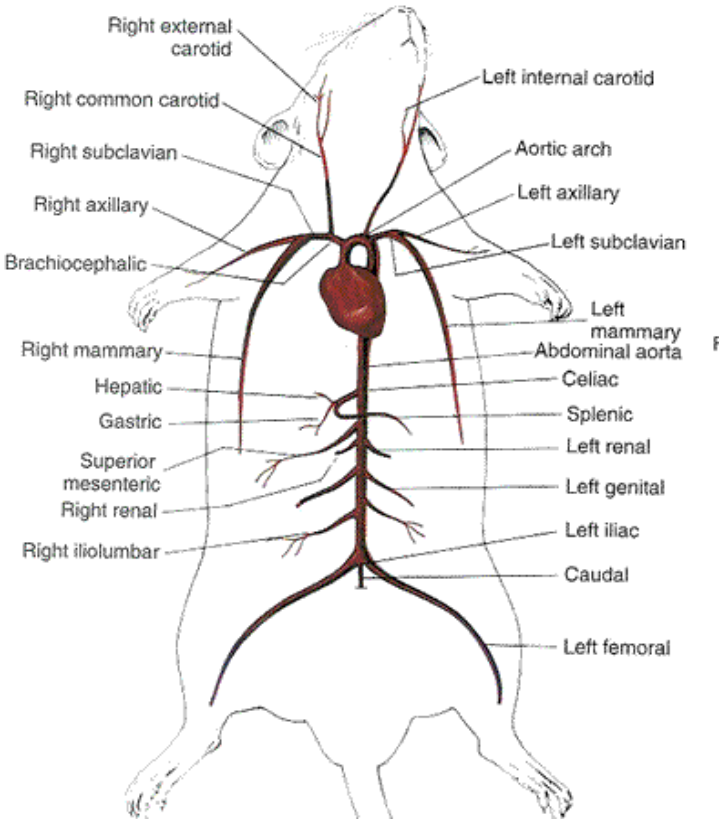

Figure 2.f1 Oxygenated blood circulatory system of a rodent.

The common carotid brings the oxygenated blood from the Aortic arch to the head. The bifurcation divides the common carotid in an external and an internal branch. The Middle Cerebral Artery is the extension of the internal carotid; this artery delivers oxygenated blood to the Circles of Willis. This key structure is responsible for the reduction in aortic blood pressure and flow sorting in the main vessels. The occlusion of the Middle Cerebral Artery interrupts the blood flux and is responsible for neuronal damage and death. The picture was on line downloaded at http://www.biologycorner.com/worksheets/rat_circulatory.html.

2.6.4 INTRACRANIAL INJECTIONS

MATERIALS:

Hypnorm, Vetapharma

Hypnovel, Roch

Animals were anesthetised using an intraperitoneal injection of a mixture of Hypnorm, Hypnovel and water (1:1:2). After a complete anaesthesia was induced, they were placed in a stereotactic frame having the head blocked by ear bars and a mouth bar. The skin was cut and the skull exposed and drilled, then the syringe electronically inserted through it. A micro pump was used to slowly introduce the fluids in the brain. For the SVZ modulation in absence of stroke, two bilateral injections, 5µl of LV, were performed at the beginning of the RMS. For the SVZ modulation in ischemic conditions 4 injections, 3 µl each of LV, per brain, were performed. The animals were returned to their cage and 3 weeks after they were killed by transcardial perfusion. The brains were processed as described below:

The bregma was used as a reference, and alternatively the beginning of the RMS or the SVZ was injected. For the RMS the coordinates used were previously described by Goncalves B. et al. (2008), AP 0.75, ML 1.2, DV -1.7 (Goncalves, Suetterlin et al. 2008). SVZ injections were designated according to our preliminary experiments (Figure 2.f2). From preliminary data, the majority of the damage was located around bregma AP ±1. Since the SVZ neurogenic islands are mostly concentrated in the front brain, as the literature suggested, and the strength of the SVZ response is closely dependent on the distance to the neurogenic islands and the damage severity, we decided to select the SVZ injection sites as the closer regions to the front ischemic damage produced by 1h_MCAo Figure 2.f2. The coordinates were the following: SVZ_1 (AP, 0.25; ML, ± 0.96, DV -2.75), and SVZ_2 (AP, 0.86; ML, ± 0.72, DV -3).

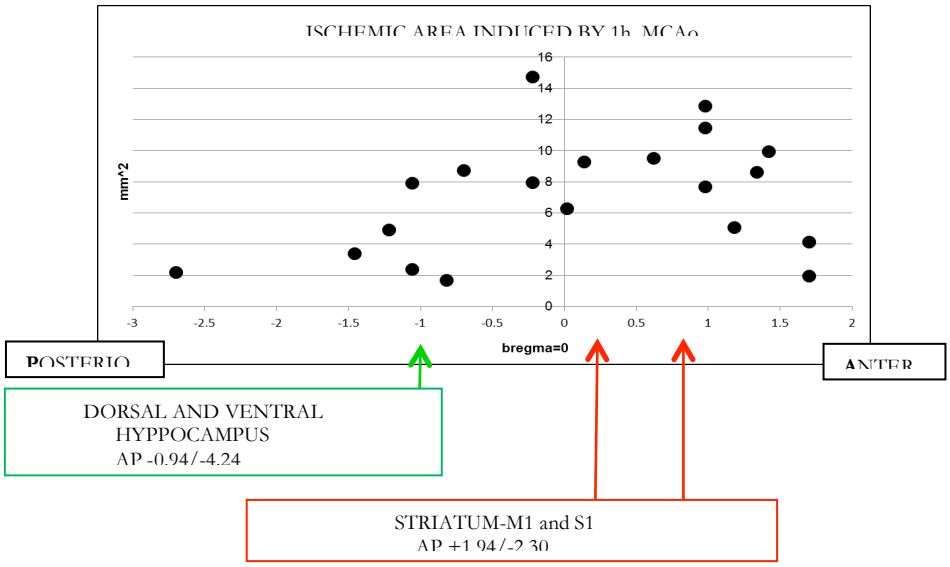

Figure 2.f2. Ischemic areas induced by for 1h_MCAo.

The picture shows the localization of the ischemic areas for 1h MCAo subjects. Each dot represents a single brain slice located at a specifically identified distance from bregma. In green the damage produce in the hippocampal formation between AP -0.94 and -4.24; in red the damage involved the front brain, AP 1.94 and -2.30 (sensorimotor cortex and striatum). The majority of the damage was located between bregma AP -1 and +1. n=7.

2.6.5 BEHAVIOURAL TESTS

MCAo animals were tested for their sensorimotor behaviour by the 0-28 focal deficit test (Clark, Gunion-Rinker et al. 1998). This test is based on observations of the sensory-motor behaviour developed post-surgery, and it is meant to detect damage in the somato-sensory (S1), motor cortex (M1, M2), and striatum. The use of a grid allows detecting defect in coordination, weakness, and motor deficit. This test comprises multiple tasks, for each of them a score from 0 to 4 was assigned (0=normal, 4=maximum defect). The final result is the sum of all the scores given for each task.

The tasks are described below:

1. Body Symmetry. To detect M1 and 2 damage. The animal is lifted through its tail and the asymmetry is observed between

forelimbs and hind-limbs. A score zero is assigned for a normal phenotype, one for a slight asymmetry, two for a moderate asymmetry, three for a prominent asymmetry and four for an extreme asymmetry.

2. Gait. To detect M1, M2 and striatal damage. The animal is left free to move and its gait is observed. A score zero is assigned for a normal gait, one if its gait looks stiff and/or inflexible, two if it limps, three if it shows trembling, drifting and/or falling and four if it doesn't walk at all.

3. Climbing. To detect M1, M2 and striatal damage. The animal is located on a centre of a grid, and after the grid is inclined 45° the motor behaviour is observed. A score of zero is assigned for normal climbing, one if it climbs with strain and limb weakness, two if it holds onto slope or it does not climb, three if the animal slides down slope and shows unsuccessful effort to prevent fall or four if it slides immediately and does not try to prevent fall.

4. Circling behaviour. To detect M1 and M2. Movement is observed when the animal is on its cage and left free to move on the bench. A score of zero is assigned when no circling behaviour is observed, one when the animal turns predominantly to one side, two when it is irregularly circling to one side, three when this circling is constant and four when it is pivoting, swaying or does not move at all.

5. Front limb asymmetry. To detect M1 and M2 damage. The front limbs are observed by lifting the animal's tail as well as allowing it to move freely on the bench. A score of zero is assigned for a normal symmetry, one when the asymmetry is slight, two when a marked asymmetry is present, three for a prominent asymmetry and four when it does not move any limb and/or the body.

6. Compulsory circling. To detect striatal damage, the animal is observed on its cage and ambulating on the bench. A score of zero is assigned when no compulsory circling is present, one when a tendency to turn to one side is observed, two when the animal makes

circles to one side, three if it pivots to one side sluggishly and four if it does not advance.

7. Whisker response. To detect S2 damage. The whiskers are lightly touched and the response on its face and limbs is observed. If the animal shows symmetrical response a score zero is assigned, one for a light asymmetry, two for a prominent asymmetry, three when the ipsi-lateral response is absent and contralateral response is diminished, and four when bilateral proprioceptive response is absent .

2.6.6 ASSESSMENT OF RECOVERY BY WEIGHT RESCUE

Surgery causes fluids to be lost as well as a release of stress hormones. Both factors affect animal body weight. Post-surgery weight recovery is a general indicator for the animal heath, and it is a well-accepted system to monitor post-surgery recovery (Modo, Stroemer et al. 2000; Ashioti, Beech et al. 2007).

2.6.7 TRANSCARDIAL PERFUSION

MATERIALS:

Paraformaldehyde, Sigma-Aldrich
PBS tablets, Sigma-Aldrich
Dolethal, Vetoquinol

Animals were killed by transcardial perfusion at different times after surgery. An appropriate dose of intraperitoneal injection of pentobarbital was used to induce deep anesthesia, whence the ribs were cut out and the heart exposed. Blood was drained from a laceration in the right atrium, and

a needle connected to the peristaltic pump was inserted on the left ventricle. The perfusion was performed by delivering an appropriate volume of PBS solution to avoid intravascular thrombi; to fix tissues, a second cycle of 4% PFA at 4 °C was transcardially administrated. Tissue fixation was evaluated by hand skin colour (turned white) and the muscle rigidity. The brain was dissected and stored in 4% PFA for no less than 4 days. .

2.7 HISTOLOGY

2.7.1 SECTIONING

Different systems were optimised for brain sectioning: cryo-sections for cryostat (12-20 μm), paraffin wax-embedded brains for microtome sections (6-12 μm) and unembedded, PFA-perfused brains for vibratome (50-100 μm).

CRYOSTAT

To process the brain with the cryostat, the tissues were quickly frozen in isopentane at -45°C and stored at -80°C. Half an hour before cutting, the brains were acclimatized in the cryostat at -20°C; the cryostat produced slices of thickness 16 μm. The sections were left to dry at room temperature and then stored at -80°C. Before any histological treatment was started brain slices were fixed in 4% PFA and then dried at room temperature.

MICROTOME

To process tissues with the microtome, perfused brains were embedded in paraffin by the St George's Histology facility. 12 μm sections were obtained with the microtome and left overnight at 37°C. Before any

treatment was performed sections were deparaffinized by Histochoice or Xylene.

VIBRATOME

To process tissues with the vibratome, perfused brains were fixed to the vibratome plate by super glue, and 50 µm sections were cut.

2.7.2 HISTOLOGICAL ANALYSIS

2.7.2.1 INFARCT VOLUME QUANTIFICATION

The infarct size for animals subjected to pMCAo and tMCAo and killed two weeks post-surgery, was estimated by Haematoxylin and Eosin staining. This technique is widely used for the assessment of the ischemic damage (Isayama, Pitts et al. 1991; Lin, He et al. 1993; Okuno, Nakase et al. 2001); differently from 2,3,5-triphenyltetrazolium chloride (TTC) staining that it is only applicable when the animal is killed within a week post MCAo, it allows damage detection also at later stages (Frankle 1976). Unfortunately the sensitivity of the system depends on the damage severity and the time between the ischemic event and the animal death. For long term experiments, such as one month or more post stroke, an Immunofluorescence to detect glia, microglia and neurons can be much more informative and sensitive (Chiamulera, Terron et al. 1993; Yoshikawa, Akiyoshi et al. 2008; Popp, Jaenisch et al. 2009). For these reasons the ischemic volume in long-term MCAo was estimated by Immunofluorescence. In this study inflammation, glial scar and neurodegeneration were first analysed singularly, and then the average between them was uses as best estimation of the ischemic environment (Figure 2.f2).

For each animal, five regions localized at +2.5, 1.7, 0, -1.7, and -3 mm distance to bregma were evaluated; consecutive sections were treated with anti-GFP and either anti-GFAP, anti-Iba1 or anti-Beta III. The Haematoxylin and eosin staining was also performed on adjacent sections. Sequentially cut sections were finally quantified for the ischemic environment, and the NPCs eGFP positive there localized (Figure 2.f2).

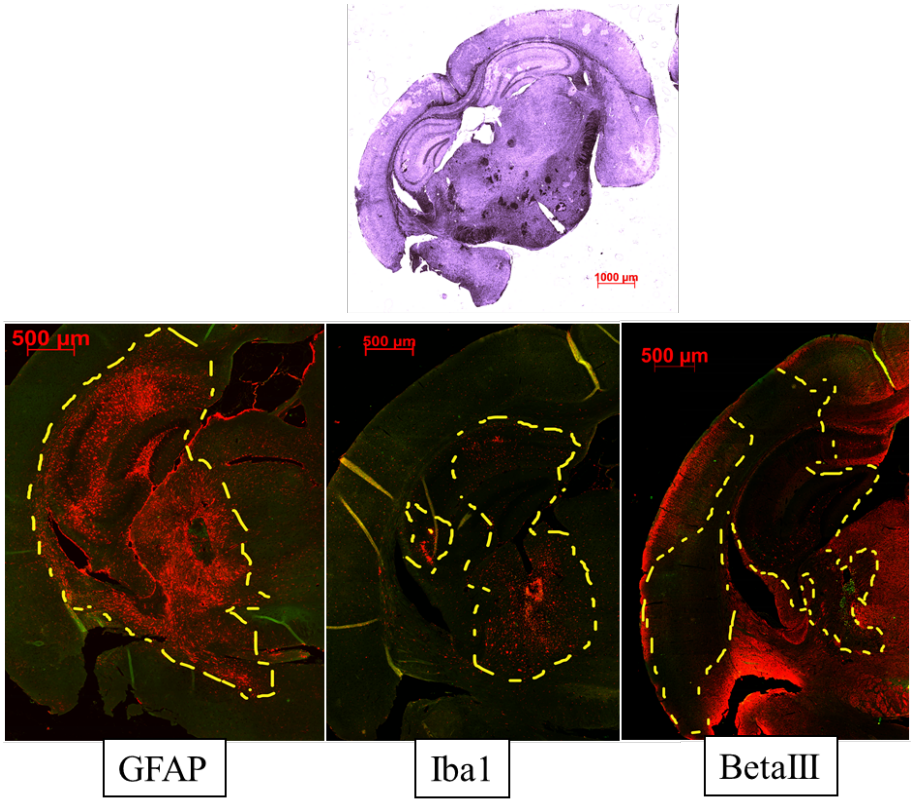

Figure 2.f2 Evaluation of the Ischemic regions by Immunofluorescence

Deparaffinized sections were treated with antibodies to detect Beta III tubulin (neurons), GFAP (astroglia) and Iba1 (microglia), for details see the Immunofluorescence paragraph. Each analysed area was evaluated by four consecutive sections, each of these treated with anti-GFP and an anti-cellular marker. The assessment of inflammation (Iba1 positive), glial scar (GFAP positive) and neurodegeneration (Beta III positive) areas were used to extrapolate the best ischemia estimation, or more simply the average between the areas. In the top image there is a section from the same animal treated with Haematoxylin and Eosin. All the section were localized at same level.

2.7.2.1.1 HAEMATOXYLIN AND EOSIN STAINING

MATERIALS:

Haematoxylin, Sigma-Aldrich
Eosin, Sigma-Aldrich
HCl, Sigma-Aldrich
Ethanol 99.9%, Fisher Scientifics
Histochoice, Sigma-Aldrich

To deparaffinise sections of tissue, slices were treated for 5 minutes at room temperature with Histochoice. The haematoxylin staining was incubated on the slides for 5 minutes at room temperature; the tissue was rinsed in water and treated with a differentiating solution (0.5%HCl and 70% Ethanol). After the differentiating solution reaction, the sections were rinsed in water and treated for 30 seconds with eosin at room temperature. Tissue re-hydration was achieved by bath with increased concentrations of Ethanol and finally the coverslips were mounted so that the sample could be observed in the microscope. The slices were evaluated with a Zeiss Observer D1 light microscope.

2.7.2.1.2 IMMUNOFLUORESCENCE

SOLUTIONS AND BUFFERS:

PERMEABILIZING SOLUTION:

PBS
Tween 20 0.5%

BLOCKING SOLUTION:

Permeabilizing solution
BSA 3%

ANTIBODY SOLUTION:

Permeabilizing solution
BSA 1%

MATERIALS:

BSA, Sigma-Aldrich
Tween 20, Sigma-Aldrich
PBS tablets, Sigma-Aldrich
Mouse GFP, Abcam
Rabbit GFP, Invitrogen
Rabbit DCX, Abcam
Rabbit GFAP, Dako
Rabbit beta III, Sigma-Aldrich
Rabbit Iba1, Wako
The details regarding the antibodies are described on Table 2.1.t2.

The immunofluorescence was performed on vibratome as well as microtome-cut sections. The tissues were permeabilized with the permeabilizing solution; 50 µm sections were incubated overnight at 4°C, while 12 µm sections were incubated for 30 minutes at room temperature. After permeabilization the sections were blocked for one hour with the blocking solution, and incubated with the primary antibody previously diluted in antibody solution; the reaction was carried out overnight at 4°C.

The day after, the slices were washed 3 times in permeabilizing solution, and then the secondary antibody was added to the sections and incubated for 1.5 hours at room temperature. After washing out the secondary antibody, the coverslips were mounted on the Superfrost Plus slides and slices observed under light microscope.
Vibratome sections were Immunofluorescence processed in a 12 well plate, then mounted on the glass slides with coverslips.

The concentrations used for the primary and the secondary antibody reactions are described in the following table (Table 2.1.t2).

Marker	*Protein*	*Company*	*Prod. #*	*Species*	*Conc.*	*secondary*	*Concentration*
neuron	Beta III	Sigma-Aldrich	T2200	Rabbit	1:500	Alexa Fluor, dokey-anti rabbit 555	1:700
glia	GFAP	Dako	Z 0334	Rabbit	1:500	Alexa Fluor, dokey-anti rabbit 555	1:1000
neuroblast	DCX	Abcam	Ab18723	Rabbit	1:500	Alexa Fluor, dokey-anti rabbit 555	1:500
microglia	Iba1	Wako	01919741	Rabbit	1:500	Alexa Fluor, dokey-anti rabbit 555	1:500
Transduced cells	GFP	Abcam	Ab1218	Mouse	1:500	Alexa Fluor, goat-anti mouse 488	1:700
Transduced cells	GFP	Abcam	Ab6556	Rabbit	1:500	Alexa Fluor, dokey-anti rabbit 555	1:700

Table 2.1.t2. Primary and secondary antibody concentration used in the Immunofluorescence experiment.

2.7.2.1.3 CELL COUNTING

To quantify SVZ neurogenesis occurring in physiological conditions, both the OBs were entirely sliced with the microtome and treated with an antibody against eGFP. The quantification reflects the actual number of eGFP positive cells that migrated to OBs within three weeks of injection.

Quantification in ischemic conditions was estimated by counting the eGFP positive cells located in the damaged area. Five regions per brain, situated at specific distance points from bregma were quantified: AP +2.5, 1.7, 0, -1.7, and -3 mm distance to bregma. To evaluate the ischemic environment and estimate the number of the migrated SVZ progenitor cells expressing eGFP, each of these regions were evaluated by immunofluorescence performed on four consecutive sections (10 μm each) located at the specified points distance to bregma (AP +2.5, 1.7, 0, -1.7, and -3 mm).

The number of green cells in the ischemic area was first assessed on the four consecutive sections (10 μm each) used to analyse the brain region in study (AP +2.5, 1.7, 0, -1.7, and -3 mm). The cell density was first estimated for each of these regions (40 μm) and in the whole ischemic damage.

The total number of green cells in the ischemic environment was then estimated by multiplying the density of the green cells in the whole damage for the total damage thickness (μm).

2.7.3 STATISTICAL TESTS

Batteries of statistical tests were used to analyse behaviour, histology and weight rescue. To evaluate the model two parameters were observed: the sensorimotor behaviour measured by the 0-28 focal deficit test, and the

variation of the body weight. Because the focal deficit assessment is a non-parametric test, it is not based on a Normal distribution, and so is evaluated by the Mann-Whitney rank sum test. The weight variation does follow the Normal distribution and is affected by time and treatment. It was evaluated by the two-way ANOVA; further analysis at selected time points were also evaluated by the Student's t test. All the cellular and infarct volume quantifications were analysed by the un-paired Student's t test and two-way ANOVA. Western Blot analysis and MTT were compared by the one-way ANOVA; when a comparison of multiple MOIs was involved a two-way ANOVA was used instead. The data correlation was performed by a linear regression when both the variables were distributed on a Normal curve; for non-parametric data the Spearman's rank Correlation Coefficient was calculated. The survival proportion was evaluated by the Gehan-Breslow-Wilcoxon test. This test was selected because compared with the log-rank (Mantel-Cox) test that gives same "weight to deaths" at all-time points, it assigns the score differently depending on when the death occurs and for this specific analysis is considered more sensitive.

PART 2

RESULTS

UNDERSTANDING THE IMPORTANCE OF NEUROGENESIS IN ISCHEMIC CONDITIONS

The aim of this project is to understand the effect of positive and negative modulation of the SVZ'NPCs naturally-occurring post-ischemia. Part 2 of the manuscript reports the results to assess the question, and it is divided in four main chapters:

1. Development of an efficient cell cycle inhibitor system.
2. Optimisation of conditions for the long-term study of the Middle Cerebral Artery occlusion model.
3. Evaluation of the efficiency of SVZ-RMS neurogenesis stimulation and inhibition in absence of stroke.
4. Evaluation of the effect of SVZ neurogenesis modulation in ischemic conditions.

CHAPTER 3

3.1 INHIBITION OF CELL CYCLE

SUMMARY

As discussed in Chapter 1, EGF1, EGF2 and IGF1 are widely used in research to improve the survival ability of neurons in culture. Moreover they are activated during embryogenesis, after stroke, and are also involved in cell fate determination and differentiation. The pathway shared by these mitogens involves an early binding with a Tyrosine Kinase receptor and the activation of a Map Kinase pathway producing the Cyclin D1 cytoplasmic accumulation. Last steps concern the Cdk4-CyclinD1 complex formation, nuclear imports, releases of E2F by the Rb suppressor, and activation of the S phase genes (Kornmann, Arber et al. 1998).

In this project the cell cycle arrest was achieved by direct inhibition of the Cyclin D1 activity. The goal was accomplished by a LV-based system in vitro validated on NIH3t3 fibroblasts. Two different strategies were attempted in order to obtain an efficient cell cycle inhibition: the first one was intended to block Cyclin D1 activity by cloning a dominant negative Cyclin D1 cDNA into a third generation Lentiviral backbone. The plasmid was packed into LV and was assessed in vitro. This approach was not successful and although much effort was invested to produce the clone and to test it in vitro, there was no convincing evidence of an in vitro cell cycle inhibition. The second approach we evaluated was based on a second generation LV encoding for a shRNA_CyclinD1. The two commercial transfer plasmids pGIPZs we tested were designed and cloned by Thermo Scientific: pGIPZs_shRNA_CyclinD1_92 (clone 92) and pGIPZs_shRNA_CyclinD1_95 (clone 95). Each clone encodes for a different hairpin sequence that binds different regions in the CyclinD1 mRNA. Both plasmids were used to produce LVs and they were evaluated in vitro by Cyclin D1 protein down regulation and cell viability assays. Although both hairpins were able to make the G1 phase shorter and to

induce cellular death, we decided to select clone 92 because vector packaging was highly efficient.

During these in vitro investigations we observed a diffuse death phenotype already occurring at 24 hours post transduction; according to the literature, Cyclin D1 is not just a cell cycle checkpoint factor but it is also involved in cellular fate and apoptosis (Han, Ng et al. 1999; Ino and Chiba 2001). From the data collected, we concluded the LV_ pGIPZs_shRNA_CyclinD1is a valid system to block cellular multiplication by either blocking of the G1 phase or apoptosis induction.

3.2 METHODS

3.2.1 CLONING A DOMINANT NEGATIVE CYCLIN D1 INTO A THIRD GENERATION LV

pRRLsc_Segfp_CdnCCND1W construct was made using the standard cloning procedure described in Chapter 2. The dnCyclin D1 gene sited into pFlex_dnCyclinD1 was kindly gifted by Dr. Diehl from Howard Hughes Institute, Memphis, and it was inserted into a double expression cassette backbone, pRRLsc_Segfp_CNCS1W created by Dr. Yip Ping from Kings College London.

The peculiarity of pRRLsc_Segfp_CNCS1W plasmid is the double gene expression cassette, where two genes are driven by two different promoters, CMV and SFFV. The first cassette is driven by the SFFV promoter leading the eGFP expression, while the second cassette contains the NCS1 gene under the CMV promoter. The pRRLsc_Segfp_CdnCCND1W transfer plasmid produced and used in this project was obtained replacing the NCS1 gene with the dnCyclinD1 sequence. The ability of the mutant to inhibit cell cycle in NIH3t3 cells

was previously demonstrated by Diehl and Sherr in 1997 (Diehl and Sherr 1997).

The cloning strategy was designed using Vector NTI software (Figure 3.f1); briefly the host backbone was linearized by *Spe*I digestion (*Spe*I, Promega), then a treatment with Polymerase Klenow was used to blunt the ends before a second digestion with *Xho*I was performed (*Xho*I, Promega). To obtain the excision of the dnCyclinD1 cDNA from the parental pFlex_dnCyclinD1, a first cut aimed to linearize the plasmid was obtained with *Bam*HI (*Bam*HiI, Promega), followed by a treatment with Polymerase Klenow and a second digestion with *Xho*I. Ligation was performed as previously described in Chapter 2; successful cloning was validated by diagnostic restriction digests and gel electrophoresis (Figure 3.f1).

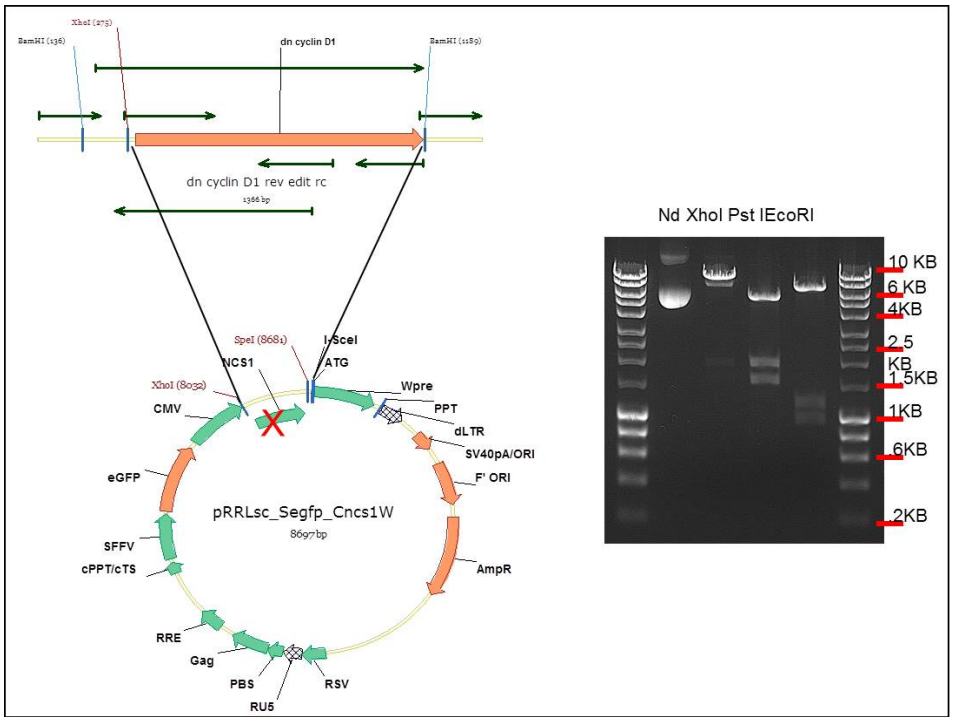

Figure 3.f1. pRRLsc_Segfp_CdnCND1W lenti backbone.

The map above was elaborated by Vector NTI software and shows the replacement of NCS1 gene with the dnCyclin D1 cDNA. On the right is the restriction analysis. Cloning was performed by the classical cloning technique; the lentibackbone was introduced into Top ten E.Coli cells by heat shock transformation and after DNA extraction the selected clone was digested with restriction enzymes. Expected bands: XhoI 8966 kb, PstI 6739 kb, 1178 kb, 962 kb, 87 kb, EcoRI 5494 kb, 1924 kb, 1551 kb.

3.2.2 SEQUENCING

The original dnCyclin D1 sequence contains two point mutations producing a Threonine conversion in an Alanine in position 156 and 286. The substitution in position 156 results in a lack of the ability to form an active complex with Cdk4, in turn responsible for the phosphorylation of the Rb protein, which heads E2F activation. Moreover, the position 286 is a proline-directed phosphorylation site that drives protein ubiquitination and degradation; the mutation at this site prevents protein phosphorylation, polyubiquitination and stabilizes dnCyclin D1 (Diehl et al 1997).

The pRRLsc_Segfp_CdnCyclinD1 expected sequence was confirmed by DNA sequencing techniques performed by Eurofins Mwg/ Operon. In

addition, an alignment between dnCyclinD1 and the WT orf isoform was made by BLAST in order to ensure the location of the mutation sites (Figure 3.f2).

The alignment confirmed the two mutations in position 156 and 286. Furthermore, two additional mutations had arisen; a point mutation in position 18 responsible for a substitution of a Serine with a Proline, and another one in position 160, which changes a Phenylalanine with a Leucine (Figure 3.f2).

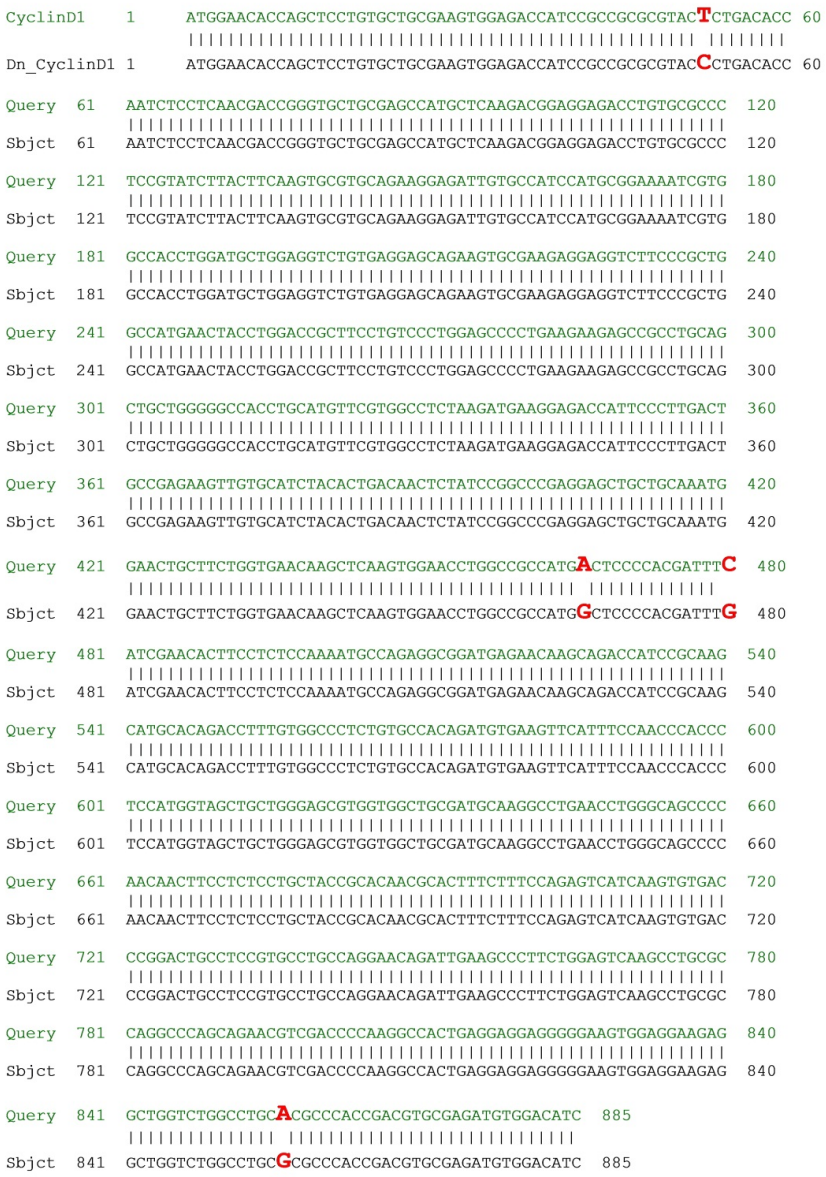

Figure 3.f2. Alignment between mouse dnCyclin D1 (in black) and the mouse wt Cyclin D1 (in green).

The alignment shows the two point mutations producing the expected Threonine conversion into Alanine (position 156 and 286 on amino acid chain). Two extra mutations were identified, causing Serine-18 to be substituted with a Proline, and Phenylalanine-160 was substituted with a Leucine.

3.3 LV_pRRLsc_Segfp_CdnCND1W IN VITRO ASSAYS

pRRLsc_Segfp_CdnCND1W was packed into LV and in vitro tested for protein expression and the effect on the cellular multiplication.

As control, we used a second-generation LV carrying and expression cassette for eGFP: LV_pHR'SIN-cPPT-SEW.

3.3.1 pRRLsc_Segfp_CdnCND1W: PROTEIN EXPRESSION ANALYSIS

Western Blot analysis was done with the assumption that the mutant's amino acid substitutions do not significantly affect the protein size, and that the immunoblotting reaction is not sensitive enough to discriminate between the endogenous and the exogenous isoforms. Under these conditions the translation of the exogenous dnCyclin D1 protein would be detectable as a general increase in the cytoplasmic amount of Cyclin D1.

LV_ dnCyclinD1, 1.62 x 10^8 IU/ml, or control LV_pHR'SIN-cPPT-SEW[9] 1.7 x 10^9 IU/ml, were used to transduce 2 x 10^5 NIH3t3 cells. The transduction conditions were set up in order to achieve MOI 3, 15 and 30. Although the blotting analysis revealed a general trend of increasing Cyclin D1 protein, especially for MOI 3, the two-way ANOVA did not highlight any significant difference between groups (Figure 3.f3).

The cells were harvested at day 8 post-transduction. Higher MOI and different harvesting days were also tested with similar results.

[9] LV_pHR'SIN-cPPT-SEW, Second generation Lentiviral used as control, it only expresses the eGFP gene.

a)

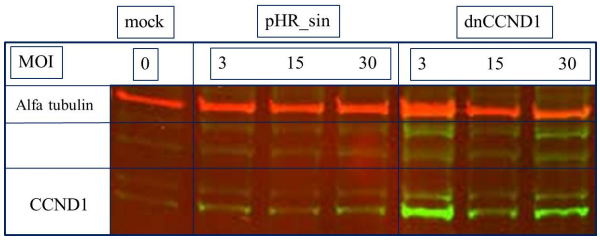

b)

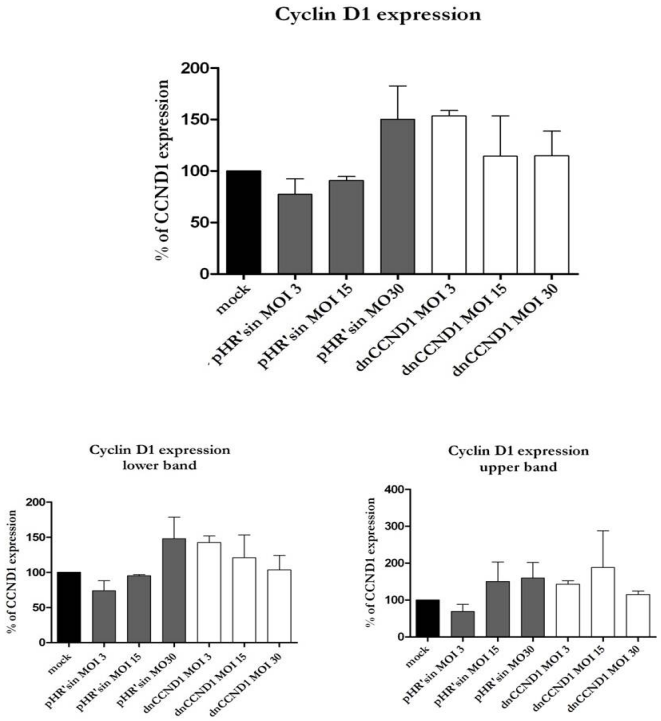

Figure 3.f3. Cyclin D1 protein variation after LV_dnCyclinD1 transduction.

NIH3t3 transduction by LV_dnCyclinD1 and LV_ pHR'SIN-cPPT-SEW. Cells were transduced at different MOI and harvested at day 8 post-transduction. (a) The two green bands in the Western Blot lower panel are both Cyclin D1 and they were quantified singularly (CCND1 lower band and CCND1 upper band) as well as together (CCND1), part b of the figure. The quantifications were obtained comparing the relative Cyclin D1 expression to the endogenous alpha-tubulin. (b) The samples were normalized with the mock. Values represent mean ± SEM (n=3). No statistical significance using two-way ANOVA was found.

3.3.2 LV_pRRLsc_Segfp_CdnCND1W: VIABILITY ASSAY BY MTT

The ability to induce a blockage of the cell cycle and/or apoptosis was evaluated by a viability assay. The test used is based on the colour variation of the yellow, water-soluble dye 3 – (4,5-dimethylthiazol-2-yl) 2,5-diphenyltetrazoliumbromide (MTT) into a blue-violet water insoluble formazan. This reaction is partially dependent on the succinate dehydrogenase, and it could be used as cellular respiration indicator as well as to detect live cells.

LV_dnCyclin D1 (6.6×10^7 IU/ml) and LV_ pHR'SIN-cPPT-SEW (5.10×10^8 IU/ml) were used to transduce 5,000 NIH3t3 cells in a 24 well plate. The MTT assay was performed at day 8 post-transduction.

The assay did not detect any significant change in proliferation in the LVs_dnCyclin D1 treated NIH3t3 cells, as shown by two-way ANOVA (Figure 3.f4).

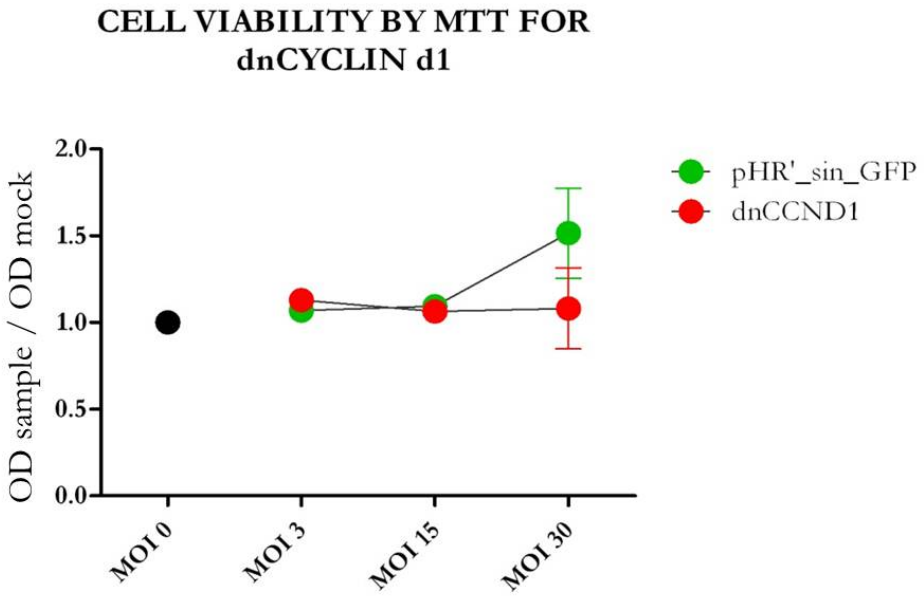

Figure 3.f4. MTT assay for LVs_dnCyclin D1.

The MTT assay was performed with three different MOI (3, 15 and 30) and the samples analysed at day 8 post-transduction. Transduced cells were treated with MTT for 3 hours at 37°C and crystal formations were left to dry overnight at room temperature. The absorbance was read at wavelength 560nm and the samples were normalized to the mock. Values represent mean ±SEM (*n*=3). There was no statistical difference in MTT conversion (live cell number) within the LVs treated groups, as shown by two-way ANOVA.

3.4 CELL CYCLE INHIBITION BY A shRNA_Cyclin D1

The second approach tested was a second-generation LV based system, encoding a small hairpin shRNA direct against Cyclin D1 mRNA. The two tested hairpins were commercially available from Thermo Scientifics (Figure 3.f5) and were packed into a second generation LV. For this experiment, the same control used for the pRRLsc_Segfp_CdnCND1W *in vitro* assays was used.

The hairpin sequences were elaborated by Thermo Scientific:

1. Clone pGIPZ_shRNA_640492,
   Mature sense (5'-3'): ATTGCATGTTCGTGGCCTCTAA
   Mature antisense (3'-5'): TTAGAGGCCACGAACATGCAAG
2. Clone pGIPZ_shRNA_640495,
   Mature sense (5'-3'): ATGCCACAGATGTGAAGTTCAT
   Mature antisense (3'-5'): ATGAACTTCACATCTGTGGCAC

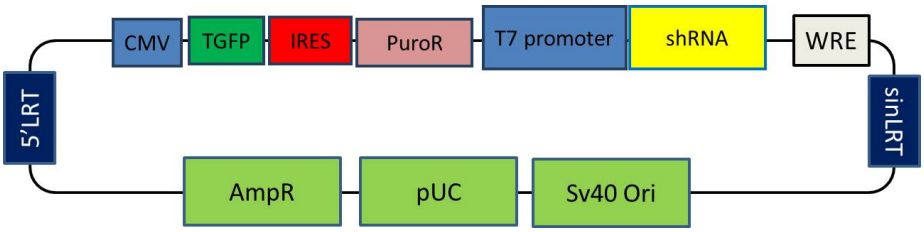

Figure 3.f5. Thermo scientific pGIPZ_shRNAs expression cassette map.

The CMV promoter led the turbo-GFP expression while the IRES is an Internal Ribosomal Entry Site for the Puromicin resistance translation. The shRNA is driven by the T7-promoter. The WRE or Woodchuck Hepatitis Virus Posttranscriptional is a regulatory element that enhances expression of the transgenes. The pUC is the bacterial origin of replication, for high copy replication and maintenance in E. coli while the AmpR transcription (Ampicillin resistance). The LRTs are the Long Terminal Repeats that are important to start the viral reverse-transcription. Ultimately the Sv40 Ori is the Simian vacuolating virus 40 origin of replication.

2.4.1 DOWN REGULATION OF CYCLIN D1 PROTEIN BY shRNA_CYCLIN D1

Cyclin D1 down regulation was evaluated by Western Blot at day 1 post-transduction in NIH3t3 cells; the method is described in Chapter 2. Briefly, NIH3t3 cells were transduced with LVs_shRNA_Cyclin_D1_92 (5×10^7 IU/ml) or LVs_shRNA_Cyclin D1_95 (9×10^7 IU/ml) or control LVs_ shRNA_empty (10^8 IU/ml). The day after the cells were scraped from the plate and the proteins extracted and separated by SDS-page gel electrophoresis. After protein transfer to a nitrocellulose membrane the immunoblotting was performed. The bands' relative intensity was estimated by Odyssey technology and analysed by one-way Anova.

The analysis was performed in four groups:

- LV_shRNA_Cyclin_D1_95
- LV _shRNA_Cyclin_D1_92
- LV_ pHR'SIN-cPPT-SEW
- mock.

After evaluating the best experimental conditions to achieve an efficient protein down regulation, MOI 75 was selected as the more effective.

At day 1 post-transduction, cells treated with both the hairpins directed against Cyclin D1 drastically reduced cell number and caused extensive damage (Figure 3.f6, part a).

The LV_shRNA_Cyclin_D1_95 treated group showed efficient Cyclin D1 protein down regulation, but it was difficult to pack the transfer plasmid into LV (Figure 3.f6). The impossibility of producing a large LV stock did not allow for repetition of the experiment for the purpose of statistical analysis.

Cyclin D1 protein down regulation by clone 92 was repeated in triplicate analysed by one-way ANOVA and the Bonferroni's post hoc test. Cyclin D1 protein was statistically significant lower in the samples treated with LV_shRNA_Cyclin_D1_92 compared to the group treated with LV_pHR'SIN-cPPT-SEW; **$p<0.01$ by one-way ANOVA (parts b) and c) of Figure 3.f6).

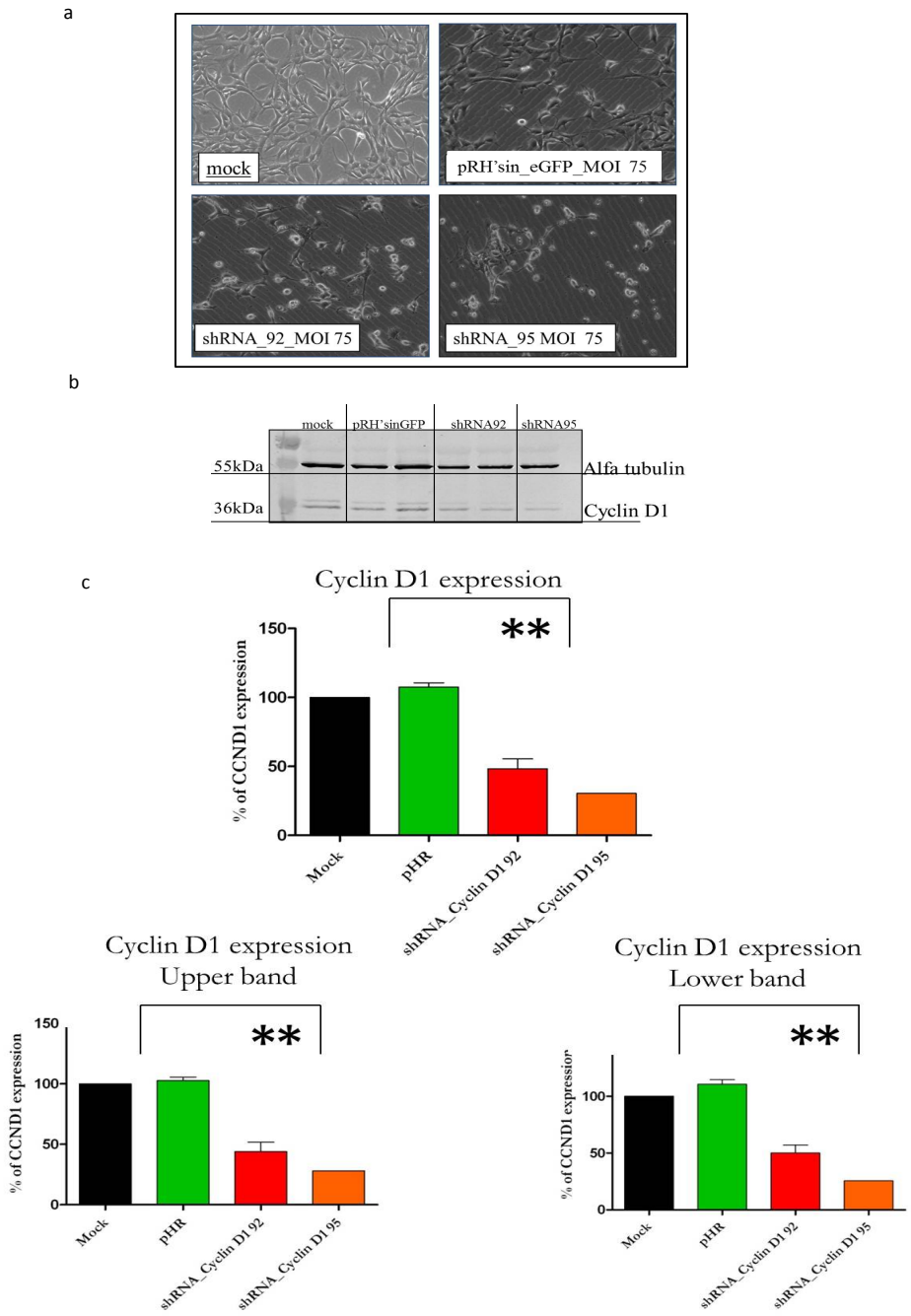

Figure 3.f6. Western Blot analysis for LVs_shRNA_Cyclin_D1_92 and 95.

a) Images show the NIH3t3 cells at day 1 post transduction, just prior to harvesting. b) Down regulation of Cyclin D1 induced by LV_shRNA_Cyclin D1 clone 92 (red) and 95 (orange) c) LV_shRNA_Cyclin_D1_92 induced a statistically significant Cyclin D1 protein down regulation when compared to the LV_ pHR'SIN-cPPT-SEW **$p<0.01$. Statistical analysis by one-way ANOVA, values represent mean ±SEM (n=3).

3.4.2 EFFECT OF CYCLIN D1 DOWN REGULATION ON THE CELL CYCLE: CELL VIABILITY BY MTT

NIH3t3 cells were transduced with LV_shRNA_Cyclin_D1_92 (5 x 10^7 IU/ml) or LV_shRNA_Cyclin_D1_95 (9 x 10^7 IU/ml) or LV_ shRNA_empty (10^8 IU/ml). After 24 hours the viability assay was performed by MTT, for details see Chapter 2. The experimental conditions were planned to achieve MOI 25, 70, 100 and 150, and the data were normalized with the mock, analysed by two-way ANOVA and the Bonferroni's post hoc test. Both tested hairpins reduced cell viability (reductase level) at MOI 70, whilst at MOI 150 the LV_shRNA_Cyclin_D1_92 reduced the reductase level to 60% of the level present in the control group, and the LV_shRNA_Cyclin_D1_95 at MOI 100 reduced it to 50% of the control group. Metabolically active cells were significantly reduced in the LV_shRNA_Cyclin_D1_92 treated group at MOI 70, *$p<0.05$, MOI 100, **$p<0.01$, and at MOI 150, ***$p<0.001$ (a) and b) Figure 3.f7). Metabolically active cells were reduced also for the LV_shRNA_Cyclin_D1_95 treated group, for which a significant reduction was observed at MOI 70 and 100, ***$p<0.001$ (c) and (d) of Figure 3.f7)

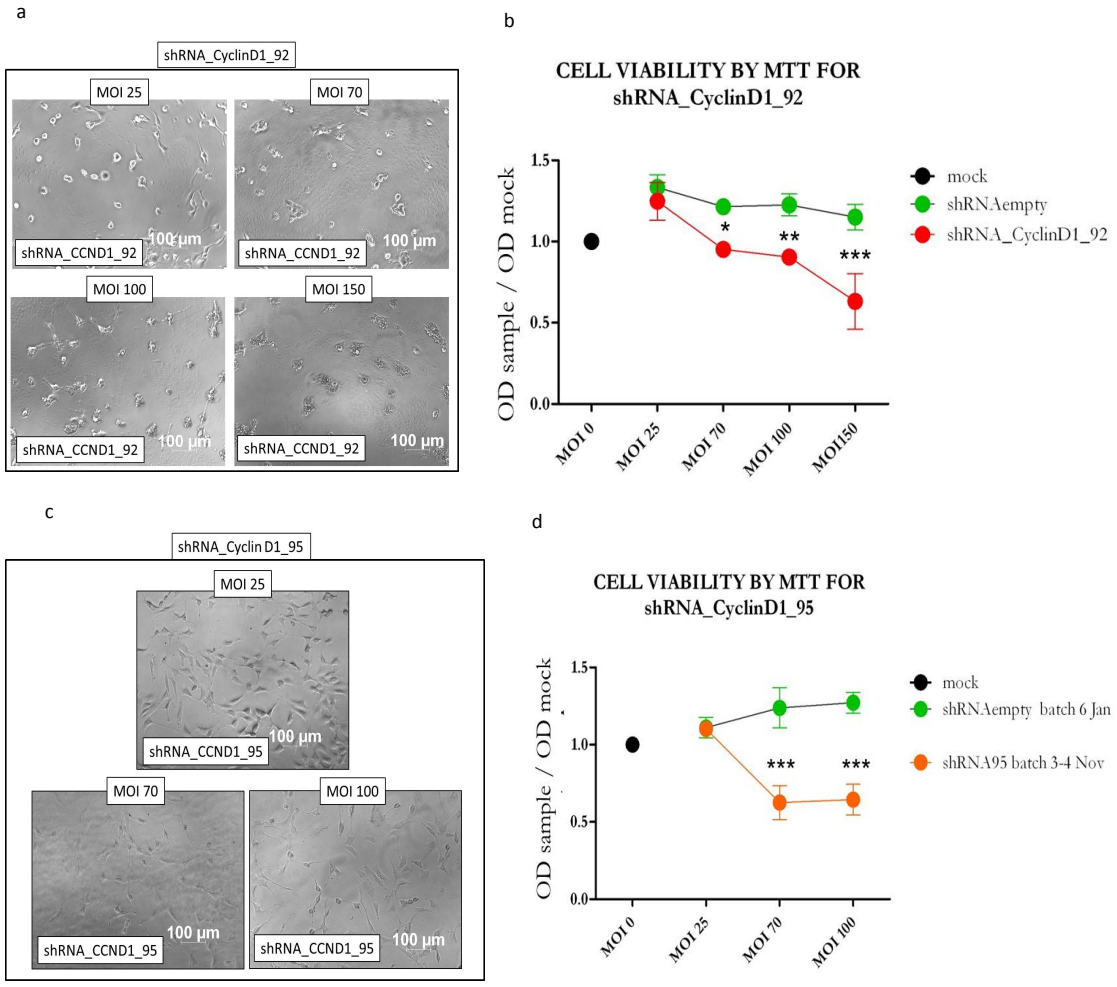

Figure 3.f7. Viability assay by MTT, shRNA_Cyclin_D1_92 and 95.

a), c) effect of shRNA_Cyclin D1 on NIH3t3 cells 24 hours post transduction b), d) both clones 92 and 95 showed reduced cell viability which was linearly dependent on the vector concentration (MOI), *$p<0.05$, **$p<0.01$ and ***$p<0.001$ for clone 92, and ***$p<0.001$ for clone 95 (MOI 70 and 100), both were compared to the LV_shRNA_Empty. Values represent mean ±SEM (n=3); the data were analysed with two-way ANOVA.

3.5 CONCLUSION

The inhibition of the cell cycle was attempted using two LV based systems. The first was meant to introduce a dominant negative isoform of the Cyclin D1 protein, in turn causing a reduction of the endogenous isoform activity and the G1 phase block. Although we found a trend of increasing Cyclin D1 protein (as results of the endogenous and exogenous protein detection by western blot), especially at MOI 3, we found no evidence for the dominant negative activity; possibly a result of the two extra mutations that the sequencing pointed out.

The second cell cycle inhibitor system was intended to induce a down-regulation of the Cyclin D1 mRNA, in turn responsible for a reduction of the protein translation and consequently G1 phase blocking. Both hairpins in the study produced the Cyclin D1 protein down-regulation with clear inhibitory effects on cell cycle and apoptosis. The analysis of protein and the cell viability accordingly suggest that the LV_shRNA_Cyclin D1 system is an efficient tool to block cell cycle in G1. It was repeatedly found that Clone 95 was difficult to pack into LVs, and for this reason shRNA_CyclinD1_92 was selected for the in vivo studies.

CHAPTER 4

4.1 MIDDLE CEREBRAL ARTERY OCCLUSION - A LONG TERM STUDY

SUMMARY

The use of animals in this study was conducted in agreement with the Animals Scientific Procedures Act 1986, and approved in detail by the local research ethics committee.

The MCAo is the ischemic model we selected to study the effect of neurogenesis modulation in post ischemic recovery.
We can divide this project into two main experiments:

1. To evaluate the effect of SVZ neurogenesis inhibiting in the post ischemic recovery
2. To evaluate the effect of SVZ neurogenesis enhancing in the post ischemic recovery

The experiments were planned in order to study the effect of the treatments across the 30 days following MCAo. The first milestone in achieving these goals was to develop and set up the stroke model.

Ischemic models are quite variable in terms of damage severity and survival expectations, and because in this study we planned to combine LV intracranial injections with MCAo, the first concern was to find the best conditions to have a reliable ischemic model which was robust enough to survive and exhibit recovery over 30 days post-ischemia.

The aim of this chapter is to demonstrate the efforts made to develop and analyse the MCAo models, so that the best conditions to apply experiment 1 and 2 as described above can be selected.

The MCAo model is a very invasive procedure that produces the obstruction of the Middle Cerebral Artery, in turn responsible for extended neuronal damage and cell death. The damage severity is closely dependent on the duration of the artery occlusion and on the subject's ability to respond to the specific treatment. For the successful experiment, there needs to be a good number of ischemic animals which are able to survive for long term study; a necessity for a rigorous statistical evaluation of the model. Three different variants of the ischemic model were studied: pMCAo, 1 hours MCAo (1h_MCAo) and 30 minutes MCAo (30'_MCAo).

A high proportion of the deaths as well as the majority of the recovery took place during the first ten days after the artery occlusion. The recovery curve for tMCAo models covered the first ten days post-surgery, after which the majority of the animals acquired an almost normal phenotype. The permanent occlusion produced the enduring blood flow interruption which was minimally stabilized over time, and the risk of death was high across all periods in this case.

4.1.1 ANIMALS

C57 Bl/6, male, six to ten week-old were used for the MCAo animals. This strain was selected above the others because of its sensitivity to MCAo, which is due to the reduced development of Willis' Circle (Yang, Kitagawa et al. 1997).

Post-surgery, the animals were injected daily with glucose-saline until they showed ability to feed themselves autonomously. In accordance with the UK standard animal cage conditions, a stimulating environment was introduced through the use of white tubes in the cage. The animals were killed by a transcardial perfusion two weeks after surgery; method described in Chapter 2.

4.1.2 MODEL EVALUATION

The MCAo animals were evaluated daily for two weeks after the operation using the 0-28 focal deficit test described in Chapter 2. After death, the ischemic volume was estimated using Haematoxylin and Eosin staining described in Chapter 2. To assess the effectiveness of the surgery the ischemic animals were compared to the sham. In addition, the difference between the effects of the occlusion time was evaluated to highlight the most suitable model for long term study.

4.1.2.1 ANIMALS LOST AND EXCLUDED FROM THE ANALYSIS

Thirty-two animals were permanently occluded in the MCA but only four survived for two weeks post-surgery. In this group, three brains where lost during the cryo-processing. The tMCAo allowed a better survival; ten 1h_MCAo animals were produced and eight survived, for 30'_MCAo, six animals were produced and all of them survived. We assumed all the animals died because of the ischemia.

4.1.2.2 0-28 FOCAL DEFICIT TEST

MCAo induced neurological damage responsible for a post-surgery sensory-motor impoverishment. The ischemic outcome is very strong during the first 36 hours, where the majority of deaths were also concentrated. An improvement was observed across the first ten days, after which the phenotype looked very similar to the sham subjects.

All groups presented a strong deficit in the sensorimotor phenotype significantly different from the correspondent sham operated animals, as shown by the Mann-Whitney rank sum test which gave ****$p<0.0001$ (Figure 4.f1).

The neurological recovery for the tMCAo models was evaluated by the analysis of the mean's rank Mann-Whitney, and there was no statistical difference between the groups (Figure 4.f2).

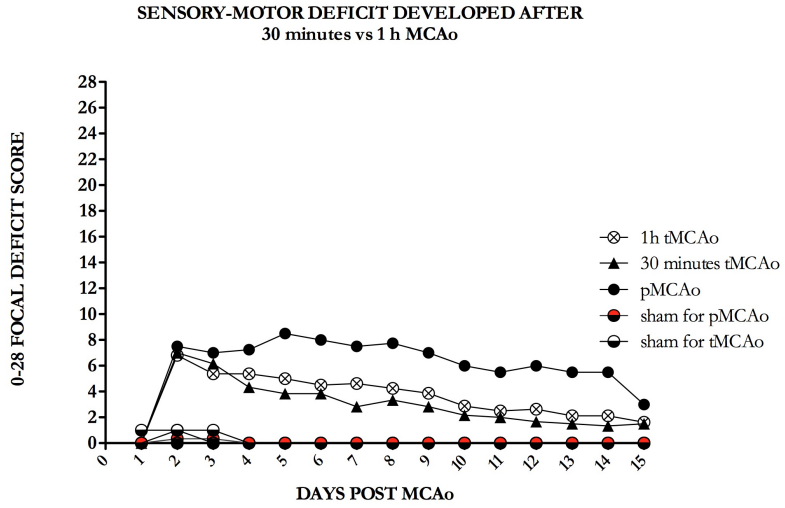

Figure 4.f1. 0-28 focal deficit test: MCAo groups vs. sham operated animals

The neurological improvement was monitored daily by the 0-28 focal deficit test. The test is a battery of sensory-motor tasks, for which, based on the severity of damage, a score between 0-4 is assigned. The final score is the sum of the scored from each single task. The MCAo behaviour (pMCAo, 1h_MCAo or 30'_MCAo) was evaluated in comparison with the sham categories by the mean rank analysis Mann-Whitney, with each data point corresponding to the mean rank for the group at the specific day after surgery. Each group was individually compared to the correspondent sham, and all of them showed a significant post-surgery sensory-motor impoverishment, ****$p<0.0001$, analysis of mean's rank Mann-Whitney. pMCAo n =4, 1h_MCAo n =8, 30'_MCAo n=6.

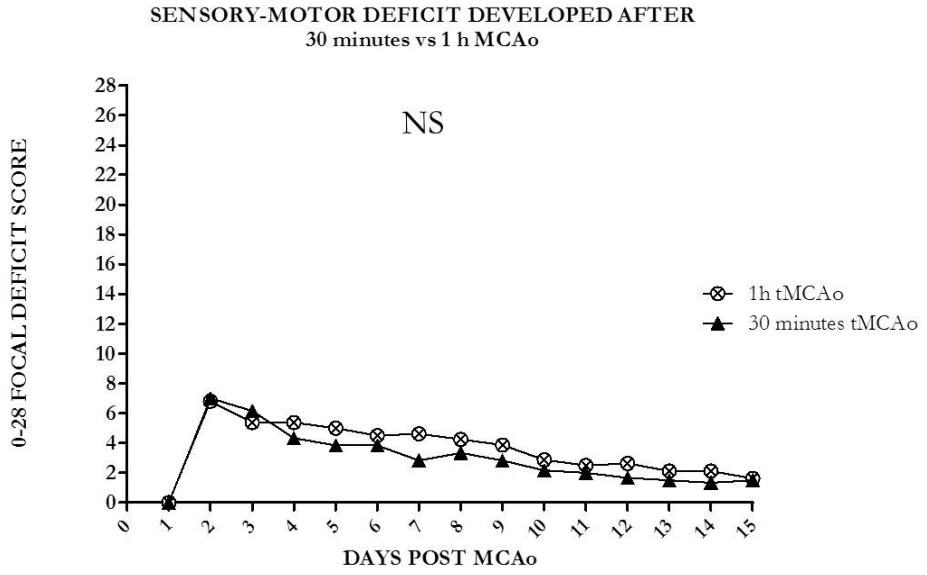

Figure 4.f2. 0-28 focal deficit test in the survived population. 1h_MCAo vs 30'_MCAo

Neurological improvement post tMCAo. The Mann-Whitney rank sum test did not highlight any significant difference in the sensorimotor impoverishment and post-surgery recovery produced by 1 hour and 30 minutes of MCA occlusion. 1h_MCAo *n* =8, 30'_MCAo *n*=6, sham n=3.

4.1.2.3 WEIGHT RESCUE

A significant body weight variation was observed in all groups after the surgery, ****$p<0.0001$, analysis by the two-way ANOVA. Except for the 30'_MCAo, no difference between groups was observed. The Bonferroni's post hoc test revealed significant difference between the sham and the 30'_MCAo at day 2, ***$p<0.001$, day 3, ****$p<0.0001$, day 4, ****$p<0.0001$, day 5, ***$p<0.001$ and day 6, *$p<0.05$ (Figure 4.f3).

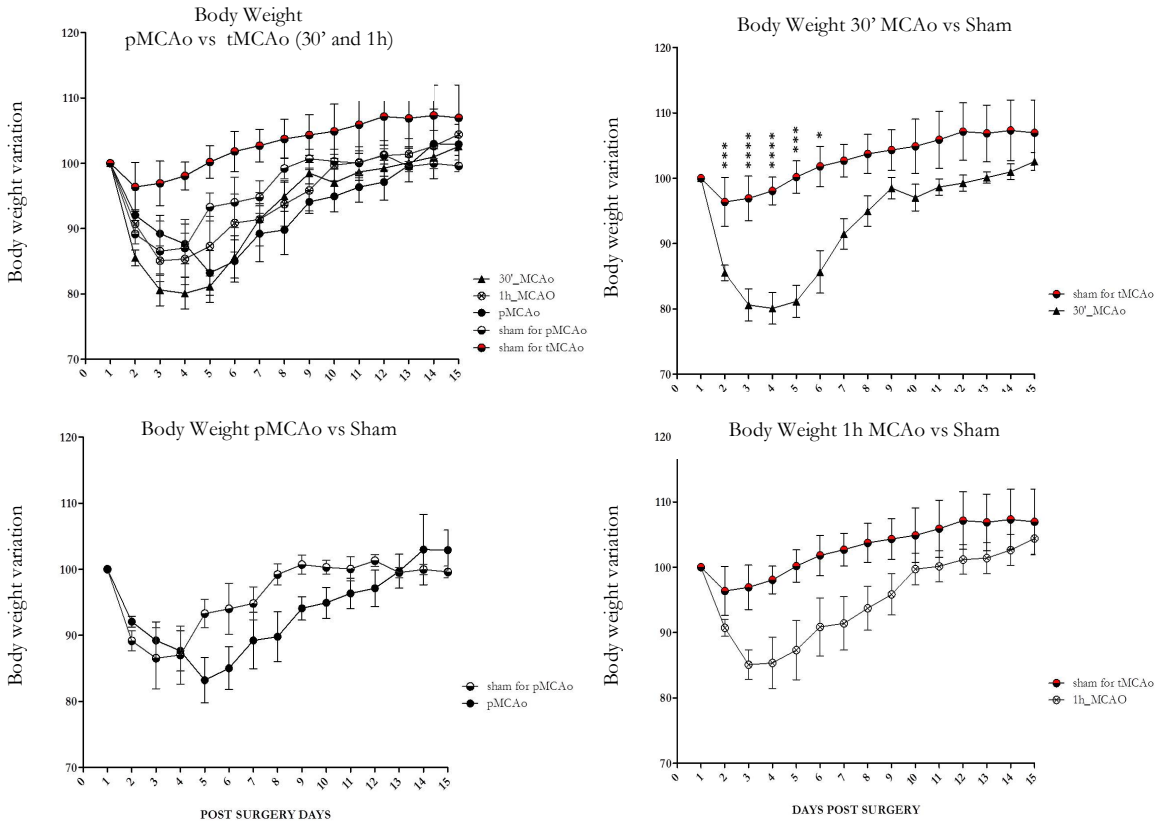

Figure 4.f3. Body weight variation

The body weight was expressed as percentage of the pre-operative weight. The data were analysed by two-way ANOVA, where the value represents mean ± SEM. Although the surgery affected the weight variation in all groups analysed, ****p<0.000, there was no difference between groups. Only 30'_MCAo group was significant different from the control, *p<0.05 by the two-way ANOVA. The Bonferroni's post-hoc test revealed significant difference at day 2, ***p<0.001, day 3, ****p<0.0001, day 4, ****p<0.0001, day 5, ***p<0.001 and day 6, *p<0.05. pMCAo *n* =4, 1h_MCAo *n* =8, 30'_MCAo *n*=6, sham for pMCAo n=3, sham for tMCAo n=3.

4.1.2.4 SURVIVAL PROPORTION

After MCAo the number of survivors was drastically reduced. This was closely dependent on the occlusion time, which in turn was responsible for the severity of the damage. According to the survival curve in Figure 4.f4, the occlusion time negatively affected the number of survivors. After the permanent occlusion, only 4/32 of animals survived for two weeks post-surgery, 1 hour occlusion showed 6/10 survivors for the same period of time, while 30'_MCAo had a 6/6 survival rate for two weeks. According to the survival curve the first week is considered a time where the risk of death for both 1h_MCAo and pMCAo is high. There was significantly different survival proportion between the pMCAo and 30'_MCAo, ***$p<0.001$, and between pMCAo and 1h_MCAo, **$p<0.01$; moreover, the survival fraction was significant different between the pMCAo and the sham operated animals, ***$p<0.001$. The 1h_MCAo group was not statistically different from the 30'_MCAo or the sham, analysis by the Gehan-Breslow-Wilcoxon Test (Figure 4.f4).

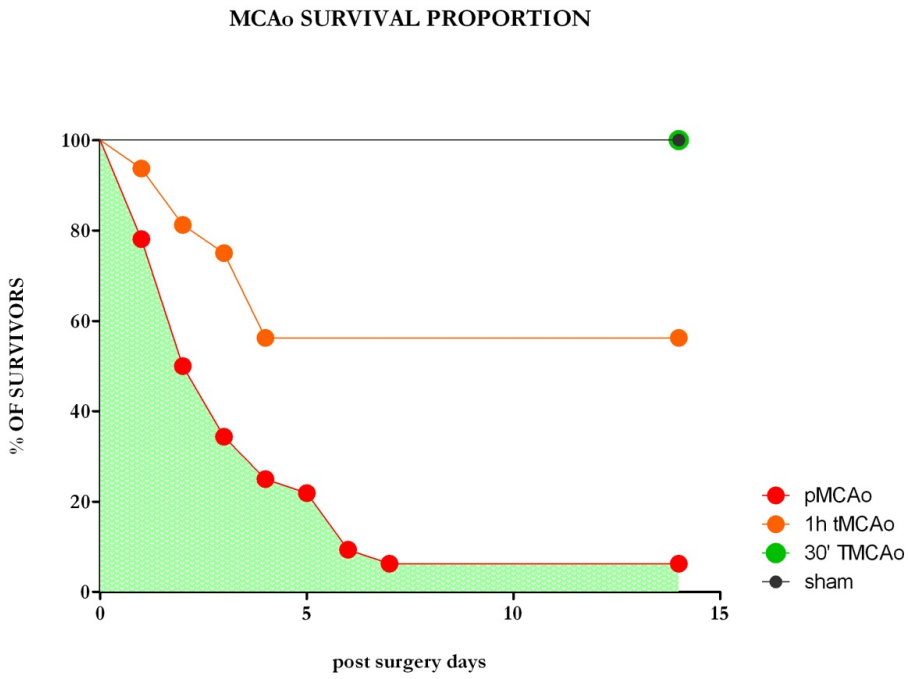

Figure 4.f4. Survival curve.

Percentages of survivors post MCAo. pMCAo showed significant different survival proportion comparing to 1h_MCAo, **p<0.01, to 30'_MCAo, ***p<0.001 and the sham group, ***p<0.001, analysis by the Gehan-Breslow-Wilcoxon Test. pMCAo n=32, 1h_MCAo n=10, 30'_MCAo n=6, sham n=6.

4.1.3 INFARCT VOLUME QUANTIFICATION AND DATA CORRELATION

MCAo brains were histologically analysed to estimate the ischemic volume. The histology of the model depends on the occlusion time and the duration of the recovery. Increasing severity of damage was observed in an occlusion time-dependent manner, with. the histology of permanent MCAo being characterized by a large oedema that extends throughout almost the whole ipsilateral hemisphere (Figure 4.f5).

The temporary occlusion was much more variable, with damage in the somatosensory cortex, motor cortex, striatum and hippocampus, and is often characterized by a variation in the topographic organization of the neural network (Figure 4.f6). Moreover, vacuolation (taken as evidence of oedema) was not evident, but extended regions with "accumulation of nuclei" visible with the Haematoxylin and Eosin staining (part b) and c) of Figure 4.f6) could be observed.

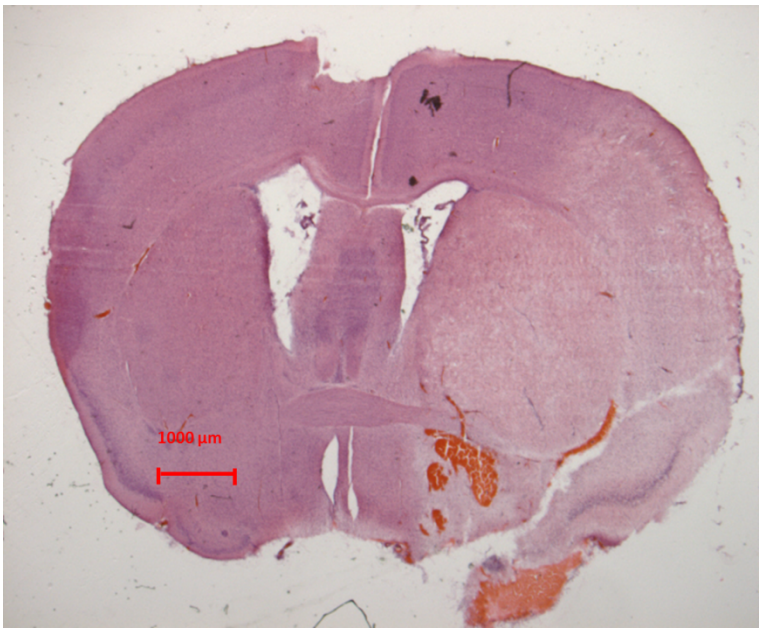

Figure 4.f5. Ischemic pMCAo brain.

Ischemic pMCAo brain two weeks after the occlusion of the Middle Cerebral Artery. Haematoxylin and Eosin staining in cryo-section. The oedema was extended to the ipsilateral hemisphere; at the right bottom of the picture the haemorrhagic blood caused by the microcanula insertion.

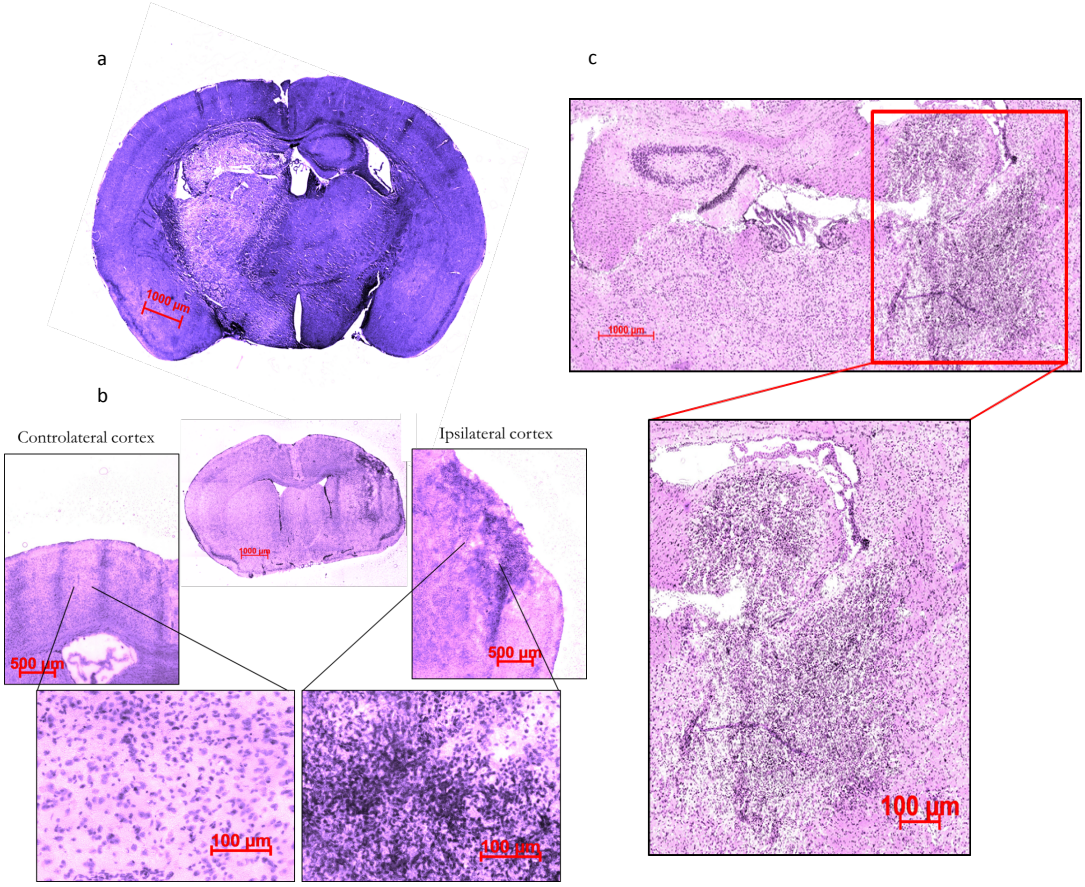

Figure 4.f6. tMCAo brain.

a) Haematoxylin and Eosin staining in microtome cut-sections. 1h_MCAo brain two weeks after ischemia b) Detail of the sensory cortex and comparison between hemispheres. C) Hyppocampal region in MCAo brain; highlighted the ipsilateral region.

4.1.3.1 ISCHEMIC VOLUME QUANTIFICATION

The ischemic volume was estimated (see Materials and Methods) and statistical significance evaluated by one-way ANOVA. For the permanent occlusion group three brains were damaged during the cryo cuttings at the Cryostat and were not used for the volume quantification.

The brain processing for the temporarily occluded groups was performed with a different technique as it was found that the MCAo tissues were not easily cut by cryostat; for this reason we decided to embed the brains in paraffin and to cut them using a Microtome instead.

The average for the ischemic volume in the 30'_MCAo group (n=6) was 12.3 mm^3 with Std Err=4.5, but, possibly because of the limits of the technique used, two subjects did not have a clear ischemic damage and 0 mm^3 was assigned. The damage in 1h_MCAo (n=7) was much more clear and extended, with an average of 21.4 mm^3. The ischemic volume for the pMCAo brain was 57.2 mm^3 (Figure 4.f7), and although the variability in size and location of the ischemic regions was high, the 1h_MCAo's ischemic volume was significantly higher than the sham operated animals, $^{**}p<0.01$, one-way ANOVA. There was no statistical difference between 30'_MCAo's ischemic volume and the sham operated animals (Figure 4.f7).

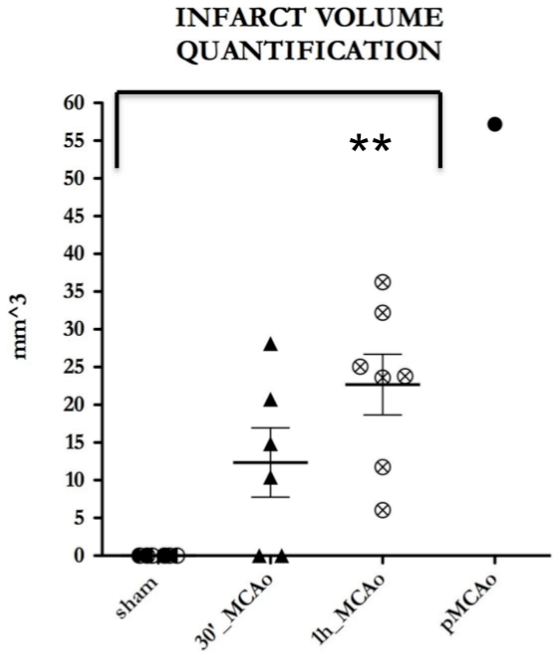

Figure 4.f7. Infarct volume quantification.

The infarct volume quantification was estimated performing Haematoxylin and Eosin staining on five different brain regions, as described in Chapter 2; the ischemic areas were observed and quantified using a Zeiss Observer D1 light microscope. Significantly higher ischemic volume for 1h_MCAo, **p<0.01; values represent mean ± SEM, by one-way ANOVA.

4.1.4 SPEARMAN'S RANK CORRELATION COEFFICIENT

The ischemic damage is responsible for the specific neurological phenotype raised after surgery. Although there is a clear assumption about this correlation, its effectiveness depends on the data acquisition and a proper analysis. To evaluate the effectiveness of the systems a Spearman's rank Correlation Coefficient test was performed.

The Spearman's rank correlation coefficient is a non-parametric test to assess the extent to which the relationship between two variables can be described by a monotonic function; is the rank of the two variables correlated by a well-defined relationship?

The direction and the strength of the correlation is described by the ρ (rho) coefficient; for $\rho = 0$ there is no correlation, $\rho = 1$ max positive correlation and $\rho = -1$ maximum negative correlation, or in other words for $\rho = \pm 1$ the variables' relationships is perfectly described by a monotonic function.

Specifically, the histological data were correlated with the score assigned to the behavioural phenotype the day the animals were killed. The Spearman's rank Correlation Coefficient test demonstrated a significant correlation between the behaviour at day 14 and the ischemic volume, $*p<0.05$, $\rho = 0.46$ (Figure 4.f8).

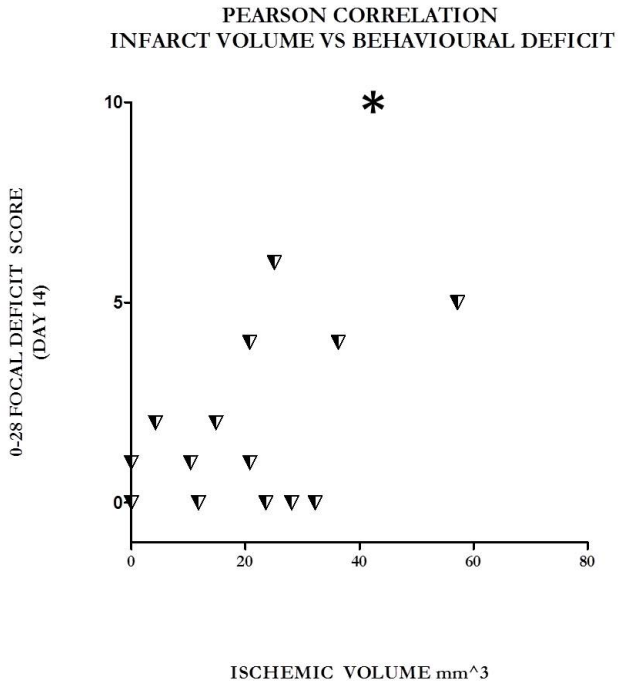

Figure 4.f8. Positive correlation between the behavioural score at day 14 and the ischemic volume quantification

Data were analysed by the Spearman's rank Correlation Coefficient; each triangle corresponds to an animal for which the ischemic volume was correlated to the behavioural score assigned at day 14. There was a significant positive correlation between the data, *$p<0.005$, $\rho = 0.46$.

4.1.5 CONCLUSION

The MCAo models were produced and evaluated based on the behavioural phenotype and the ischemic volume quantification. pMCAo and 1h_MCAo demonstrated strong ischemic phenotypes which were behaviourally and histologically assessed. The 30'_MCAo animals demonstrated a clear ischemic phenotype which was statistically different from the sham, and presented a smaller ischemic volume, sometimes not very different from the sham operated brains.

The analysis of the body weight showed a significant post-operative variation in all groups, although difference between groups was demonstrated significant only for 30'_MCAo compared to the sham.

There were only 4/32 of pMCAo survivors at day 14 post-surgery; this was significantly different comparing to the tMCAo and sham groups, $**p<0.01$ and $***p<0001$ by the Gehan-Breslow-Wilcoxon Test. Because of this small fraction of survivors, we decided the pMCAo model was not adequate for further experiments. The 1h_MCAo and 30'_MCAo groups showed good survival ability and ischemic phenotype, although the second one was much milder.

The reduced lesion volume in the 30'_MCAo group was not statistically different from the sham, and for this reason was not selected for the project's next step. The 1h_MCAo group demonstrated reasonable survival ability and good ischemic phenotype, clearly visible at behavioural and histological level.

The effectiveness of the model analysis, by behavioural and histology tests was validated by the Spearman's rank correlation coefficient, $*p<0.005$, $\rho=0.46$.

CHAPTER 5

5.1 SVZ-RMS NEUROGENESIS MODULATION IN NON-ISCHEMIC CONDITIONS

SUMMARY

Neurogenesis naturally occurs in physiological conditions. The SGZ in the hippocampal formation replaces the granular cells of the dentate gyrus (DG) over its entire lifetime. Similarly the SVZ on the wall of the lateral ventricles controls the replacement of the glomerular and periglomerular cells of the OBs (Bovetti, Gribaudo et al.). The tangential migration toward the OBs occurs in a well-known pathway by the RMS (Lennington, Yang et al. 2003).

As previously discussed, this project is aimed at understanding the importance of neurogenesis occurring in ischemic conditions, using LV-based systems. The efficiency of the LV_shRNA_Cyclin D1 to inhibit the cell cycle *in vitro*, was already demonstrated and discussed in chapter 3.

The systems we selected to boost SVZ neurogenesis were based on integration-deficient lentiviral vectors expressing GDNF or TTC from the CMV promoter. IDLV_GDNF and IDLV_TTC were produced using transfer plasmids produced by Dr. Sherif Ahmed, having already had their in vitro effectiveness proven.

1) pRRLcC_TTC_IRESeW
2) pRRLcC_pGDNF_IRESeW

The peculiarities of these two lentiviral backbones are: i) the expression cassette containing a CMV promoter that drives a precursor GDNF or a TTC, ii) an internal ribosome entries site (IRES) and iii) a sequence encoding for an eGFP. The IRES is a ribosome binding sequence, which

allows translation initiation in the middle of a messenger RNA. The translation of the eGFP is under control of the IRES activity.

Unfortunately, once the plasmids were packaged into LVs, the IRES functionality was fairly low and for this reason we decided for the *in vivo* study to co-inject the IDLV_GDNF and IDLV_TTC with a separate LV carrying an eGFP cassette under the SFFV promoter (LV_ pHR'SIN-cPPT-SEW).

In Chapter 3 I already discussed and demonstrated that LV_shRNA_CyclinD1_92 can inhibit cell cycle *in vitro* in NIH3T3 cells. For *in vivo* experiments, the LV_shRNA_CyclinD1_92 was used in combination with LV_ pHR'SIN-cPPT-SEW to inhibit SVZ progenitor multiplication, and for long-term cellular detection (14 days). As a control another pGIPZ plasmid carrying an empty hairpin (LV_shRNA_Empty) was packed into LV, and used in conjunction with the LV_ pHR'SIN-cPPT-SEW.

GDNF and TTC were packed into IDLVs. These vectors, as discussed in Chapter 1, do not integrate the viral DNA in the host genome; rather in a mitotic cell population such as the NPCs of the SVZ, the episomal vector is expected to be diluted as the cells divide. As the IDLV cassette is lost toward the migration, it is assumed that the effect of GDNF or TTC is circumscribed within the SVZ area. Because the eGFP cassette is also located in the LV_ pHR'SIN-cPPT-SEW, which has the ability to integrate the provirus in the host genome, the detection of the SVZ progenitors by eGFP expression is ensured over a long time period.

This chapter reports the evaluation of the neurogenesis modulation in physiological conditions, based on the injections of the IDLV_ pRRLcC_pGDNF_IRESeW, IDLV_ pRRLcC_TTC_IRESeW,

LV_shRNA_CyclinD1_92 or LV_shRNA_Empty at the beginning of the RMS, in combination with LV_ pHR'SIN-cPPT-SEW for cell marking.

5.2 METHODS

C57 Bl/6, male, six-ten week old were injected at the beginning of the RMS as previously described by Goncalves B. et al. (2008), AP 0.75, ML ±1.2, DV -1.7. A total of 10 µl of LVs was injected at day zero, 5 µl of vector for each hemisphere (LVs were administrated in un-supplemented DMEM). Details of the vector batches used in this experiment are shown in Table 5.t1.

After the injections the animals were housed in their own cage with normal diet and housing conditions. Three weeks later they were killed by transcardial perfusion. The tissues were embedded in paraffin by the St George's Histology facility, and immunofluorescence was performed to detect and quantify eGFP-positive cells into the OBs; methods described in Chapter 2.

SAMPLE	shRNA_Empty	TTC	GDNF	shRNA_CyclinD1
SVZ MODULATOR SYSTEM	(no modulation) LV_shRNA_Empty Produced: 29/4/2011	(-) IDLV_TTC Produced: 5/3/2011	(-) IDLV_GDNF Produced: 5/3/2011	(+) LV_shRNA_CyclinD1_92 Produced: 5/5/2011
qPCR titre	3.78×10^{8} IU/ml	3.05×10^{9} IU/ml	3.35×10^{9} IU/ml	2.1×10^{8} IU/ml
Flow Cytometer titre	1.4×10^{8} IU/ml	no	no	2.3×10^{8} IU/ml
µl injected	6.6	6.6	6.6	6.6
LV_pHR'SIN-cPPT-SEW	YES Produced 13/3/2011	YES Produced 13/3/2011	YES Produced 13/3/2011	YES Produced 13/3/2011
Flow cytometer titre	2.3×10^{8} IU/ml	2.3×10^{8} IU/ml	2.3×10^{8} IU/ml	2.3×10^{8} IU/ml
µl Injected	3.3	3.3	3.3	3.3

Table 5.t1. SVZ neurogenesis modulators based on LVs and IDLVs.

The table illustrates the batches used for the *in vivo* experiment with the related titre. IDLV_GDNF and IDLV_TTC due to the lack of the ability of the IRES sequence to start the eGFP translation, and the consequential reduction of the gene expression were not titrated by flow cytometer.

5.3 HOMOLOGY BETWEEN RAT AND MOUSE GDNF

The pRRLcC_pGDNF_IRESeW plasmid used to produce IDLV_GDNF encodes a precursor gene from rat. Because our experiments were performed in mice, we checked the similarity between mouse and rat sequences by a Blast alignment.

Figure 5.f1 presents the results for the Blast alignment between the protein sequences: rat GDNF and mouse GDNF. The chain is composed of 199 amino acids and the identity between the two proteins is 99% (197/199) with no gaps.

```
mouse 9   VCLVLLHTASAFPLPAGKRLLEAPAEDHSLGHRRVPFALTSDSNMPEDYPDQFDDVMDFI  68
          VCLVLLHTASAFPLPAGKRLLEAPAEDHSLGHRRVPFALTSDSNMPEDYPDQFDDVMDFI
Rat  1    VCLVLLHTASAFPLPAGKRLLEAPAEDHSLGHRRVPFALTSDSNMPEDYPDQFDDVMDFI  60

mouse 69  QATIKRLKRSPDKQAAALPRRERNRQAAAASPENSRGKGRRGQRGKNRGCVLTAIHLNVT  128
          QATIKRLKRSPDKQAAALPRRERNRQAAAASPENSRGKGRRGQRGKNRGCVLTAIHLNVT
Rat  61   QATIKRLKRSPDKQAAALPRRERNRQAAAASPENSRGKGRRGQRGKNRGCVLTAIHLNVT  120

mouse 129 DLGLGYETKEELIFRYCSGSCESAETMYDKILKNLSRSRRLTSDKVGQACCRPVAFDDDL  188
           DLGLGYETKEELIFRYCSGSCE+AETMYDKILKNLSRSRRLTSDKVGQACCRPVAFDDDL
Rat  121  DLGLGYETKEELIFRYCSGSCEAAETMYDKILKNLSRSRRLTSDKVGQACCRPVAFDDDL  180

mouse 189 SFLDDNLVYHILRKHSAKR  207
           SFLDD+LVYHILRKHSAKR
Rat  181   SFLDDSLVYHILRKHSAKR  199
```

5.f1 Blast alignment between mouse GDNF [mus muscolus, GenBank: AAB52953.1] and rat GDNF [Rattus norvegicus, GenBank: AAM18096.1]

Length=199

Score = 407 bits (1046), Expect = $7e^{-119}$, Method: Compositional matrix adjust.
Identities = 197/199 (99%), Positives = 199/199 (100%), Gaps = 0/199 (0%)

5.4 IDLV_GDNF and IDLV_TTC

The neurogenesis boosting was achieved with a IDLV based system rather than the integrative conformation, LV. The integration deficient conformation circumscribed the effect of the boosting to the SVZ, as result of the cellular proliferation. Moreover because the IDVL_ neurotrophic

factor was co-injected with the LV_ pHR'SIN-cPPT-SEW, that carried the eGFP cassette, the long-term detection of the NPCs was also possible after the migration in the ischemic regions.

5.5 HISTOLOGY AND CELL COUNTING

Three weeks after the injections the animals were killed and immunofluorescence labelling was performed to assess effectiveness of the injections and to evaluate the efficiency of the SVZ modulator systems, based on LVs.

LV_ pHR'SIN-cPPT-SEW in conjunction with the pGIPZs plasmids carrying the shRNAs (Figures 5.f1, 5.f2, 5.f3 and 5.f7), or the LV_pRRLcC_pGDNF_IRESeW (Figures 5.f4 and 5.f5), or the LV_pRRLcC_TTC_IRESeW (Figure 5.f6), was an efficient tool to detect SVZ neurogenesis occurring in physiological conditions, to monitor migration toward the RMS, and to assess the integration of the neo-born neurons into the OBs neuronal network (Figure 5.f7).

Three weeks post injection the LV_shRNA_CyclinD1_92 treated group had significantly reduced eGFP positive cells in the OBs, relative either to the control group (LV_srRNA_Empty), GDNF and TTC groups (Figure 5.f2 and Figure 5.f3). Student's t-test ***$p<0.001$ (Figure 5.f8).

Under the same conditions, IDLV_GDNF treated group increased the number of eGFP positive cells that migrated to the OB, relative to the control group (Figure 5.f4 and Figure 5.f5). Student's t test, *$p<0.05$, (Figure 5.f8).

The IDLV_TTC treated group did not exhibit any difference in the number of eGFP positive cells migrated to the OBs when compared to the other groups (Figure 5.f6 and Figure 5.f8).

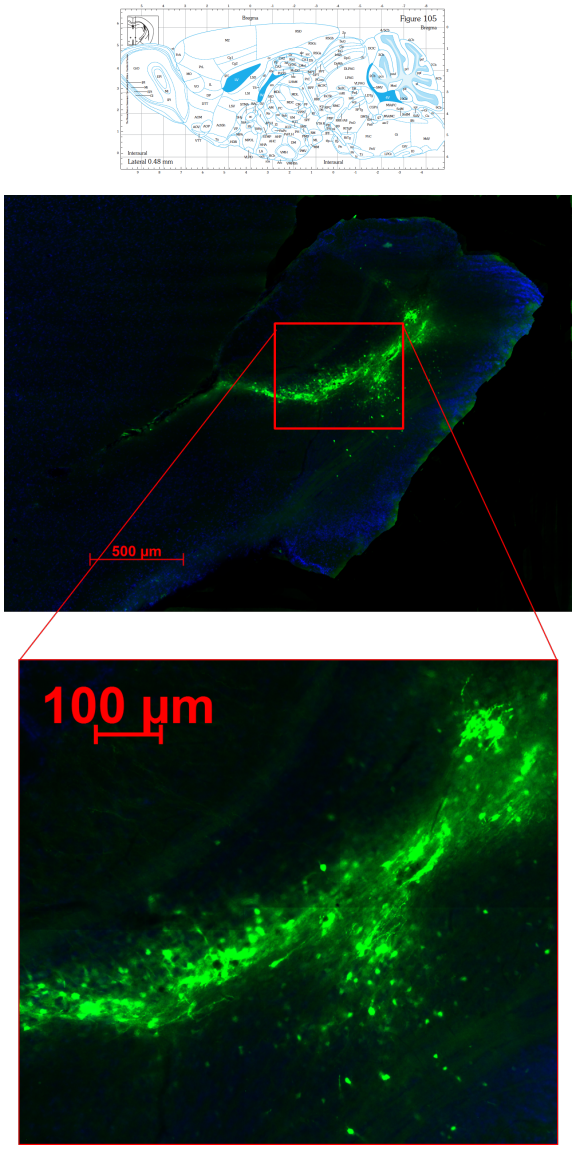

Figure 5.f1. Migrated eGFP positive cells in the OB: LV_shRNA_Empty group.

This animal was injected at the beginning of the RMS with LV_shRNA_Empty and LV_ pHR'SIN-cPPT-SEW; the histological analysis was performed three weeks later. Anti-mouse eGFP by Abcam (green), nuclear chromatin was visualised with DAPI (blue).

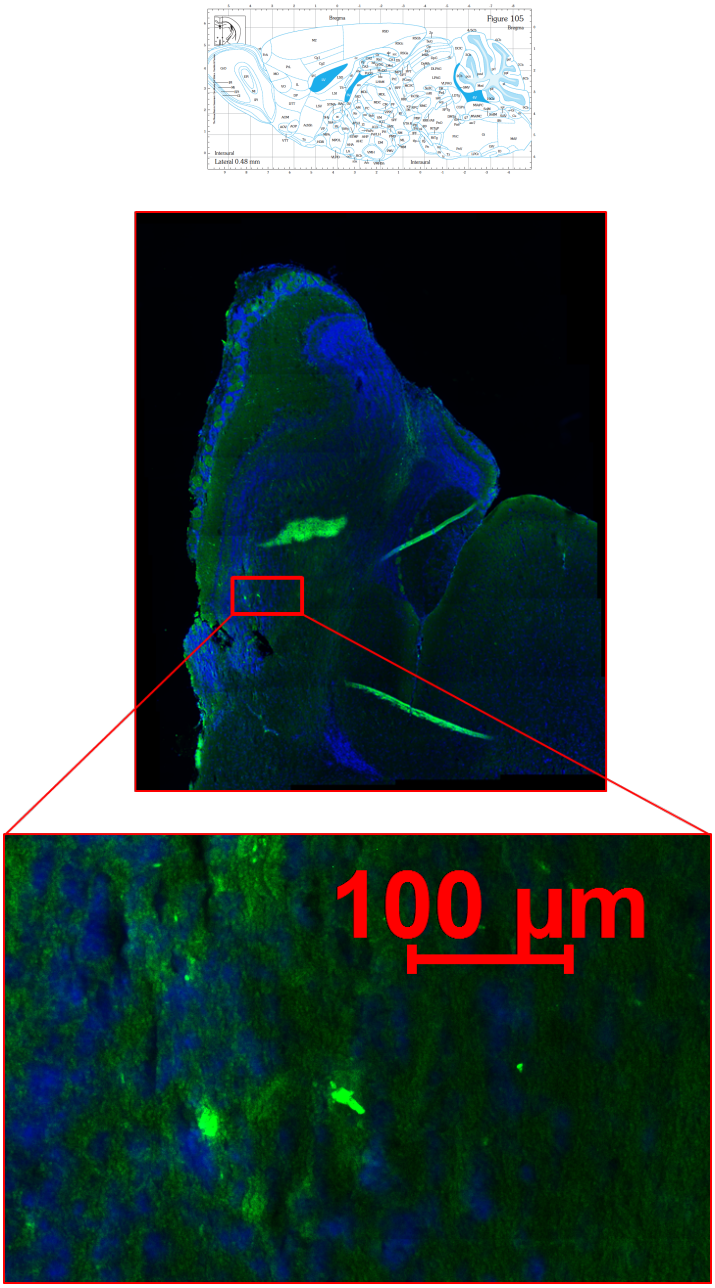

Figure 5.f2. SVZ-RMS neurogenesis inhibition by LV_shRNA_CyclinD1

Sagittal section of a mouse OBs injected as previous described with LV_shRNA_CCND1 and pHR'SIN-cPPT-SEW. Anti-mouse eGFP by Abcam (green), nuclear chromatin was visualised with DAPI (blue).

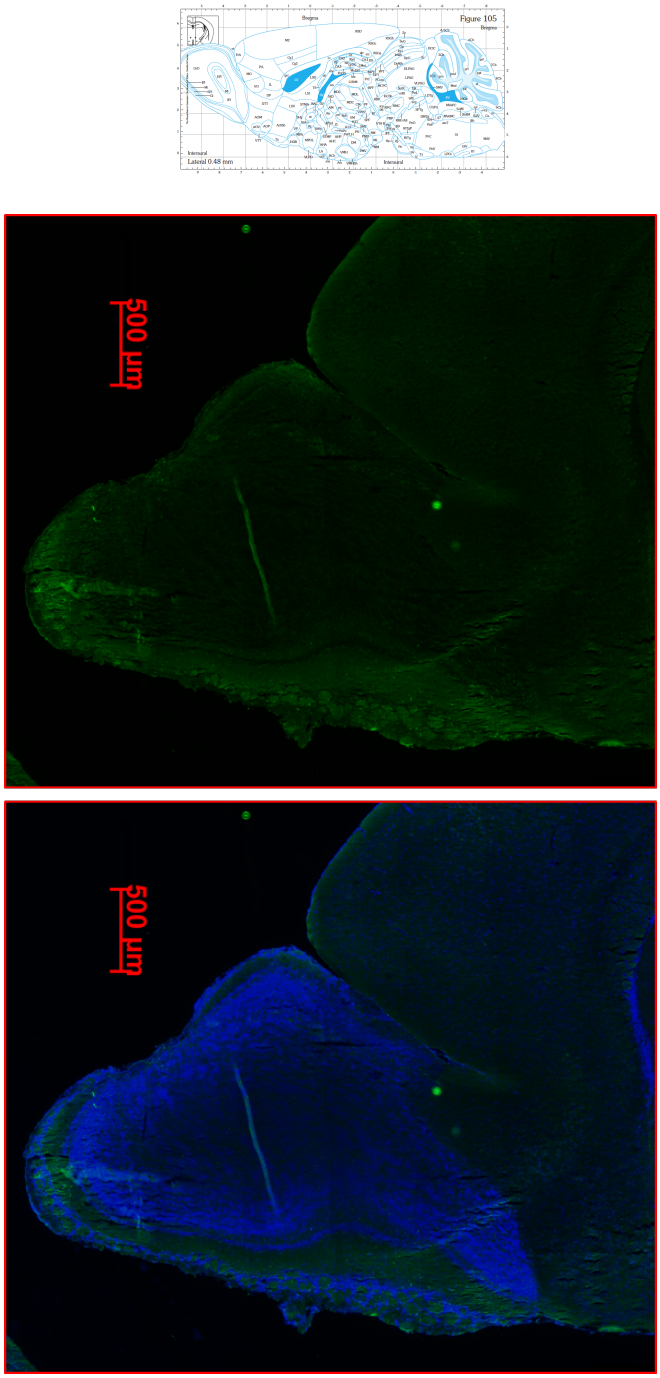

Figure 5.f3. SVZ-RMS neurogenesis inhibition by LV_shRNA_CyclinD1

Sagittal section of a mouse OBs injected with LV_shRNA_CCND1 and pHR'SIN-cPPT-SEW. Anti-mouse eGFP by Abcam (green), nuclear chromatin was visualised with DAPI (blue).

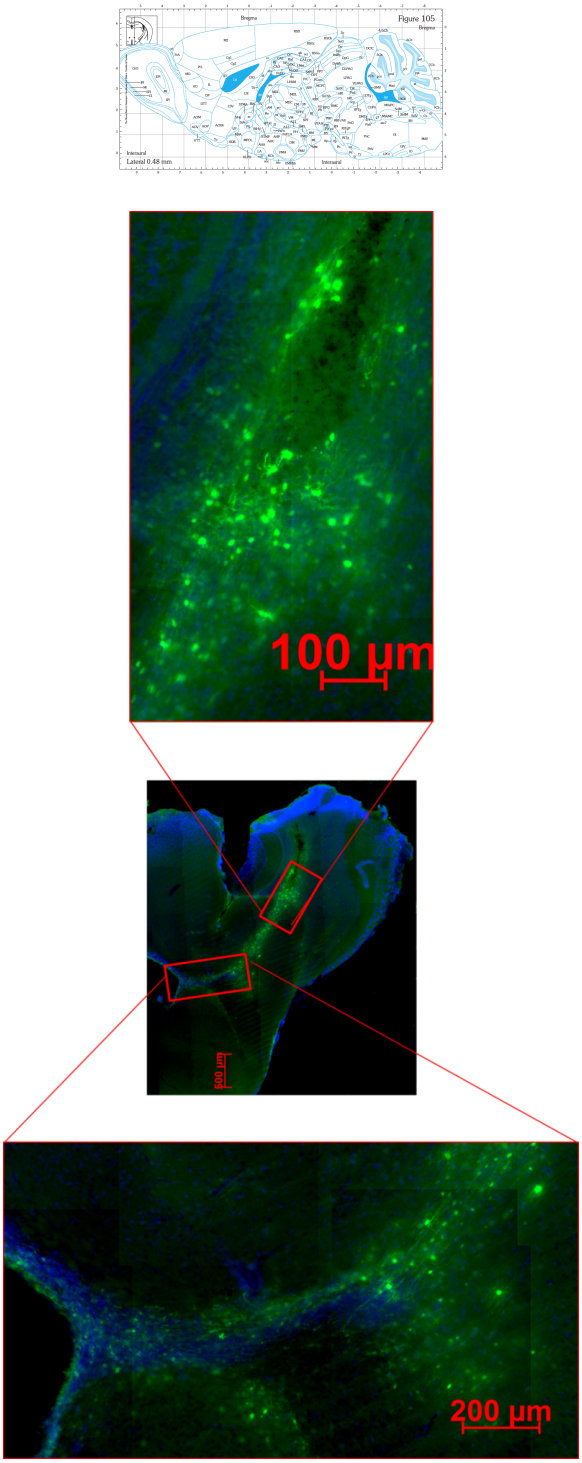

Figure 5.f4. SVZ-RMS neurogenesis enhancement by IDLV_GDNF

Animal injected with IDLVs_pRRL_GDNF and pHR'SIN-cPPT-SEW as before reported. Anti-mouse eGFP by Abcam (green), nuclear chromatin was visualised with DAPI (blue).

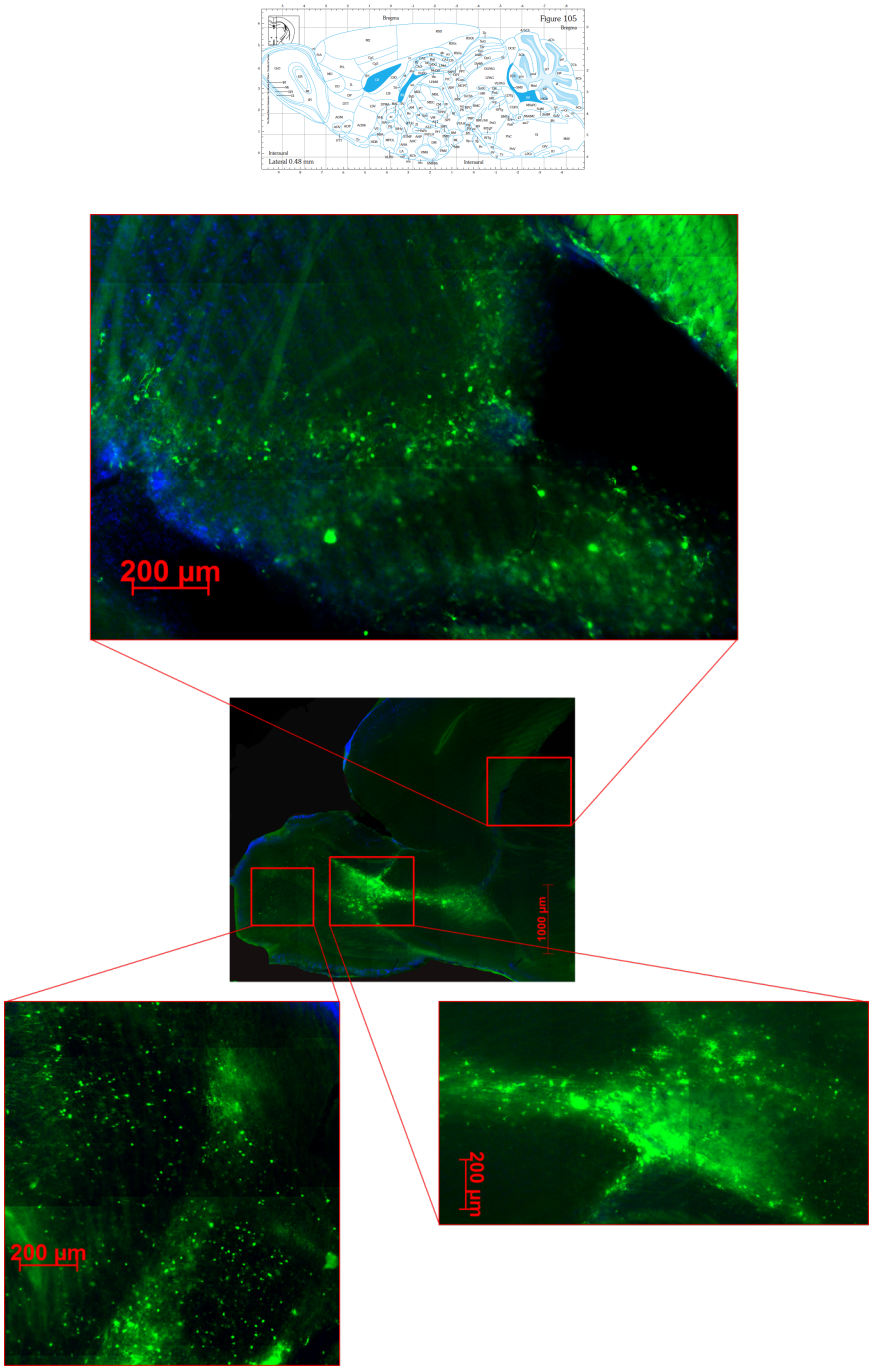

Figure 5.f5. SVZ-RMS neurogenesis enhancing by IDLV_GDNF

This animal was injected with IDLVs_pRRL_GDNF and pHR'SIN-cPPT-SEW. Anti-mouse eGFP by Abcam (green), nuclear chromatin was visualised with DAPI (blue).

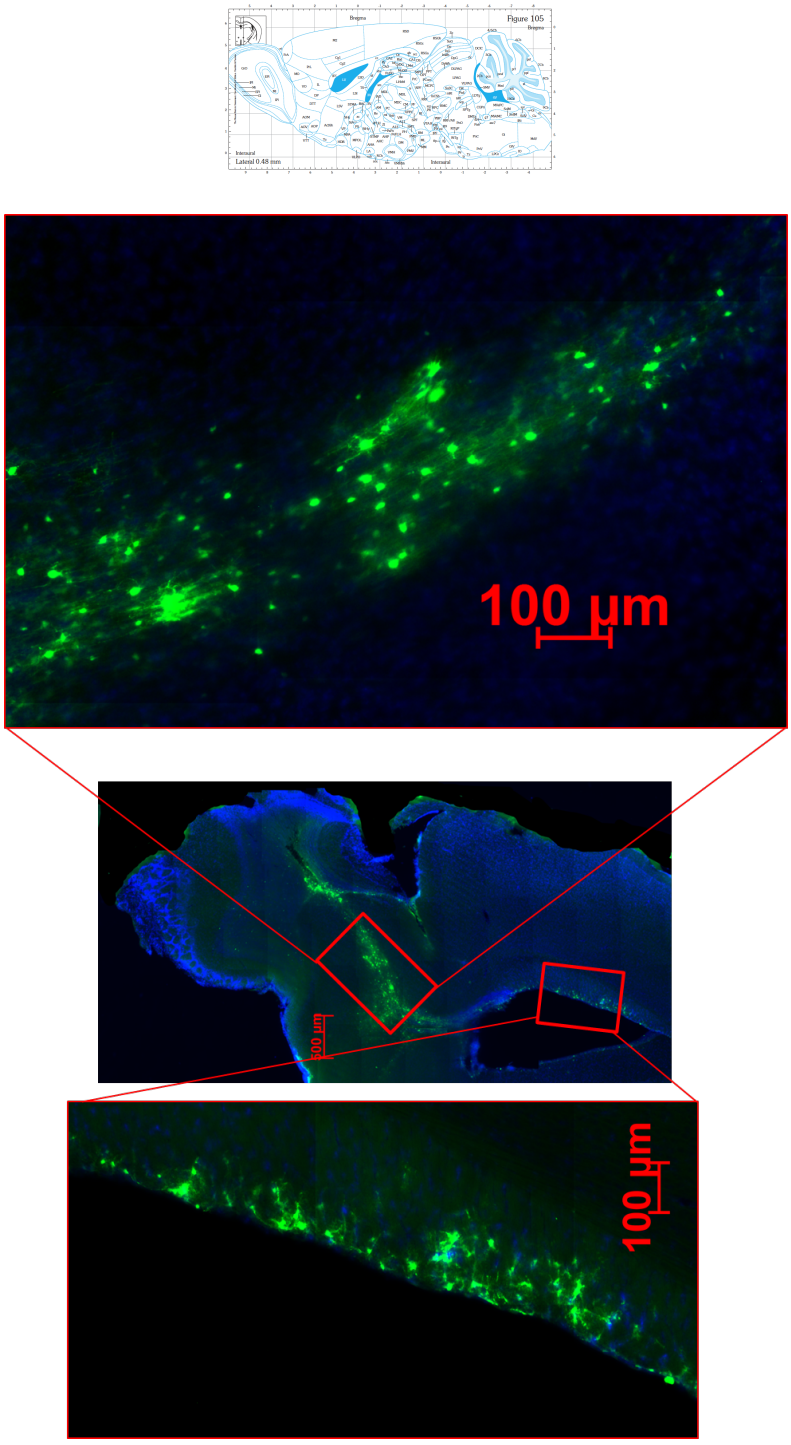

Figure 5.f6. SVZ-RMS-OB migration in an animal treated with LV_ pHR'SIN-cPPT-SEW and LV_pRRLcC_TTC_IRESeW

Animal injected with LVs_pRRL_TTC and pHR'SIN-cPPT-SEW. Anti-mouse eGFP by Abcam (green), nuclear chromatin was visualised with DAPI (blue).

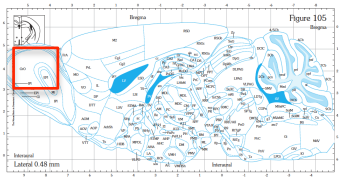

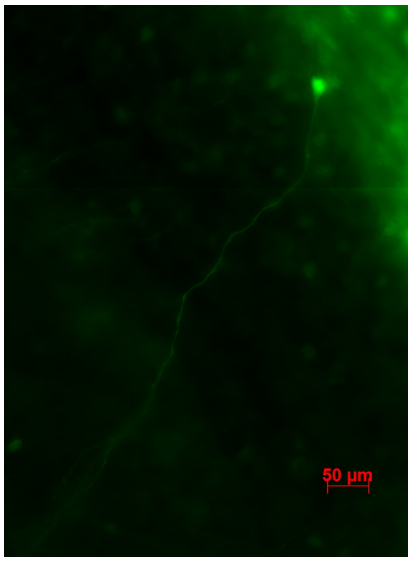

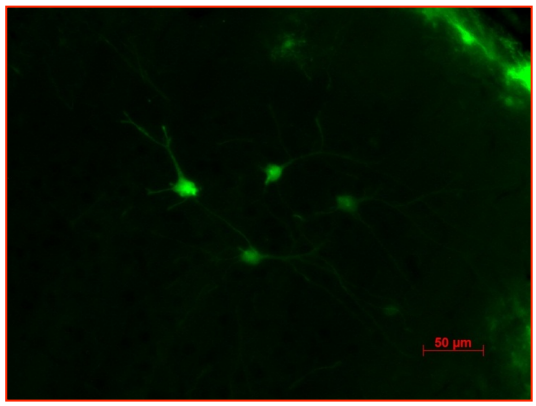

Figure 5.f7. NPCs derived cells in the OB three weeks after LV_shRNA_Empty injection.

Detail of the OB region in a mouse treated with LV_shRNA_Empty and pHR'SIN-cPPT-SEW. The histology was performed three weeks later.

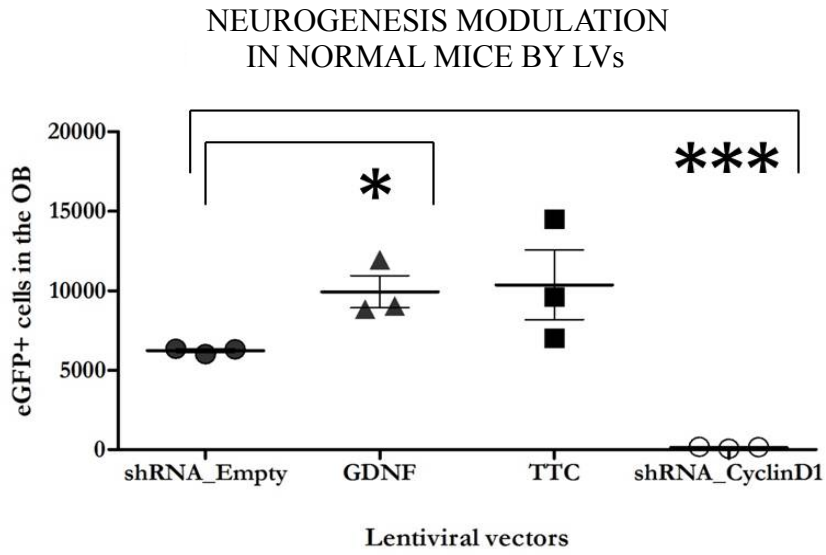

Figure 5.f8. SVZ's neurogenesis quantification after lentiviral modulation.

Quantification of the eGFP positive cells migrated into the OBs three weeks post intracranial injections of LV vectors. Both the OBs were entirely quantified for green labelled cells. Bars represent mean ±SEM. The LV_shRNA_CyclinD1 significantly reduced the green cells in the OBs, ***$p<0.001$. Moreover there was a significant increase of eGFP positive cells in the OBs as effect of the IDLV_GDNF, when compared to the control (LV_shRNA_Empty) group, *$p<0.05$. Student's t-test. Data from n=3 animals per group.

5. 6 CONCLUSION

The effectiveness of the SVZ modulator systems based on intracranial LV injections was evaluated in absence of stroke.

The animals received 10 µl of vectors divided into two bilateral injections at the beginning of the RMS and the histology was performed three weeks later. Each group received an LV carrying either the shRNA_CyclinD1 sequence, the rat precursor GDNF, the TTC or an Empty hairpin, in combination with the LV encoding eGFP (LV_ pHR'SIN-cPPT-SEW).

The LVs-eGFP based system was an efficient tool to detect the SVZ progenitors and to monitor them along the migration toward the OBs, as previously shown by Goncalves et al, 2008.

The SVZ neurogenesis was efficiently inhibited by the LV_ shRNA_CyclinD1, ***$p<0.001$. Moreover the treatment with IDLV_GDNF significantly increased the eGFP positive cells into the OBs, where *$p<0.05$, by the Student's t-test. LV encoding TTC was without effect.

CHAPTER 6

6.1 SVZ-RMS NEUROGENESIS MODULATION IN STROKE

SUMMARY

Neurogenesis occurs in ischemic conditions in the SVZ and the SGZ (Wang, Zhang et al.; Yamashita, Ninomiya et al. 2006). It was demonstrated that the neuronal precursors can produce not only neurons but also glial cell types. Because of the high mobility of microglia, a possible origin from the SVZ's progenitors is still debated (Levison, Druckman et al. 2003).

Intrastriatal infusion of GDNF by subcutaneous minipump performed just before the ischemia and up to day 7 after MCAo produced GDNF diffusion to the SVZ and increased cell proliferation (Kobayashi, Ahlenius et al. 2006). In addition, intrastriatal infusion between day 13 and day 23 post ischemia increased the survival of mature neurons generated after MCAo (Kobayashi, Ahlenius et al. 2006).

GDNF can be provided as polypeptide or the gene can be delivered by vectors. It was demonstrated that there was a lack of ability of the recombinant intracerebral administered GDNF in ALS patients, to provide trophic support for the degenerating motor neurons (Deierborg, Soulet et al. 2008). This lack of the efficacy could be the result of a poor bioavailability of the polypeptide in the mammalian brain.

TTC was demonstrated to be an efficient tool for delivering the mature and the recombinant GDNF to the extracellular space, where the growth factor can provide trophic support to neighbouring cells (Benn, Ay et al. 2005; Li, Chian et al. 2009). In addition, a recent publication demonstrated that a growth factor-like property of TTC compound can positively influence

degenerating motor neurons in an ALS mouse model (Moreno-Igoa, Calvo et al. 2010).

The aims of this chapter are:

- To compare the effects of negative and positive modulators of SVZ proliferation on stroke outcome, in order to assess the importance of neurogenesis in ischemic conditions
- To assess possible protective effects of TTC and GDNF pre-ischemia administered to the SVZ.

6.2 METHODS

C57 BL/6, male, 6-10 weeks old were injected with 12µl of vector suspension. LV was used to deliver the shRNA_CyclinD1 and shRNA_Empty while IDLV was used for GDNF and TTC. As described in the methods, the SVZ was targeted by two injections performed in each hemisphere. The coordinates used were the follow: **SVZ_1** AP, 0.25; ML, ± 0.96, DV -2.75, and **SVZ_2**, AP, 0.86; ML, ± 0.72, DV -3), as described in the methods chapter, the coordinates were estimated based on previous experiments, as the regions with the major probability to develop an ischemic lesion after 1h_MCAo.

In this experiment four different groups of mice were investigated (n=10 per group);

i) SVZ neurogenesis inhibition by LV_shRNA_CyclinD1,
ii) SVZ neurogenesis boosting by IDLV_GDNF,
iii) SVZ neurogenesis boosting by IDLV_TTC,
iv) LV_shRNA_Empty (control).

All vectors were co-injected with the LV_ pHR'SIN-cPPT-SEW that carried an eGFP cassette. Except for the LV_shRNA_CyclinD1_92, the batches used in this experiment were the same as used for the experiment

described in Chapter 5. The information about batches and titres used is illustrated in Table 6.f1.

After the intracerebral injections the animals were returned to their own cage with food and water *ad libitum*. Animals were monitored daily for unexpected adverse effects and signs of distress, weighed to monitor post-surgical recovery; animals underwent 1 hour MCAo at day 14 after intracerebral injections. In all cases weight had returned to pre-injection level. After the ischemia induction the animals were closely monitored for their weight and the temperature, and it was ensured that their conditions were not beyond the humane limits set for termination. During the first 2-4 days the animals were left in a warm cage and glucose-saline was intraperitoneally administered.

After MCAo animals' recovery was followed daily for 30 days by the 0-28 focal deficit test. They were killed by transcardial perfusion and the brains were analysed by immunofluorescence and Haematoxylin and Eosin staining as described in Chapter 2.

The experiment was conducted blind; the groups were named as A, B, C and D to identify the injections (respectively LV_shRNA_CyclinD1, LV_shRNA_Empty, IDLV_GDNF and IDLV_TTC). All histological analysis was carried out by myself on this coded material. Only after the histology was completed and the green cell numbers and ischemic volume quantified, the treatment performed in each group was revealed, and data pooled.

SAMPLE	shRNA_Empty	TTC	GDNF	shRNA_CyclinD1
SVZ MODULATOR SYSTEM	(no modulation) LV_shRNA_Empty Produced: 29/4/2011	(-) IDLV_TTC Produced: 5/3/2011	(-) IDLV_GDNF Produced: 5/3/2011	(+) LV_shRNA_CyclinD1_92 Produced: 29/4/2011
qPCR titre	3.78×10^8 IU/ml	3.05×10^9 IU/ml	3.35×10^9 IU/ml	2.8×10^8 IU/ml
Flow cytometer titre	1.4×10^8 IU/ml	no	no	7.2×10^8 IU/ml
µl Injected	6.6	6.6	6.6	6.6
pHR'SIN-cPPT-SEW	YES Produced 13/3/2011	YES Produced 13/3/2011	YES Produced 13/3/2011	YES Produced 13/3/2011
Flow cytometer Titre	$2.3\ 10^8$ IU/ml	$2.3\ 10^8$ IU/ml	$2.3\ 10^8$ IU/ml	$2.3\ 10^8$ IU/ml
µl Injected	3.3	3.3	3.3	3.3

Table 6.f1. LVs and IDLVs used in the experiment with the related titre.

6.3 ANIMALS LOST AND EXCLUDED FROM THE ANALYSIS

10 animals per group were investigated, two of them died because of the effect of the anaesthesia during the 1h_MCAo. A total of 21 animals across all groups died after the ischemia.

1 brain injected with the IDLV_TTC was not properly processed with paraffin, and it was not possible to perform the histological evaluation.

1 animal from the LV_shRNA_Empty was excluded from the analysis because the behaviour and the histology data deviated from the group's means by more than 2 standard deviations (Chauvenet's criterion).

6.4 HISTOLOGY

6.4.1 POSITIVE CONTROL: SVZ-DERIVED NEURONAL PROGENITOR CELLS IN THE OLFACTORY BULBS

As discussed in Chapter 2, injection coordinates were decided based on previous experiments. SVZ regions close to the focus of ischemic damage produced by 1h_ MCAo were selected.

To demonstrate effectiveness of the injections and long-term detection of the NPCs, the OBs were examined to identify eGFP positive cells, assumed to have migrated from the neurogenic islands of the SVZ (Figure 6.f1 and Figure 6.f2).

eGFP positive cells were found in the intrabulbar part of the anterior commissure (aci) and in the granular cell layer of the OB (GrO), (Figure 6.f1).

Under the same conditions, and to demonstrate effectiveness of the SVZ neurogenesis inhibition, the OBs of the animals treated with the LV_shRNA_CyclinD1 were analysed, and compared to the other groups. LV_shRNA_CyclinD1 efficiently inhibited neurogenesis as demonstrated by the absence of eGFP positive cells in the OB (Figure 6.f2).

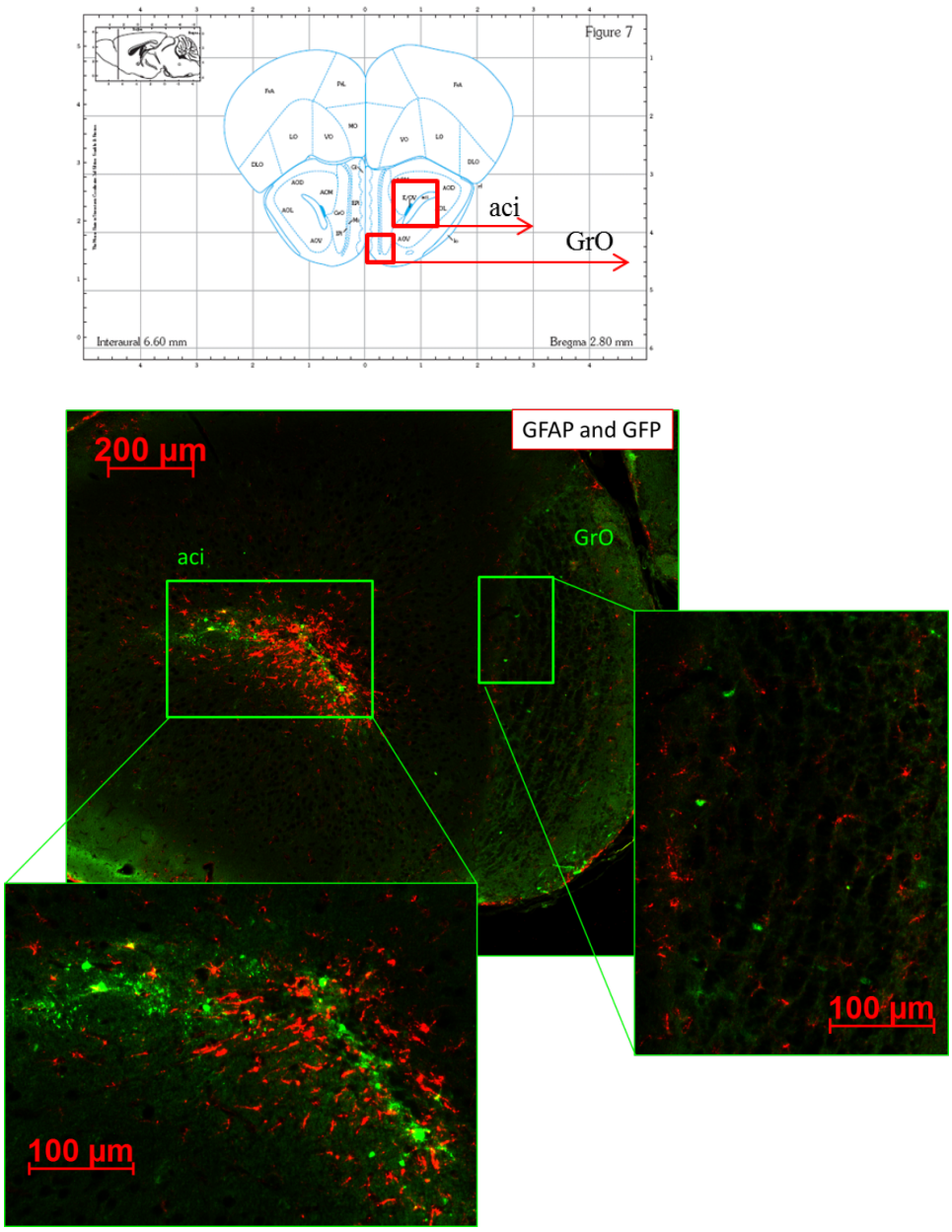

Figure 6.f1. Positive control: eGFP positive cells migrated into the OBs

OBs of an MCAo animal pretreated with IDLV_GDNF and and LV_ pHR'SIN-cPPT-SEW. The eGFP positive cells localized within the aci and GrO at 2.80 mm anterior from bregma, top picture. The histology was performed 30 days after reperfusion by Immunofluorescence; co-staining anti-GFP, (green), and anti-rabbit GFAP antibody (red)).

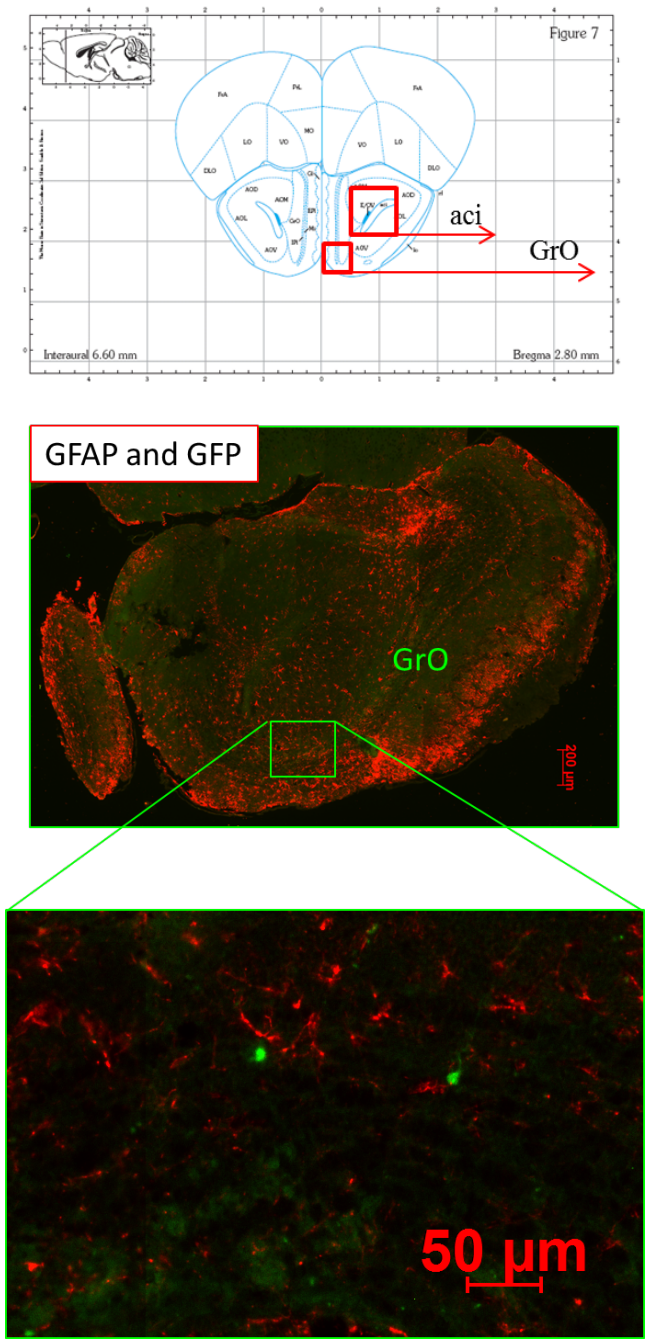

Figure 6.f2. Positive control: effect of the inhibition of the SVZ neurogenesis in the OBs

Animal injected with LVs_shRNA_Cyclin D1/LV_ pHR'SIN-cPPT-SEW and underwent to MCAo two weeks later; the OBs region is highlighted. The eGFP positive cells localized within the aci and GrO at 2.80 mm anterior from bregma, top picture. Histology performed by Immunofluorescence; co-staining mouse anti-GFP (Abcam) and rabbit anti-GFAP (Dako).

6.4.2 EFFECT OF MCAo ONE MONTH AFTER: THE ISCHEMIC BRAIN

Transient focal ischemia (1h_MCAo) induced migration of NPCs in the ipsilateral ischemic area. The neuronal progenitors were found along the anterior part of the anterior commissure (aca) and surrounding the lateral ventricle (lv) in the ipsilateral hemisphere; some cells extended to the caudate putamen (CPu) already in the forebrain at 1.70 mm anterior from bregma, (Figure 6.f3). Only a few eGFP positive cells co-expressed a marker for differentiated cell types (Iba1, DCX, or GFAP).

eGFP positive cells were found in the CPu: the migrated cells were found at 1.17 mm from the ventricles, and some of them looked differentiated, but they were not positive for any of the cellular markers tested (GFAP, Iba1, Beta III and DCX), Figure 6.f4.

The ipsilateral SVZ (i.e. ipsilateral to the focal ischemic lesion) but not the contralateral was found expanded with an increase of the eGFP positive cells (Figure 6.f5 and Figure 6.f6). In addition, some eGFP-labeled cells grouped like neurogenic islands were found in the ischemic cortex and striatum (Figure 6.f6 and Figure 6.f7). In the cortex the eGFP positive cells were found at 1.87 mm from the SVZ (Figure 6.f7).

eGFP positive cells were repeatedly found in white matter tracts (the aca, and the corpus callosum; Figure 6.f8 and Figure 6.f9). As previous authors suggested, MCAo induced an increase in cell number in these regions (Gotts and Chesselet 2005). Moreover, the ipsilateral SVZ expansion presented in Figure 6.f9 suggests a possible migratory pathway between the SVZ and the aca.

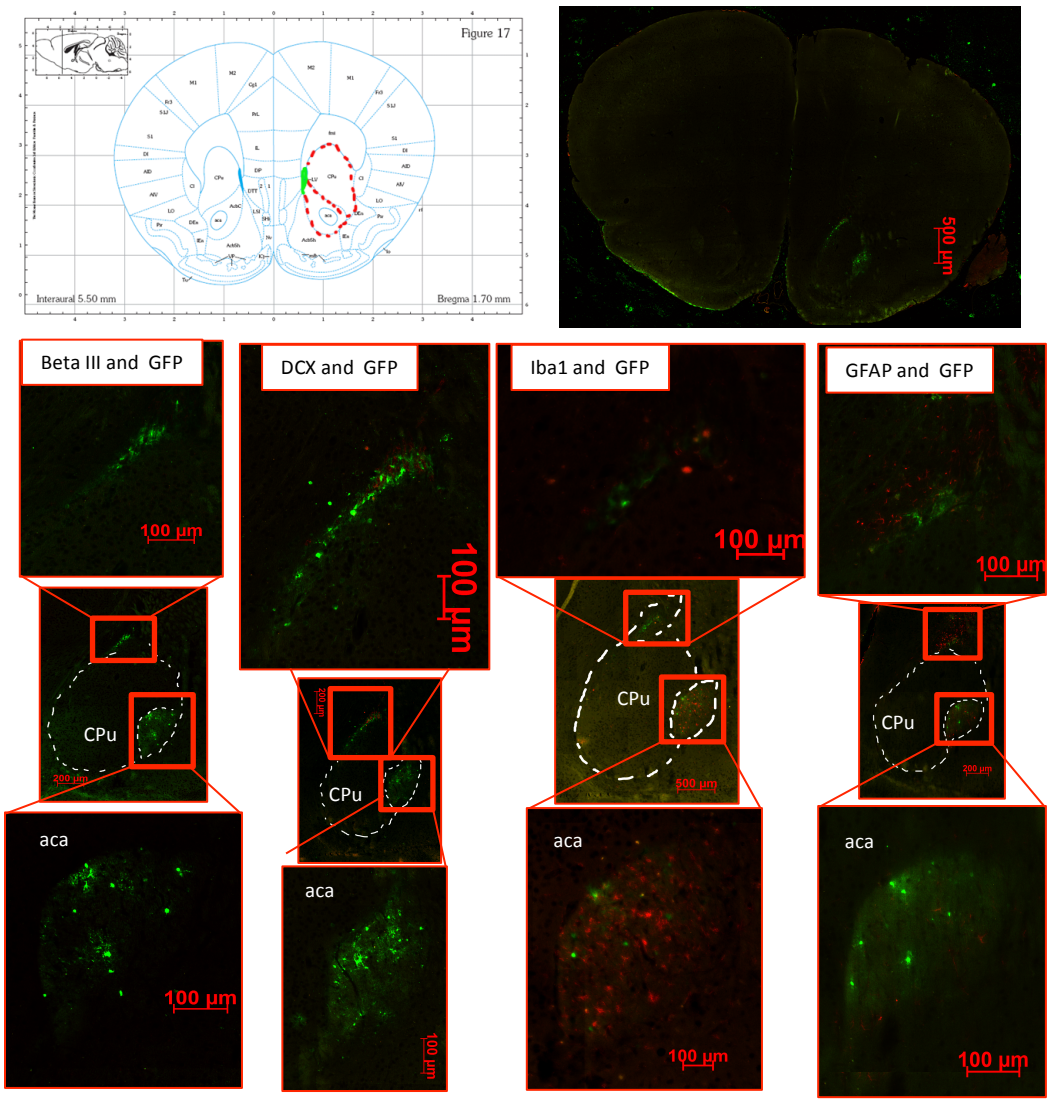

Figure 6.f3. MCAo-induced migration of NPCs to the lesion areas.

eGFP positive cells in ischemic striatal regions. In the above images an animal was injected with a mix of IDLV_GDNF and LV_ pHR'SIN-cPPT-SEW close to the wall of the lateral ventricles and two weeks later underwent to 1h_MCAo. The histology was performed by Immunofluorescence; sequentially cut sections were treated with a mouse anti-eGFP (Abcam) and a cellular marker to detect microglia (rabbit anti-Iba1, Wako), glia (rabbit anti-GFAP, Dako), neurons and neuroblasts (rabbit anti-Beta III, Sigma-Aldrich and rabbit anti-DCX, Abcam). The eGFP positive cells were found in the aca and CPu, as described by the top map, AP 1.70 mm from bregma. Brain map taken from The Brain Mouse Atlas by Franklyn and Paxinos.

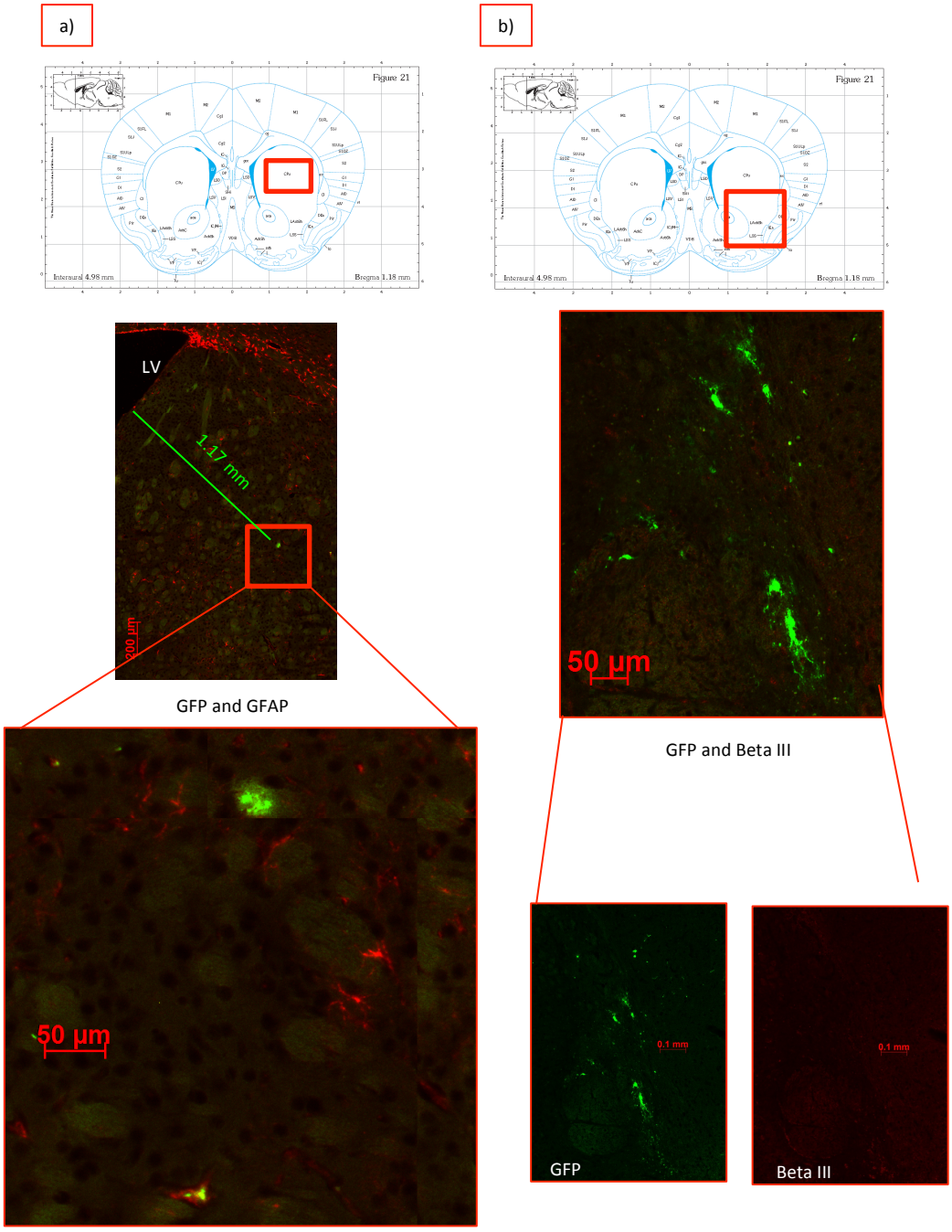

Figure 6.f4. eGFP positive cells in the ischemic striatal region.

The animals were injected close to the wall of the lateral ventricles with a) IDLV_TTC and LV_ pHR'SIN-cPPT-SEW b) IDLV_GDNF and LV_ pHR'SIN-cPPT-SEW. Two weeks later they were subjected to 1h_MCAo. The immunostaining was performed with a mouse anti-eGFP (Invitrogen) and alternatively a rabbit anti-Beta III (Sigma-Aldrich), or a rabbit anti-GFAP (Dako). Region locxalized at AP 1.18 mm from bregma. Brain map taken from The Brain Mouse Atlas by Franklyn and Paxinos.

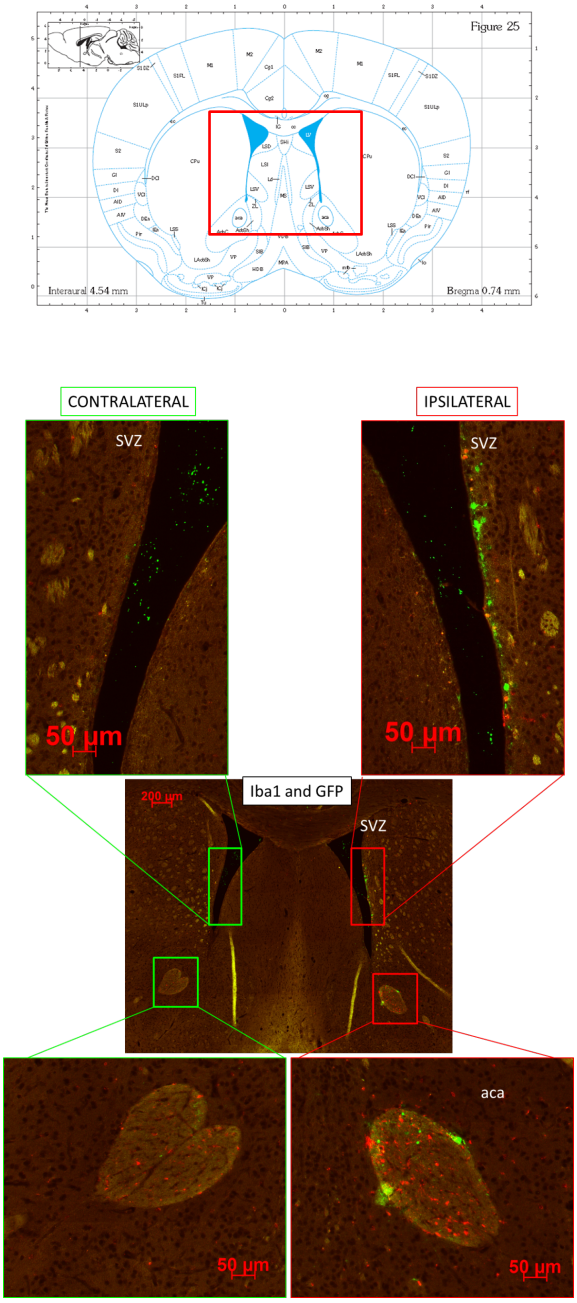

Figure 6.f5. Increase in eGFP expressing cells in the ipsilateral SVZ and aca

The pictures above derived from an animal treated with IDLV_GDNF/ LV_pHR'SIN-cPPT-SEW and consequently subjected to 1h_MCAo; eGFP positive cells localized in the ipsilateral SVZ and aca. The immunofluorescence staining was performed with a mouse anti-eGFP (Invitrogen) and a rabbit anti-Iba1 from (Wako). Section located at AP 0.74 mm from bregma. Brain map taken from The Brain Mouse Atlas by Franklyn and Paxinos.

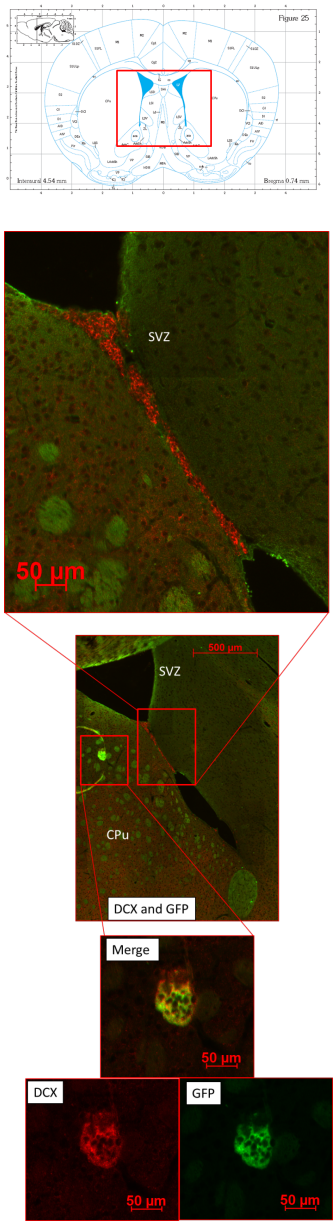

Figure 6.f6 eGFP and DCX positive niche like structure in the ischemic striatum.

Expansion of the SVZ region in MCAo brain; the neurogenic area was positive for DCX, moreover groups of progenitor cells expressing DCX were found in the closer striatum. The animal was injected on the wall of the lateral ventricles with IDLV_TTC /LV_ pHR'SIN-cPPT-SEW and two weeks later subjected to 1h_MCAo. The histology was performed by Immunofluorescence; mouse anti-eGFP (Invitrogen) and a rabbit anti-Iba1 (Wako). The section was localized at AP 0.74 mm from bregma.

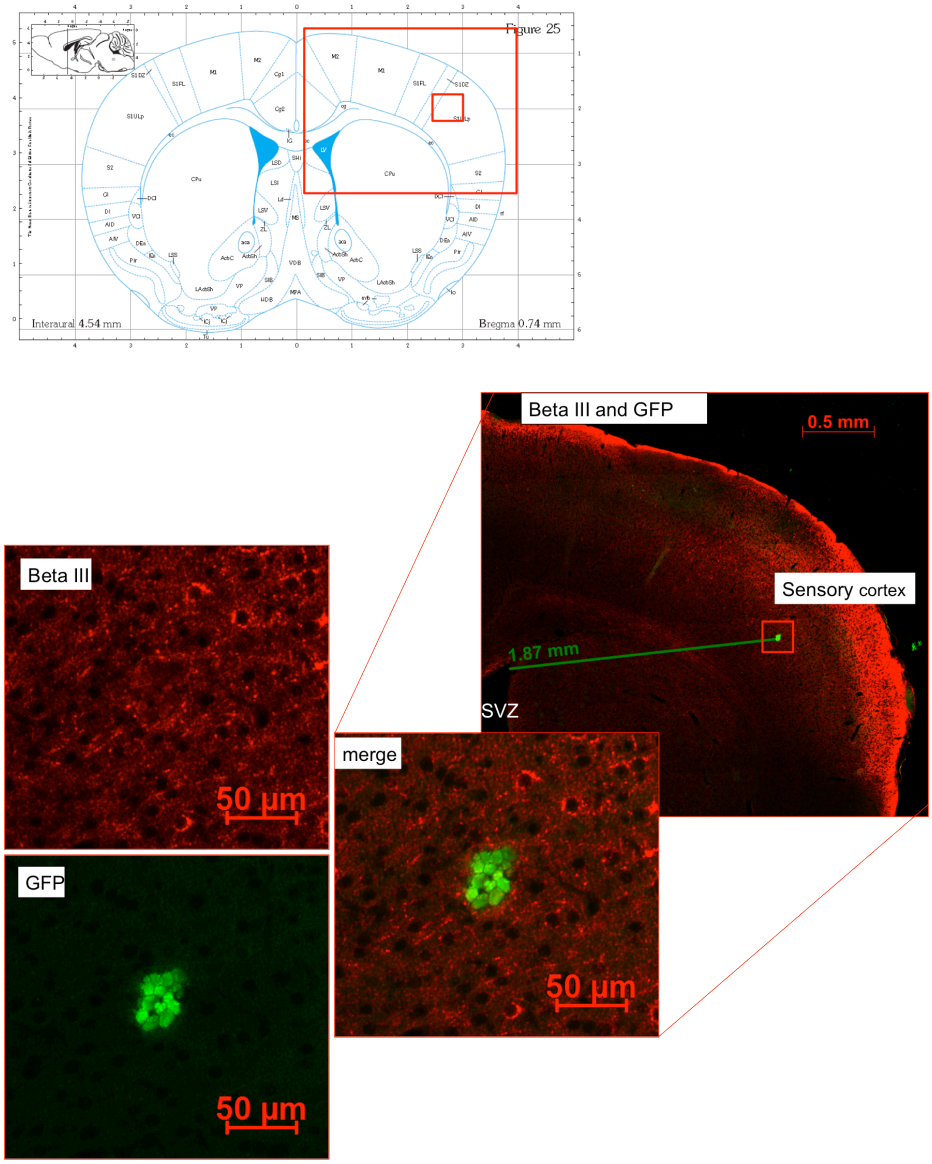

Figure 6.f7. eGFP positive niche like structure in the ischemic cortex.

EGFP positive cells localized in the sensory cortex after ischemia. The animal was injected on the wall of the lateral ventricles with IDLV_GDNF and LV_ pHR'SIN-cPPT-SEW; after two weeks it was subjected to 1h_MCAo. The histology was performed by co-staining with mouse anti-eGFP (Invitrogen) and rabbit anti-Beta III (Sigma-Aldrich). The eGFP positive cells were at 1.87 mm from the closer SVZ; AP 0.74 mm distance from bregma.

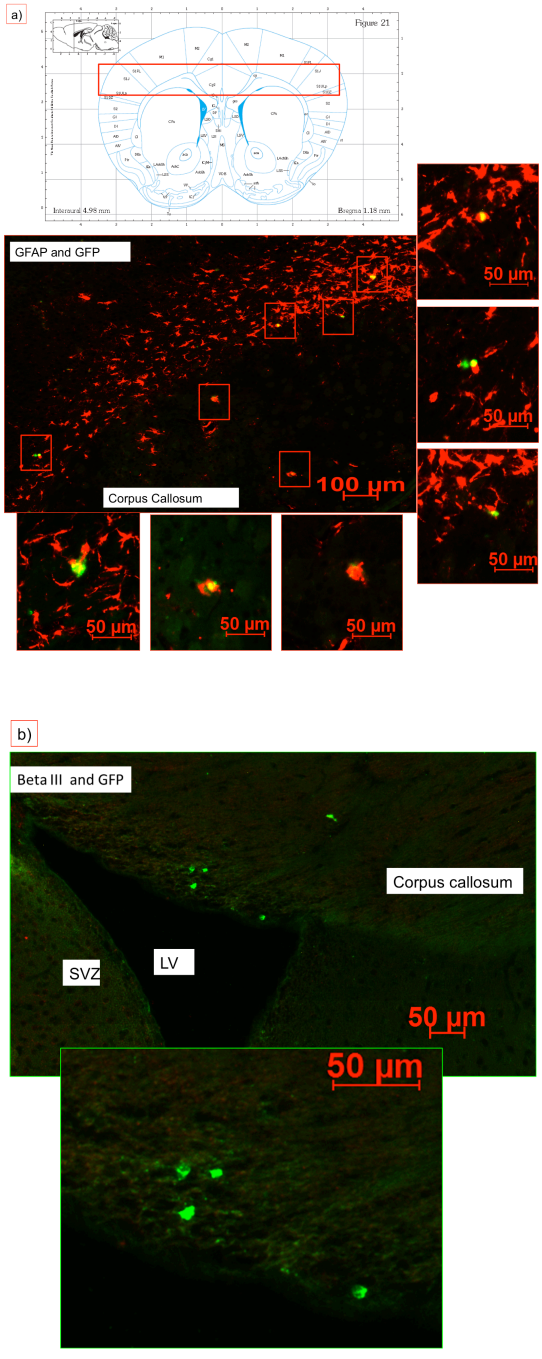

Figure 6.f8 EGFP positive cells localized within the corpus callosum

EGFP positive cells localized within the corpus callosum: some of them co-expressed GFAP. The animals were injected on the wall of the lateral ventricles with LV_shRNA_Empty/LV_ pHR'SIN-cPPT-SEW a) and IDLV_TTC /LV_pHR'SIN-cPPT-SEW b), after two weeks underwent 1h_MCAo. The histology was performed by Immunofluorescence; mouse anti- eGFP (Invitrogen) and alternatively a rabbit anti-Beta III (Sigma-Aldrich) or a rabbit anti-GFAP (Dako). The sections were localized at AP 1.18 mm from bregma.

Figure 6.f9. Possible radial migration pathway SVZ-aca

Neural progenitors were localized along the SVZ with an enlargement visible at the ventral side; the DCX positive cells as well as eGFP positive cells were located within and surrounding the aca. The animals were injected on the wall of the lateral ventricles with a) IDLV_ GDNF/LV_pHR'SIN-cPPT-SEW or b) IDLV_TTC/LV_pHR'SIN-cPPT-SEW and two weeks later they were subjected to 1h_MCAo. Immunostaining was performed with a mouse anti-GFP with alternatively a rabbit anti-Beta III (Sigma-Aldrich) or a rabbit anti-DCX (Abcam). AP 1.18 mm from bregma.

6.4.3 EVALUATION OF THE ISCHEMIC ENVIRONMENT

The ischemic volume was evaluated by Haematoxylin and Eosin staining and Immunofluorescence techniques. As described in Chapter 2, the quantification by Haematoxylin and Eosin alone was not sensitive enough to detect the ischemic environment in one-month reperfusion brains. For this reason, flanking the classical histology, neurodegeneration, glial scar and inflammation process were evaluated by Immunofluorescence.

The ischemic environment is composed of degenerating neurons, glial scar and activated microglia, with each of these variables changing with time and the brain restoration. The localization and quantification of the ischemic damage by one of these parameters alone would give only a partial view of the damage. For this reason the average volume between the glial scar, the inflammation and the neurodegeneration was performed and evaluated as the best estimation of the ischemia.

IDLV_GDNF as well as the IDLV_TTC treated groups, showed significant increase of the inflammation volume compared to the control, *$p<0.05$, Student's t test (Figure 6.f10). Diversely, the volume of the glial scar and the volume occupied by degenerating neurons (ischemic core) was the same when the groups were compared (Figure 6.f11 and Figure 6.f12).

The ischemic volume was estimated to be between 5 and 15 mm^3 with no difference between groups (Figure 6.f13).

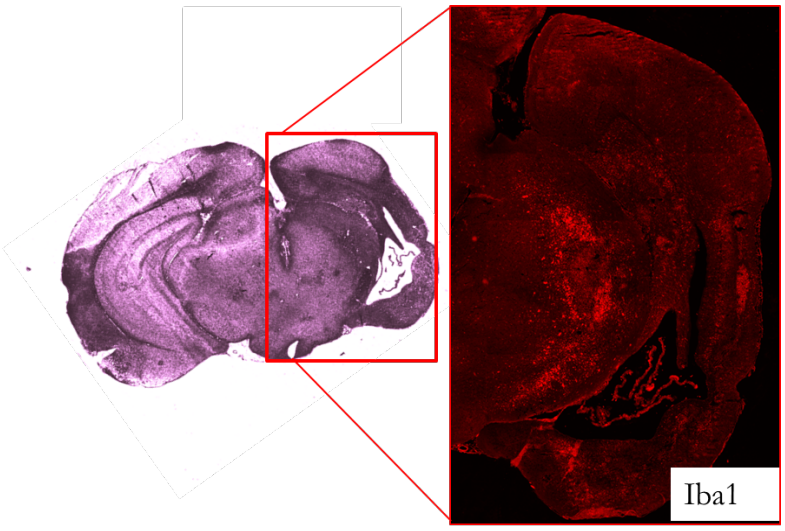

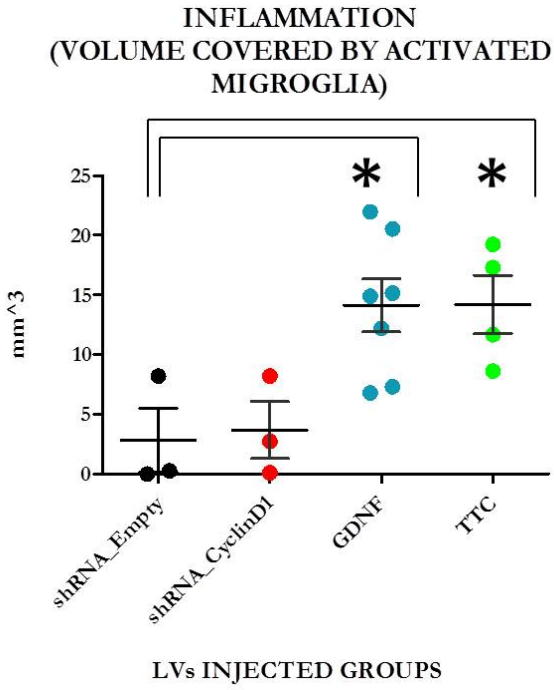

Figure 6.f10. Volume quantification of the regions covered by activated microglia.

Estimation of the inflammation reaction after ischemia. The analysis was accomplished by detecting Iba1 expressing cells using a rabbit anti-Iba1 antibody (Wako). The Student's t test pointed out an increase of the inflammation process in the IDLV_GDNF and IDLV_TTC treated groups, *$p<0.05$; values represent mean ± SEM. LV_shRNA_Cyclin D1 n=3, LV_shRNA_Empty n=3, IDLV_GDNF n=7 and IDLV_TTC n=4.

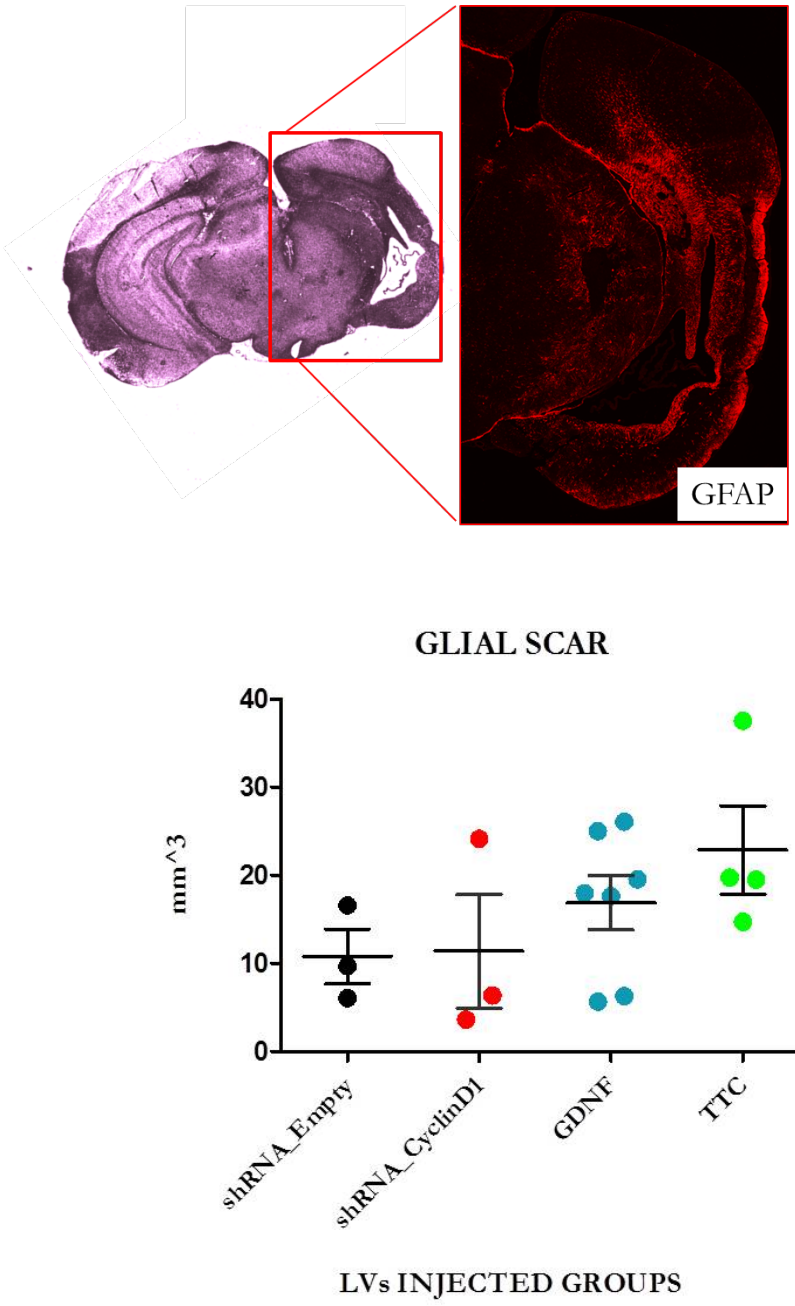

Figure 6.f11. Glial scar quantification

Estimation of the glia scar formation after ischemia. The analysis was performed by quantification of the volume covered by GFAP expressing cells. No variation was detected in the groups under analysis. In the plot the values represent mean ± SEM; analysis by the Student's t test. LV_shRNA_Cyclin D1 n=3, LV_shRNA_Empty n=3, IDLV_GDNF n=7 and IDLV_TTC n=4.

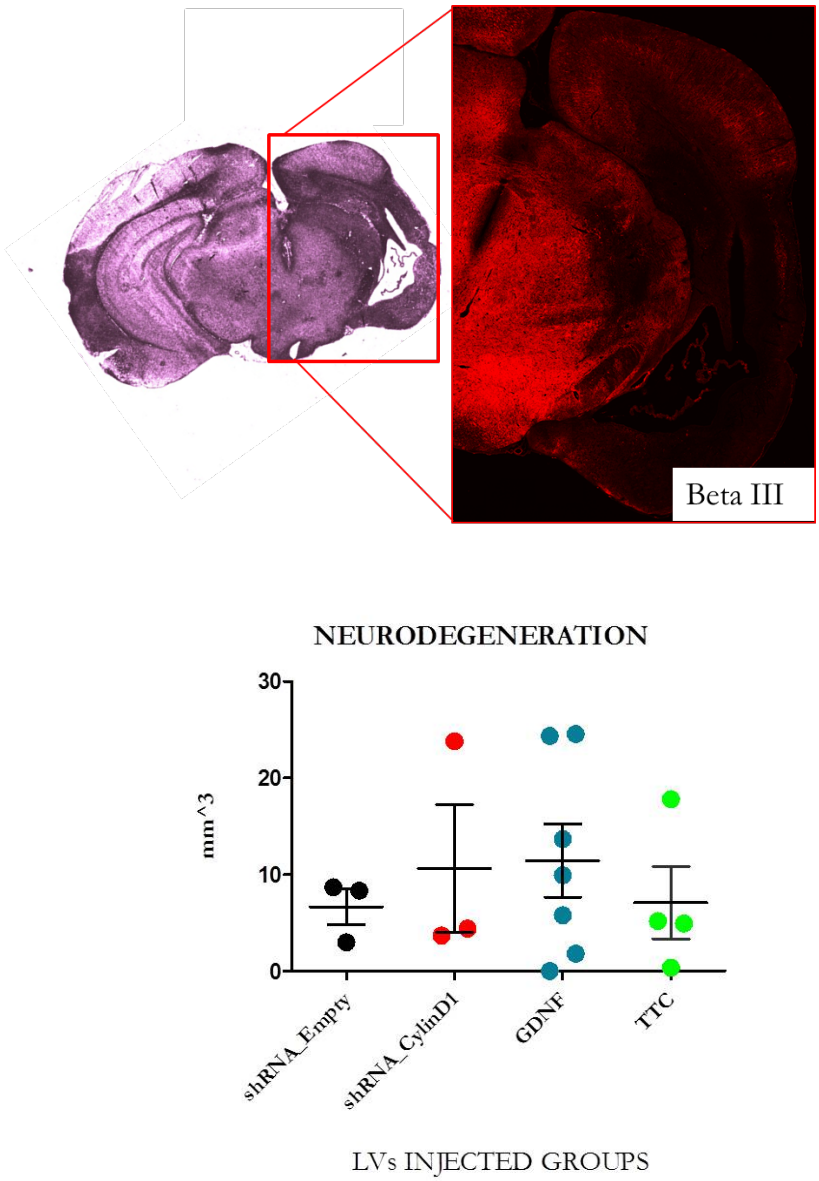

Figure 6.f12. Quantification of the neurodegenerative regions.

Estimation of the core region (neurodegeneration) after ischemia. The analysis was performed by quantification of the volume where Beta III was under expressed. No variation was detected in the groups under analysis. The analysis was accomplished using a rabbit anti-Beta III antibody (Sigma-Aldrich). In the plot the values represent mean ± SEM; analysis by the Student's t test. LV_shRNA_Cyclin D1 n=3, LV_shRNA_Empty n=3, IDLV_GDNF n=7 and IDLV_TTC n=4.

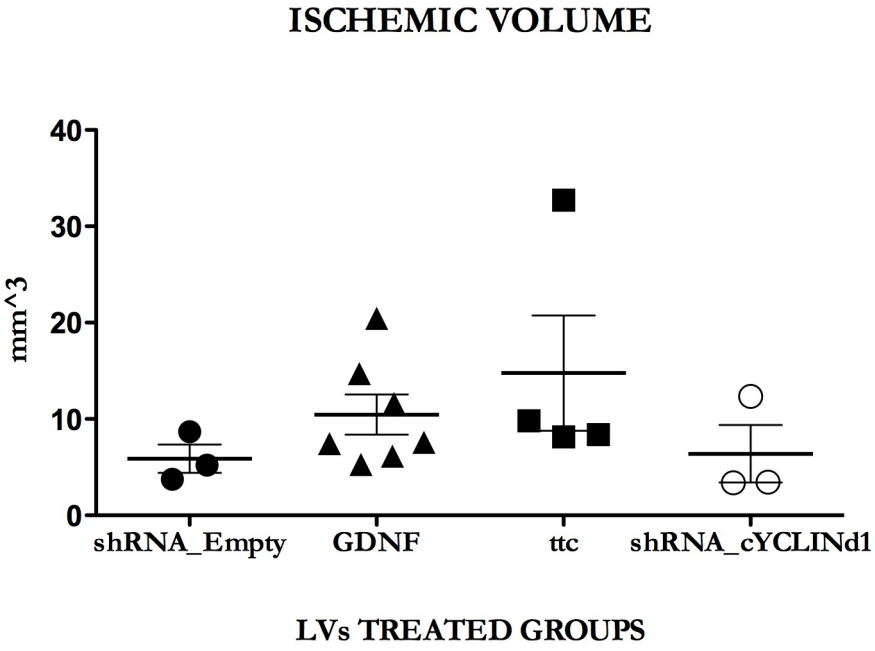

Figure 6.f13. Infarct volume quantification.

The ischemic volume quantification was estimated as the average between the volume of neurodegeneration (down-regulation of Beta III), glial scar (up-regulation of GFAP or activated astrocytes) and the inflammation (up-regulation of Iba1 or activated microglia). There was no difference in the ischemic volume produced after 1h_MCAo. Values represent mean ± SEM; analysis by the Student's t test. LV_shRNA_Cyclin D1 n=3, LV_shRNA_Empty n=3, IDLV_GDNF n=7 and IDLV_TTC n=4.

6.4.4 eGFP-POSITIVE CELLS IN THE ISCHEMIC AREA

eGFP positive cells were counted in the ischemic regions after 30 days of reperfusion. The counting was performed in 5 regions per brain, that were identified at specific position from bregma: AP +2.5, 1.7, 0, -1.7, and -3 mm. As described in Chapter 2, for each of these regions (AP +2.5, 1.7, 0, -1.7, and -3 mm) four consecutive sections were co-stained with a mouse anti- eGFP from Sigma-Aldrich and a specific cellular marker (rabbit anti-Iba1 from Wako, rabbit anti-GDNF from Dako, rabbit anti-Beta III from Invitrogen and rabbit anti-DCX by Abcam). The estimation of total number of green cells in the ischemic volume is described in the Chapter 2.

The injection of the LV_shRNA_CyclinD1in the SVZ efficiently reduced the number of eGFP positive cells in the ischemic environment, $^{**}p<0.01$, Student's t test (Figure 6.f14).

The injection of the IDLV_GDNF in the SVZ increased the eGFP positive cells in the MCAo brains, $^{*}p<0.05$, Student's test (Figure 6.f15).

Due to high variability between subjects, the IDLV_TTC treated group did not show any significant variation of the eGFP positive cells migrated to the ischemic areas (Figure 6.f16).

The characterization of the phenotype for the eGFP expressing cells did not point out a predominant phenotype (Figure 6.f17). One month post MCAo, the neural progenitors born in the SVZ and migrated in the ischemic boundaries, were for the most part not positive for any of the cellular markers tested.

There were no convincing eGFP positive cells co-expressing Beta III (Figure 6.f17). As many papers reported neurodegeneration occurs very

early after the differentiation; Lindvall and Kokaia (2004) described the 80% of the stroke-generated neurons died during the first 14 days post ischemia (Lindvall and Kokaia 2004). Moreover, a diffuse expression of lipofuscin in dying and dead cells did not allow sure discrimination between the eGFP and lipofuscin. Regarding the remaining markers: GFAP was 0.31% of the total green cells, while Iba1 0.29% and DCX 0.33%. (Figure 6.f17).

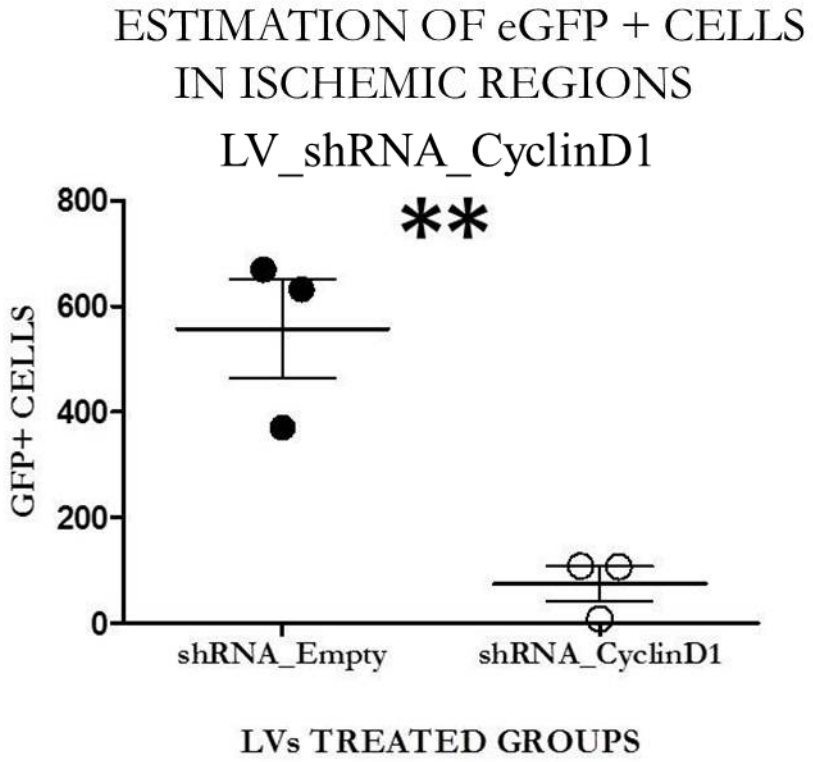

Figure 6.f14 eGFP positive cells in the ischemic area: LV_shRNA_CyclinD1 group.

Quantification of eGFP positive cells in ischemic region; group treated with LV_shRNA_Cyclin D1 and LV_ pHR'SIN-cPPT-SEW. The animals treated with LV_shRNA_CyclinD1 drastically reduced the number of eGFP positive cells estimated within the ischemic regions, **$p<0.01$. Values represent mean ±SEM; Student's t test.

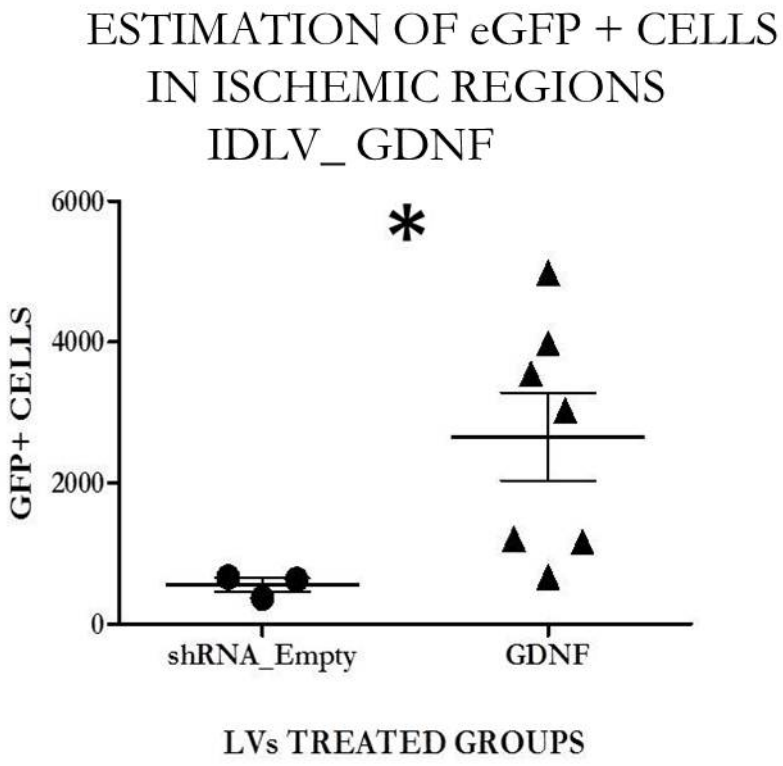

Figure 6.f15. eGFP positive cells in the ischemic area: IDLV_GDNF injected group.

MCAo group treated with IDLV_GDNF and LV_ pHR'SIN-cPPT-SEW. IDLV_GDNF increased the number of eGFP positive cells within the ischemic regions *$p<0.05$. Values represent mean ±SEM; Student's t test.

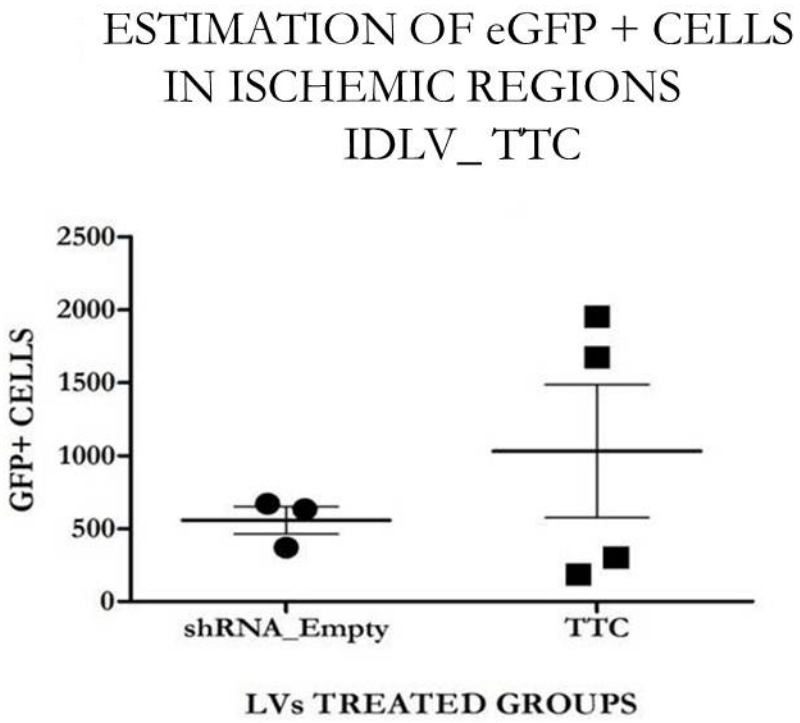

Figure 6.f16. eGFP positive cells in the ischemic area: IDLV_ TTC injected group.

Quantification of eGFP positive cells within the ischemic region; group treated with IDLV_TTC and LV_ pHR'SIN-cPPT-SEW. The number of eGFP positive cells estimated in the ischemic boundaries was not statistically different from the control. Values represent mean ±SEM; p=0.42, Student's t test.

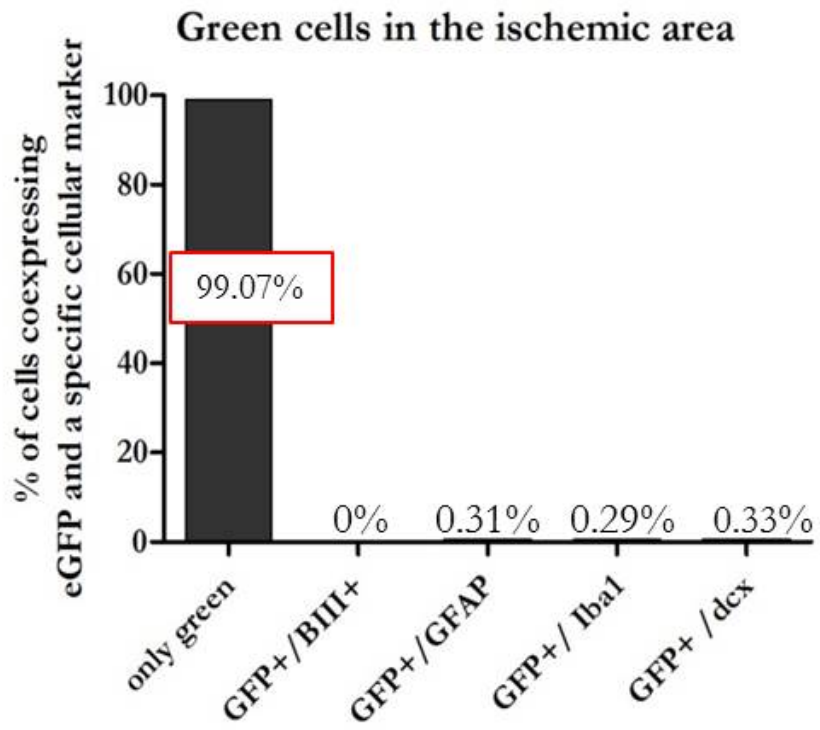

Figure 6.f17. Analysis of phenotype in the eGFP positive cells migrated to the ischemic environment.

The eGFP positive cells localized in the ischemic region where evaluated for the phenotype by Immunofluorescence. 99.07% of the eGFP positive cells did not co-express any of the marker assessed (Iba1, Beta III, GFAP, DCX).

6.4.5 IDLV_GDNF INJECTION IN THE SVZ IMPROVED THE NATURAL RESPONSE TO ISCHEMIA.

Ischemia-induced proliferation of neural progenitors has been extensively demonstrated (Le Magueresse, Alfonso et al.; Sugiura, Kitagawa et al. 2005; Yamashita, Ninomiya et al. 2006). The quiescent NPC population responds to stimuli released by the ischemic environment. With the hypothesis of a linear relationship between the damage severity and SVZ response, the correlation between the ischemic damage and eGFP positive cells located there was analysed by linear regression.

Although the relationship was not statistically significant in the control group (R^{10}=0.19), the IDLV_GDNF significantly improved it with *p<0.05 and R=0.68, as proved by the linear regression analysis. The treatment with the LV_shRNA_CyclinD1 reduced the coefficient to 0<R<0.005. The linear regression analysis for the IDLV_TTC group was not statistically significant where R= 0.16 (Figure 6.f18).

The linear relationship between the green cells migrated in the ischemic regions and the volume (or damage severity) was further analysed by possible correlation between green cells and glial scar, green cells and inflammation or green cells and neurodegeneration. Although there was no linear relationships between the green cells and glial scar or inflammation, the neurodegeneration volume (or core volume) was highly associated with the number of migrated NPCs in the ischemic regions, ***p<0.001 and R=0.92, Linear Regression analysis (Figure 6.f19).

[10] R is the correlation coefficient and is a measure of the goodness of fit of the linear regression. It can vary between 0 and 1; 0 when there is no linear relationships between the variables X and Y, while for R=1 there is a perfect distribution of the X on the line, in turn this allow a complete predictability of the Y values knowing the related X.

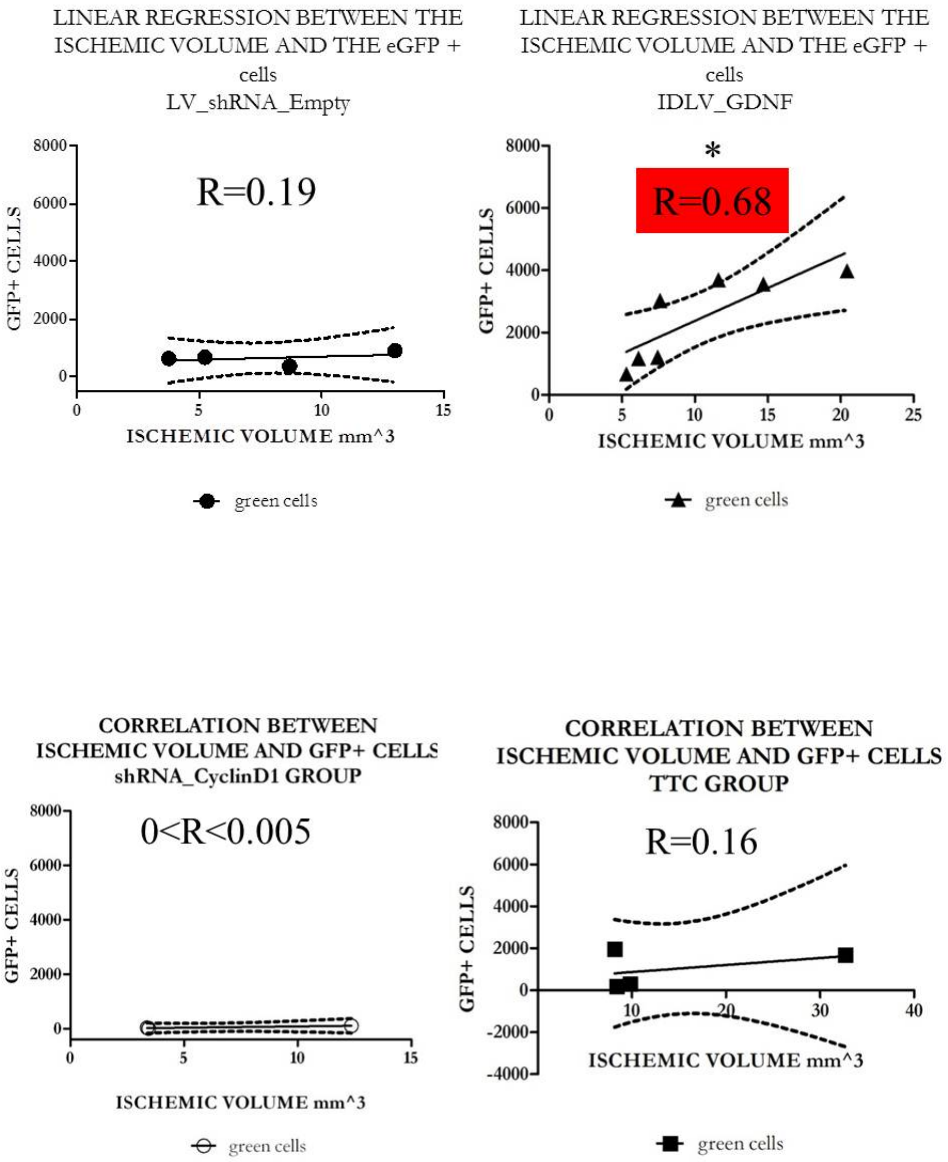

Figure 6.f18. The IDLV_GDNF increased the neurogenic response to ischemia.

1h_MCAo induced neurogenesis of the SVZ in a damage-severity dependent manner. The treatment with the IDLV_GDNF boosted the SVZ response, *p<0.05, by the Linear Regression analysis. The R values highlighted an increase in the linear relationships between the damage severity and the neurogenesis of the SVZ. IDLV_GDNF R=0.68, LV_shRNA_Empty R=0.1, IDLV_TTC R=0.16 and LV_shRNA_CyclinD1 0<R<0.005

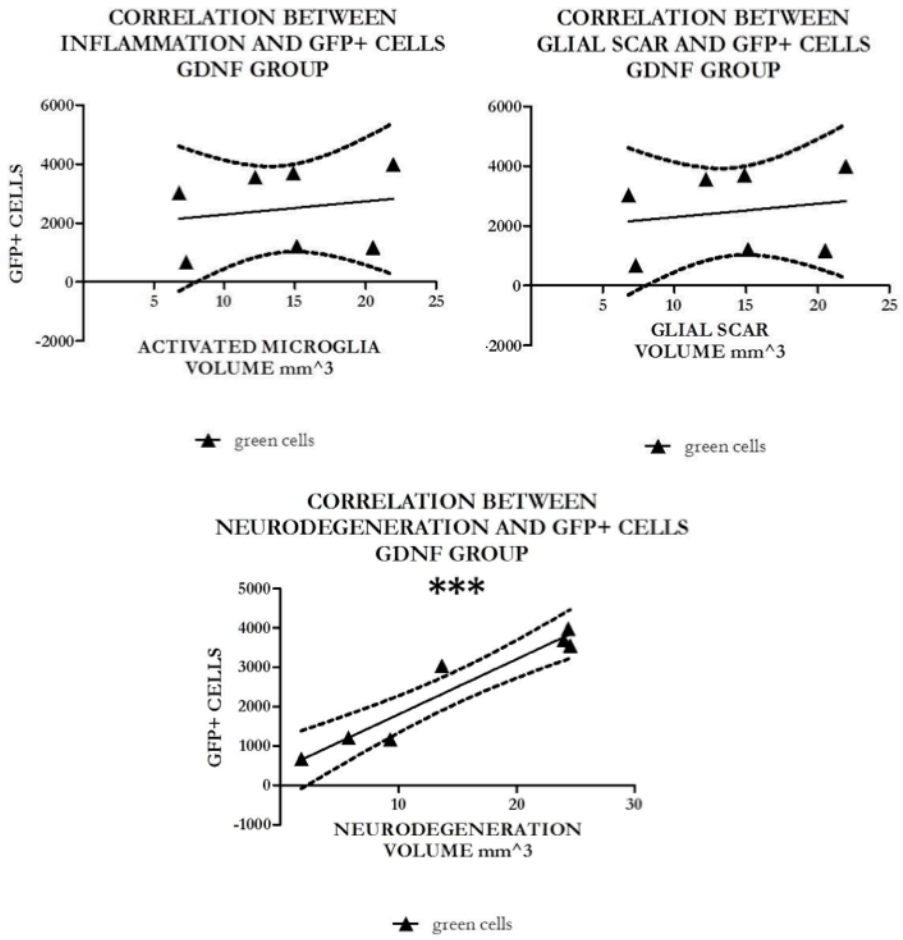

Figure 6.f19. Linear regression analysis of the ischemic volume and the eGFP positive cells located there: IDLV_GDNF injected group.

The linear regression analysis was performed to evaluate which part of the ischemic environment had influenced most the neurogenesis of the SVZ. There was no linear relationships between the number of eGFP positive cells and the glial scar, as well as the inflammation process; conversely the neurodegeneration affected the response of the SVZ the most with ***$p<0.001$ and $R=0.92$ estimated by linear regression analysis.

6.4.6 LV_shRNA_CyclinD1 REDUCED RECOVERY ABILITY AFTER MCAo

The neurological damage was evaluated on a daily basis by the 0-28 focal deficit test described in Chapter 2.

The analysis of the survivors[11] treated with the LV_shRNA_CyclinD1 showed a significant reduced recovery ability during the first two weeks post ischemia, as demonstrated by the Mann-Whitney rank sum test that gave *$p<0.05$ (Figure 6.f20). After day 14, the animals' behaviour was very similar to the LV_shRNA_Empty (control group).

LV_shRNA_CyclinD1 drastically increased the frequency of death during the first five days post ischemia, with 5 out 9 subjects suffering this fate (Figure 6.f21).

The analysis of the variation of the body weight did not show difference in the groups after the intracranial injections (part a) of Figure 6.f22). A trend to delayed recovery of pre-operative weight was visible in the LV_shRNA_CyclinD1 group after 1h_MCAo (part b) of Figure 6.f22). Moreover, day 3 after 1h_MCAo was further analysed by the Student's t test that demonstrated a statistically reduced body weight with *$p<0.001$ (part c) of Figure 6.f22)

[11] The survivors (or survival population) are the ischemic animals that were able to survive for 30 days after 1h_MCAo

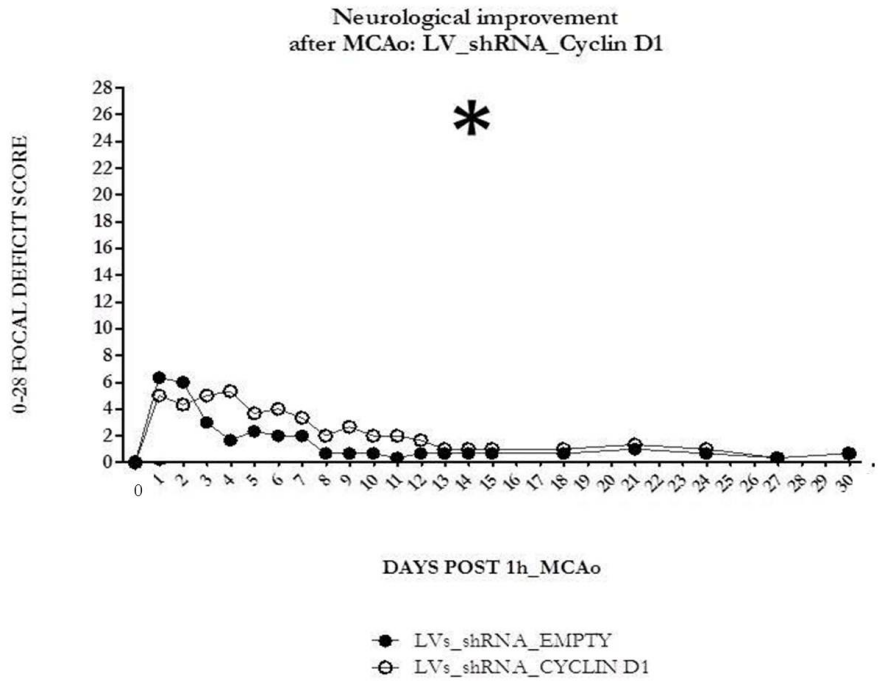

Figure 6.f20. Neurological recovery in the surviving populations: effect of LV_shRNA_CyclinD1 after 1h_MCAo

The neurological improvement was assessed on a daily basis by the 0-28 focal deficit test. LV_shRNA_CyclinD1 group showed a significant increase in the ischemic sensory-motor phenotype rose after ischemia, *$p<0.05$, Mann-Whitney rank sum test. Values represent the median of the score assigned. For the LV_shRNA_CyclinD1 group $n=3$, and for the LV_shRNA_Empty group $n=3$. One animal treated with the Empty hairpin was excluded from the analysis because it was greater than 2 standard deviations from the mean, Chauvenet's criterion.

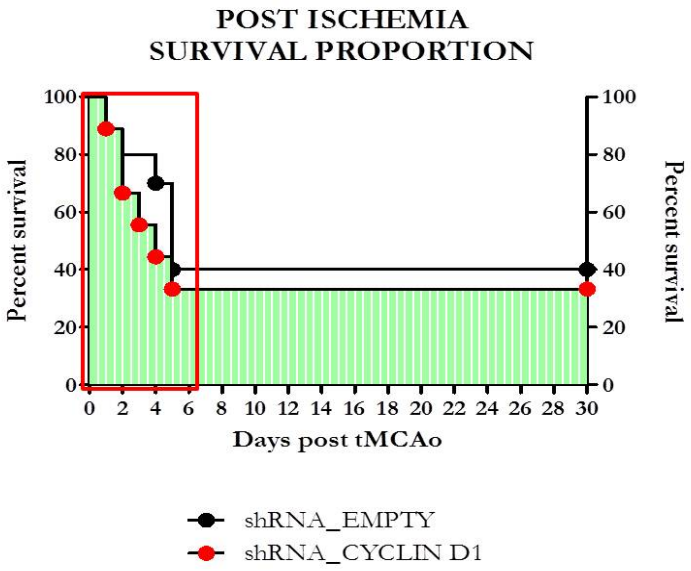

Figure 6.f21 LV_shRNA_CyclinD1 increased the number of deaths during the first 5 days post ischemia.

LV_shRNA_Cyclin D1 group reduced the number of survivors after ischemia. The curves were analysed in pair by the Gehan-Breslow-Wilcoxon.

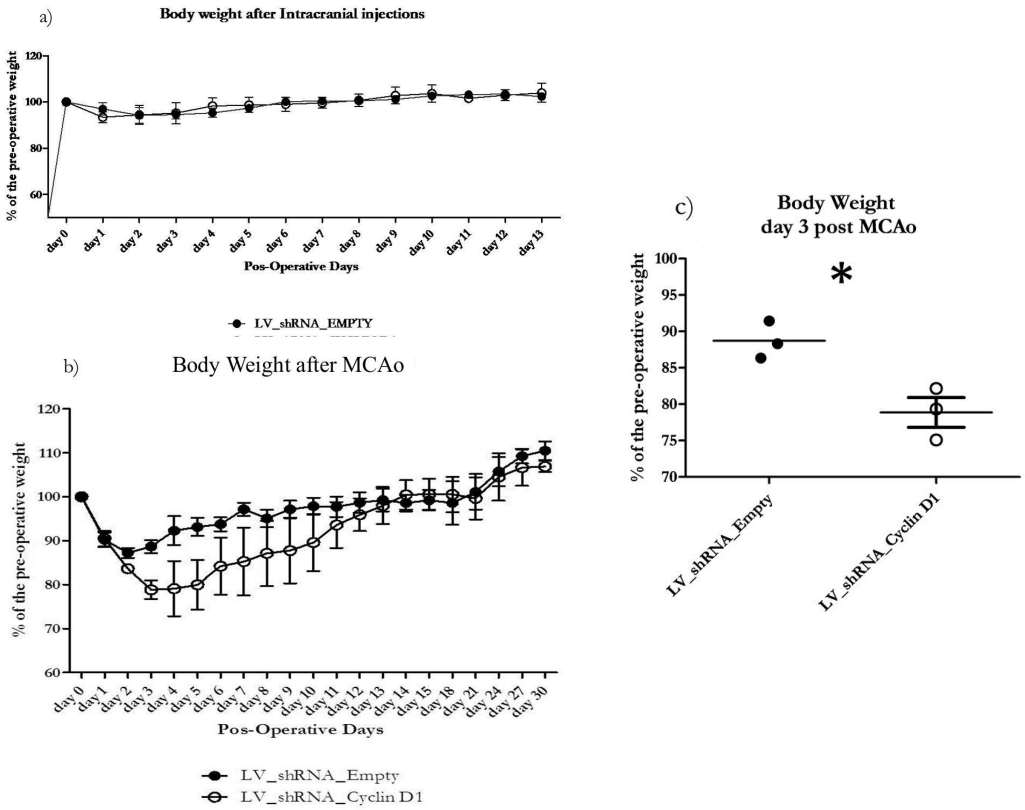

Figure 6.f22. Body weight variation after surgical procedures: LV_shRNA_CyclinD1 injected group.

Analysis of the variation of the body weight in the survival populations. There was no difference in the groups after the intracranial injections (part a) of the picture), although after 1h_MCAo there was a trend to delay the weight rescue for the LV_shRNA_Cyclin D1 injected group (part b) of the picture). Values represent mean ± SEM; analysis by the two-way ANOVA. The variation of the body weight was significantly different at day 3 post 1h_MCAo, *$p<0.005$; analysis by the Student's t test (part c) of the picture). For the LV_shRNA_CyclinD1 group n=3, and for the LV_shRNA_Empty group n=3.

6.4.7 TREND TOWARDS IMPROVED NEUROLOGICAL RECOVERY IN IDLV_GDNF AND IDLV_TTC

Post ischemic neurological improvement was assessed as previously described in Chapter 2.

From a first analysis of survivors both the IDLVs treated groups, GDNF and TTC, presented a reduction of the post-operation neurological improvement compared to the control (Figure 6.f23). The neurological improvement was analysed by the Mann-Whitney rank sum test that demonstrated a statistically reduction of the sensorimotor recovery after 1h_MCAo; ***$p<0.001$ for IDLV_TTC and ** for IDLV_GDNF, both compared to the control group.

After a detailed analysis of the subjects, a trend of surviving and of proportionally reducing damage was associated with the growth factor treated groups, especially for IDLV_GDNF. Because the control group lost many animals with a severe and intermediate ischemia, only mildly affected subjects were able to survive until day 30 post MCAo, while the survivors of the growth factors treated groups also comprised subjects with an intermediate stroke. In such circumstances the groups under comparison are extremely diverged in terms of stroke severity, in turn affecting the response to the treatments and the following statistical analysis.

To avoid a misleading data analysis due to an imbalance between the control and the growth factor-treated groups, the first five days were considered to have a bigger population with similar characteristics to compare. The analysis of the subjects alive at least until day 5 post 1h_MCAo showed a trend of improving neurological outcome after ischemia, for both the IDLV_GDNF and IDLV_TTC treated groups (Figure 6.f24 and Figure 6.f25). This trend for IDLV_GDNF injected

group was associated to p=0.065 by the Mann-Whitney rank sum test (Figure 6.f24).

Figure 6.f26 shows the entire data set of the neurological recovery for the MCAo animals under analysis. From the plots is possible to evaluate the MCAo effect on the sensorimotor behaviour across the first 7 post-operative days. The treatment with the IDLV_GDNF tended to reduce the severity of the ischemia, as shown by the reduced average and lower variability for the 0-28 focal deficit score. Moreover, the intermediate ischemic subjects that had been treated with the IDLV_GDNF survived longer compared to the other subjects with the same ischemic severity but that received a different treatment, Figure 6.f26.

The analysis of the body weight did not highlight any difference after the intracranial injections for the IDLV_GDNF and IDLV_TTC groups, although the body weight tended to be lower in the IDLV_TTC injected group (part a) of Figure 6.f27). In addition, after 1h_MCAo these groups showed a trend towards reduced post-operation weight, both in comparison with the control group (part b) and c) of Figure 6.f27); the analysis was performed by the two-way ANOVA. Day 3 and 4 were further analysed by the Student's t test that demonstrated a significant reduction of the body weight of the IDLV_GDNF treated group compared to the control, **$p<0.01$ (part d) and e) of Figure 6.f27).

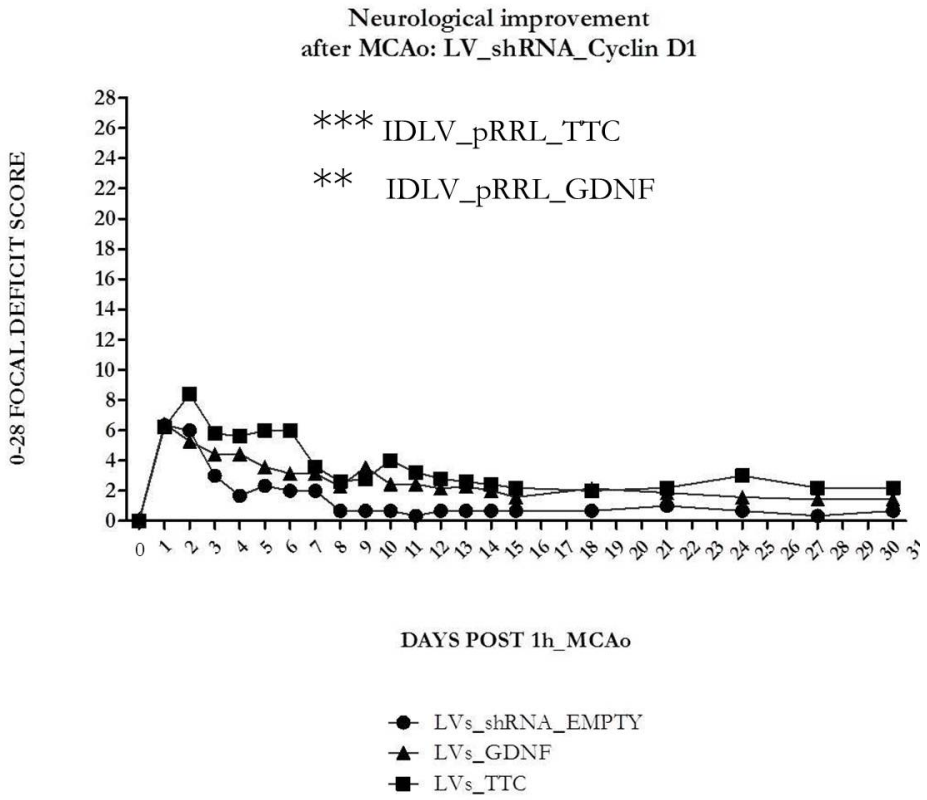

Figure 6.f23. Paradox of the neurological deterioration in the growth factor-treated groups: effect of IDLV_GDNF and IDLV_TTC.

Analysis of the animals survived for 30 days after 1h_MCAo. Neurological improvement was assessed on a daily basis by the 0-28 focal deficit test. There was a paradoxical increased of the ischemic phenotype for the growth factors treated groups. The curves were analysed by the Mann-Whitney rank sum test that assigned **$p<0.001$ for the difference between the LV_shRNA_Empty and the IDLV_GDNF; while ***$p<0.0001$ for the LV_shRNA_Empty and the IDLV_TTC. Values represent the mean of the ranks at specific time points after 1h_MCAo. For the LV_shRNA_Empty group n=3, for the IDLV_GDNF group n=7 and for the IDLV_TTC group n=5.

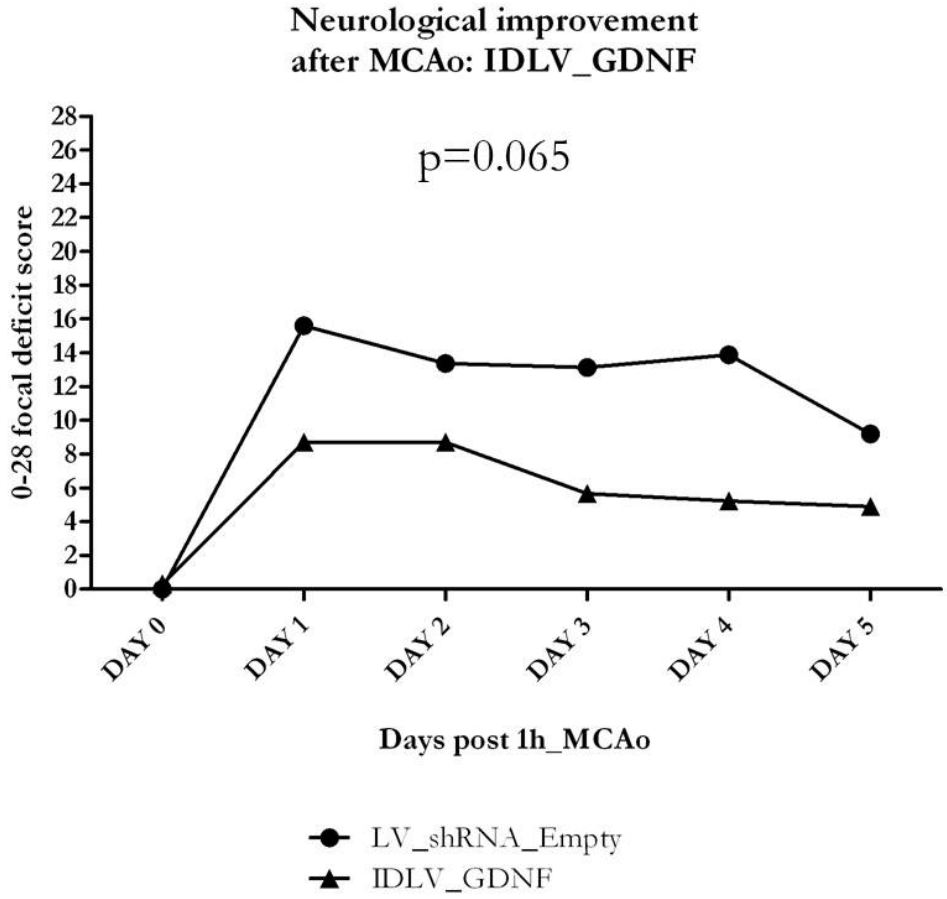

Figure 6.f24. Neurological recovery during the first five days after 1h_MCAo: IDLV_GDNF injected group.

Evaluation of the ischemic phenotype for subjects survived until day 5 post surgery. The analysis revealed a trend of improving the sensory-motor performance in the IDLV_GDNF treated group. Values represent the rank's mean, p=0.065, Mann-Whitney rank sum test. LV_shRNA_Empty group *n*=7, IDLV_GDNF *n*=9

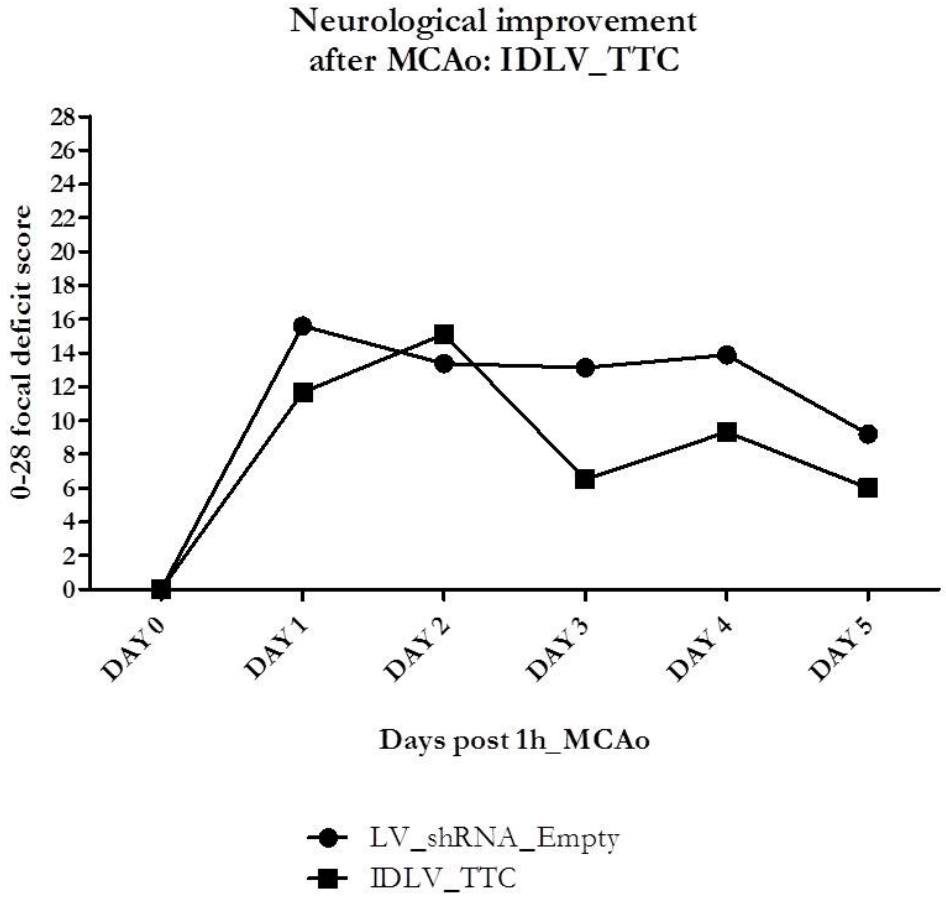

Figure 6.f25. Neurological recovery during the first five days after 1h_MCAo: IDLV_TTC injected group.

Evaluation of the ischemic phenotype for subjects surviving until day 5 post surgery. The analysis revealed a trend of improving the sensory-motor performance in the IDLV_TTC treated group. Values represent the rank's mean, p=0.11, Mann-Whitney rank sum test. LV_shRNA_Empty group *n*=7, IDLV_TTC *n*=6

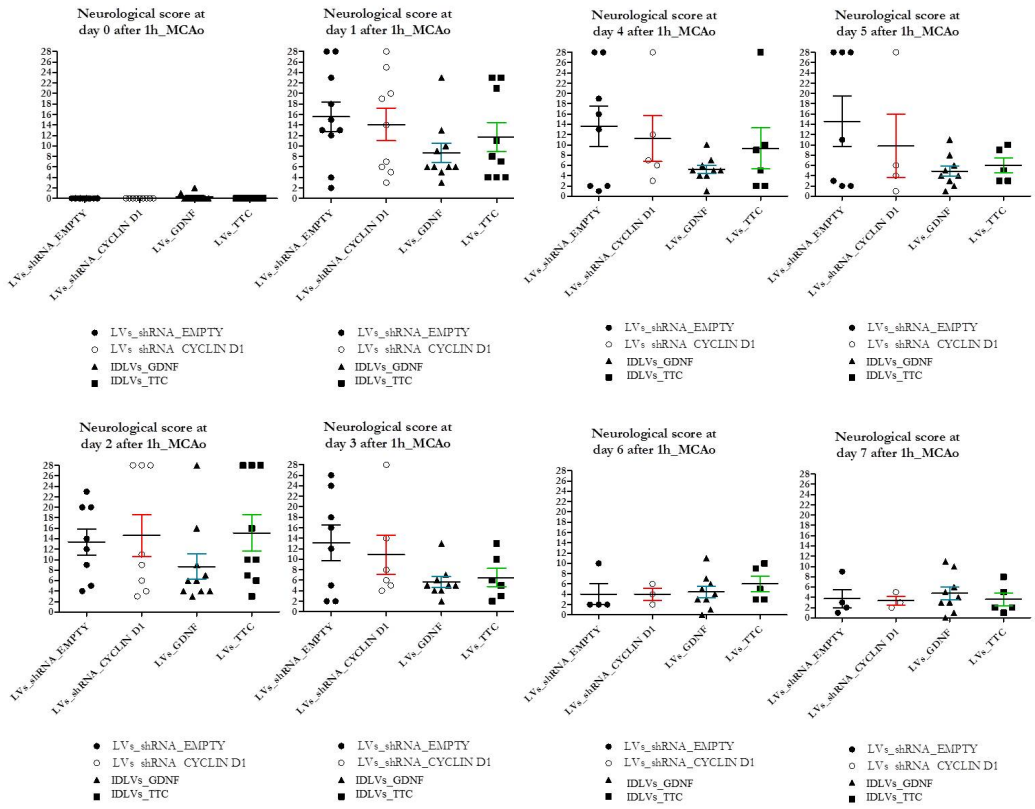

Figure 6.f26. 0-28 Focal deficit test dot plots evaluation.

The plots above show how the developing over time of the ischemic phenotype after 1h_MCAo; this was evaluated on the survival fraction by the 0-28 focal deficit test. The plots were analysed by the Mann-Whitney rank sum test but not difference between groups was found statistically significant at any time point.

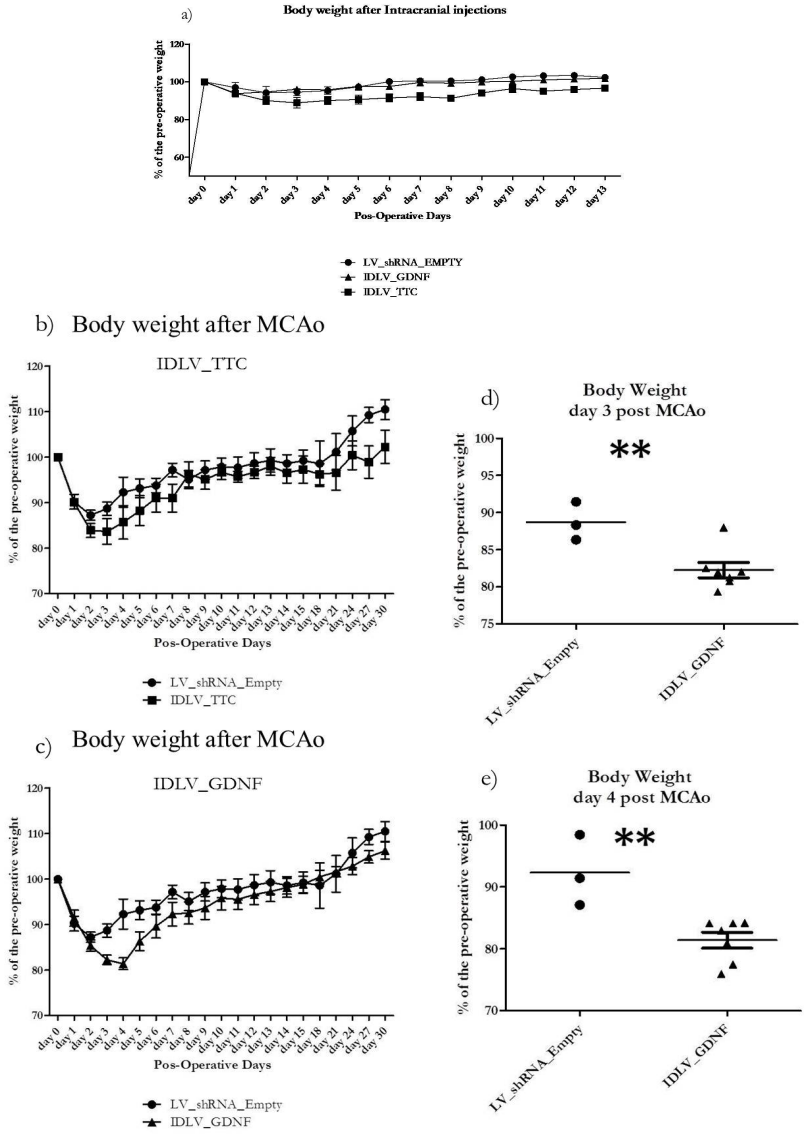

Figure 6.f27. Body weight variation after surgical procedures: IDLV_pRRL GDNF and IDLV_pRRL TTC injected groups.

There was no difference in weight variation developed after intracranial injections. In addition, no statistically different body weight variation was observed after 1h MCAo, even though a trend of reduced weight gain occurring post-operation was evident in both groups (b) and c) of the picture). Values represent mean ± SEM; analysis by the two-way ANOVA. The IDLV_GDNF treated group was further analysed at post-operational day 3 and 4 by the Student's t test; statistically significant body weight reduction in the animals treated with the IDLV_GDNF either at day 3 and 4 after 1h_MCAo, **$p<0.01$ (part d) and e) of the picture). For the IDLV_GDNF group n=7, for the IDLV_TTC n=5 and for the LV_shRNA_Empty group n=3.

6.4.8 SURVIVAL PROPORTION

Although a large proportion of subjects died across the experiment because of the ischemia, the LVs treated groups tended to deviate from the expected number of deaths depending on the treatment received.

Only 40% of subjects in the control group survived the experiment (30 days post 1h_MCAo). The survival rate was 33% for the LV_shRNA_CyclinD1, 55% for the IDLV_TTC and 70% for the IDLV_GDNF.

The comparison between the LV_shRNA_CyclinD1and the IDLV_GDNF by the Gehan-Breslow-Wilcoxon Test, demonstrated significant difference survival proportion between groups, *$p<0.05$, (Figure 6.f28).

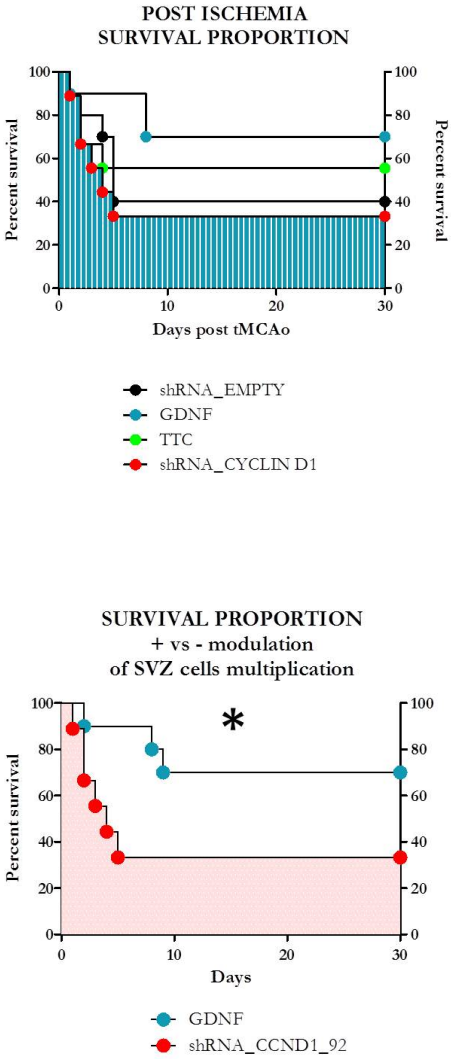

Figure 6.f28. Survival proportion.

Treatments affect survival proportion: 33% for the LV_shRNA_Cyclin D1 group, 70% the IDLV_GDNF, 55% the IDLV_TTC and 40% the LV_shRNA_Empty group. The curves were analysed in pair by the Gehan-Breslow-Wilcoxon Test; there was significant different survival fraction between the IDLV_GDNF and the LV_shRNA_Cyclin D1 treated groups, *p<0.05.

6.4.9 TREATMENTS ALTERING THE SURVIVAL EXPECTANCY

The survival expectancy is the probability of surviving with a defined ischemic status. For instance, for an extremely severe stroke (for instance a 20 score by the 0-28 focal deficit test), it is very unlikely that survival will last for more than 36 hours. In other words there is a negative correlation between the ischemia severity and life expectancy.

This analysis was performed by associating the ischemic severity, behaviourally assessed at day 2[12] post stroke, with the number of days the animals survived post-surgery. The modulation of the SVZ neurogenesis by LVs and IDLVs affected the life expectancy in MCAo animals. A $**p<0.01$ and a $\rho=-0.84$ was associated to the control group; this means there is a negative correlation between the ischemia severity and life expectancy. Animals treated with the LV_shRNA_CyclinD1 showed a stronger correlation with $***p<0.001$ and $\rho=-0.928$. On the other hand the treatment with the growth factors reduced this negative correlation: IDLV_GDNF was $*p<0.05$ with $\rho=-0.644$ and the IDLV_TTC was $*p<0.05$ with $\rho=-0.732$, Spearman's rank Correlation Coefficient (Figure 6.f29).

[12] Day 2 was selected because generally it was the day the animals presented the highest sickness score, in terms of behaviour and frequency of death. After day 2 they tended to start the recovery.

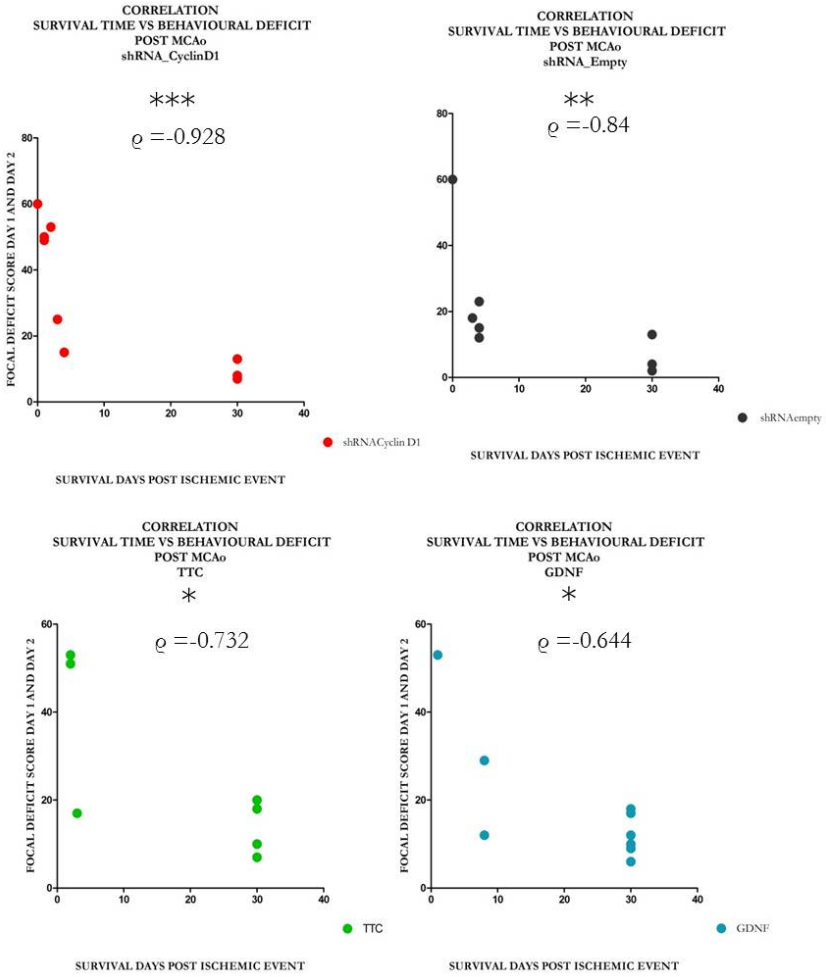

Figure 6.f29. Life expectancy

Spearman's rank Correlation Coefficient between the neurological phenotype, estimated by the 0-28 focal deficit test at day 2, and the number of days the animal survived post ischemia. There was a statistically significant correlation between the ischemia severity and the number of days the subjects survived after 1h_MCAo; for the LV_shRNA_Empty treated group, **$p<0.01$ and ρ[13]$=-0.84$. The modulation of the SVZ neurogenesis by LVs and IDLVs affected this correlation. The LV_shRNA_CyclinD1 was ***$p<0.001$ and $\rho=-0.928$, the IDLV_GDNF was *$p<0.05$ and $\rho=-0.644$ while the IDLV_TTC was *$p<0.05$ and $\rho=-0.732$. LV_shRNA_Empty group n=10, IDLV_GDNF n=10, IDLV_TTC n=9 and LV_shRNA_CyclinD1 n=9.

[13] . The ρ value quantifies the direction and magnitude of the correlation

6.4.10 SPEARMAN'S RANK CORRELATION COEFFICIENT BETWEEN THE BEHAVIOUR SCORE AT DAY 30 AND THE ISCHEMIC VOLUME ESTIMATION

The Spearman's rank correlation coefficient analysis was performed between the score assigned to the animals the last day they were alive and the related ischemic volume. As shown by Figure 6.f30 there is a positive correlation between the two variables, $*p<0.05$ with $\rho=0.5$.

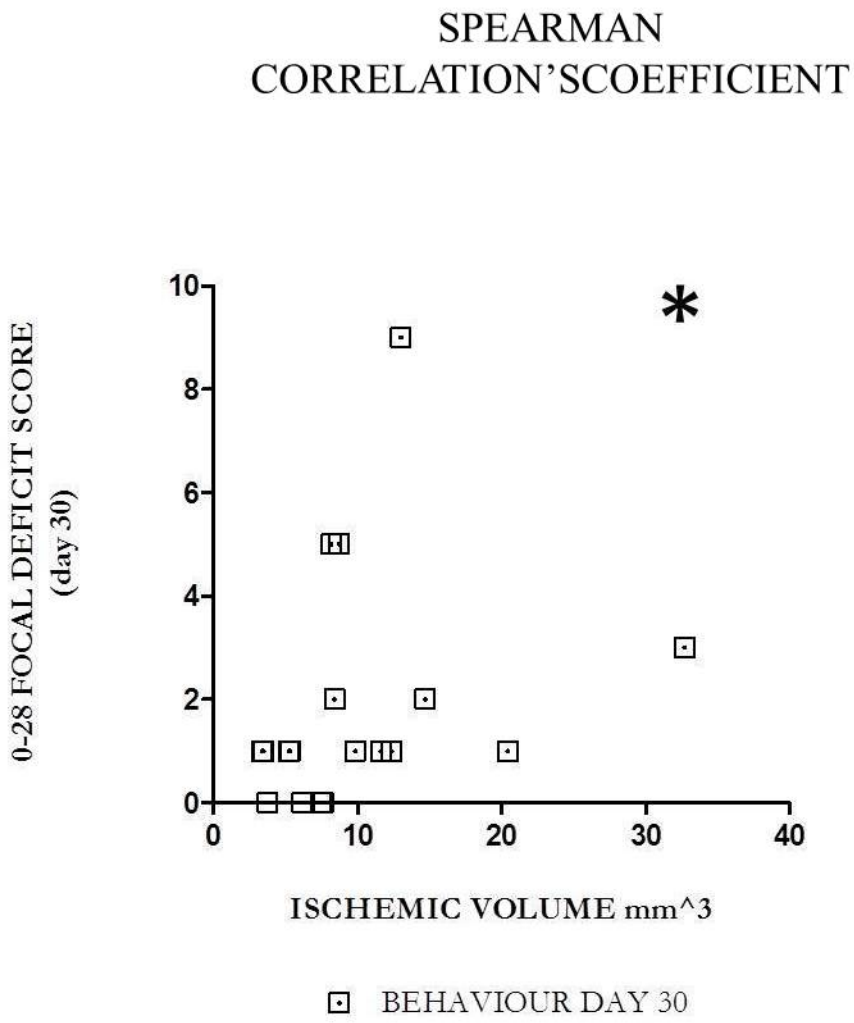

Figure 6.f30. Evaluation of the analysis: correlation between the behavioural score at day 30 and the ischemic volume quantification.

The correlation between the behavioural phenotype assessed by the 0-28 focal deficit test and the ischemic volume quantification was performed by the Spearman's rank Correlation Coefficient. There is a significant correlation between the parameters analysed, *$p<-0.05$ with $\rho=0.5$.

6.4.11 CONCLUSION

The injections of LVs and IDLVs in the SVZ were efficient tools to detect and monitor NPCs in the ischemic brain over a long time period (up to 30 days) (Figure 6.f1 to Figure 6.f9).

Suppression of Cyclin D1 by the LV_shRNA_CyclinD1 efficiently inhibited neurogenesis of the SVZ as demonstrated by the low numbers of eGFP positive cells in the OBs and in the ipsilateral region (Figure 6.f2 and Figure 6.f5). The number of eGFP-positive cells in the ischemic regions was significantly lower than in the control injected with empty vector, **$p<0.01$ by the Student's test (Figure 6.f14).

The eGFP positive cells were mainly found in the aca, CPu, cortex and corpus callosum (Figure 6.f2, 6.f6, 6.f7 and 6.f8). The maximum distance SVZ-derived cells were found from the SVZ was 1.17 mm in striatum (Figure 6.f6) and in the cortex was 1.87 mm (Figure 6.f7).

Groups of eGFP positive cells like neurogenic islands were found in the cortex and striatum (Figure 6.f6 and Figure 6.f7).

EGFP positive cells were found in the ipsilateral aca (Figure 6.f5). Moreover, the SVZ expansion was positive for DCX and eGFP and it was extended to the aca in the ispilateral but not the contralateral hemisphere; this suggests a possible radial migratory pathway for the NPCs (Figure 6.f9) (Gotts and Chesselet 2005).

The inhibition of neurogenesis in the SVZ by LV_shRNA_CylinD1 did not alter the recovery of body weight or behavioural function after the intracranial injections, but delayed the restoration of the pre-ischemic weight after 1h_MCAo (Figure 6.f22). Moreover, the neurological improvement was statistically lower than the control and growth factors

treated groups, *p<0.05, Mann-Whitney rank sum test (Figure 6.f20). The "SVZ neurogenesis inhibition group" (i.e. CyclinD1-suppressed) drastically reduced its number of animals that survived across the first 5 days post 1h_MCAo (Figure 6.f21).

IDLV_GDNF and IDLV_TTC injected in the wall of the lateral ventricles increased the number of the intermediate ischemic subjects surviving the experiment. These subjects were able to improve their initial neurological conditions, mostly evident during the first five days post stroke (Figure 6.f24 and Figure 6.f25).

From a first analysis of the survivors after 30 days of reperfusion a paradoxical worsening of neurological recovery became apparent (Figure 6.f23). This impoverishment was found statistically different to the control, respectively **p<0.01 for the IDLV_GDNF and ***p<0.001 for IDLV_TTC; analysis by the Mann-Whitney rank sum test.

MCAo is a very efficient model of stroke although high variability of ischemia severity is intrinsic to the model itself. For instance in a group of MCAo animals produced under the same conditions, three subgroups based on the damage severity and location can be recognised: the mild, the intermediate and the severe ischemic group. Each of these responds differently in terms of survival ability and post operation recovery. In this experiment the modulation of the SVZ strongly affected the ability of the subgroups to respond to ischemia, by means the IDLV_GDNF increased life expectancy for the intermediate ischemic subgroup and improved conditions in the mild animals. The comparison with the control group, which lost all the intermediate and severe subjects during the first ten days post operation, resulted in a misleading data analysis by which the treatment with growth factors looked to reduce the neurological recovery. Some laboratories avoid complications like this by a selections of the subjects based on the location and the damage size severity (Smith,

Stroemer et al.). In this project, due to the limited number of animals available, a proper selection of the subjects with similar ischemic characteristics was not possible as it would lead to insufficient statistical power. For this reason an analysis of the first five days post-surgery was performed in order to have more subjects to compare with similar features (Figure 6.f24 and Figure 6.f25).

The analysis of the animals that survived up to day 5 after MCAo and treated with LV_GDNF, showed a reduced ischemic phenotype ($p=0.065$) (Figure 6.f24).

Accordingly the number of survivors with an intermediate severe lesion, and therefore a delay of the reduction of the inflammation process and brain restoration, the IDLV_GDNF as well as the IDLV_TTC injected groups presented a statistically significant increase of the inflammation volume,*$p<0.05$, Student's t test (Figure 6.f10).

Because the LV_shRNA_CyclinD1 lost many subjects with an intermediate severe lesion already during the first 5 days after MCAo, while the control group still had subjects with an equivalent damage at the same time point, the comparison between these two groups at early stage was considered misleading, since compared groups with different stroke severity and for this reason was not introduced in this manuscript. The analysis of the survivors after 30 days post MCAo resulted in more balanced conclusion because it only included milder subjects in both groups.

The treatments differed in the survival proportion. Comparing to the control group that had a survival rate of 40%, the SVZ neurogenesis inhibition group (LV_shRNA_CyclinD1 injected) had only 33%, the neurogenesis augmented group (IDLV_GDNF) had 70% and the IDLV_TTC ended the experiment with 55% of subjects surviving. A

comparison between the effect of IDLV_GDNF and LV_shRNA_CycinD1 showed there was a significant trend to increase or decrease (respectively) survival rate depending on how the neurogenesis of the SVZ responded, *$p<0.05$ (Figure 6.f28).

The modulation of the SVZ produced variation in the animal's life expectancy. The severity of the ischemia was negatively correlated with the number of days the subject survived after the injury, as the Spearman's rank correlation coefficient proved for the LV_shRNA_Empty, **$p<0.01$ with $\rho=-0.86$. The negative correlation can change in magnitude depending on the modulation of the progenitors proliferation in the SVZ; the neurogenesis boosting by IDLV_GDNF reduced the negative correlation with *$p<0.05$ and $\rho= -0.644$, while the LV_shRNA_CyclinD1 increased it with ***$p<0.001$ and $\rho=-0.928$. IDLV_TTC also reduced the negative correlation with *$p<0.05$ and $\rho=-0.732$ (Figure 6.f29).

IDLV_GDNF injection close to the wall of the SVZ improved the natural response of neurogenesis to ischemia. The hypothesis that there is a positive linear correlation between the lesion severity and the ability of the SVZ to respond to ischemia was evaluated by a linear regression. Although it was not possible to assess a significant correlation between these variables in the control group, a strong correlation was statistically significant in the IDLV_GDNF treated group, *$p<0.05$ with $R=0.68$ by linear regression analysis (Figure 6.f18). Further studies on the correlation between the number of eGFP cells and the neurodegeneration volume demonstrated a strong relationship with ***$p<0.001$ and $R=0.92$; no correlation was found between the number green cells and the volume of glial scar, nor between the number of green cells and the volume occupied by activated microglia (Figure 6.f19).

The analysis of the body weight variation did not highlight any difference after the intracranial injections, even though the IDLV_TTC

treated group tended to have a reduced body weight already at this stage (part a) of Figures 6.f22 and 6.f27). The neurogenesis boosting and inhibiting groups showed a trend to reduce the body weight recovery comparing to the control, this was particularly evident during the first week after MCAo. The group treated with the LV_shRNA_Cyclin D1 presented a statistically significant reduced body weight at day 3 after 1h_MCAo (part c) of Figure 6.f22), for which *$p<0.05$ was estimated by the Student's t test. In addition, the animals treated with the IDLV_GDNF reduced the body weight at day 3 and 4 after 1h_MCAo, for which **$p<0.01$ was assigned by the Student's t test (part d) and e) of Figure 6.f27).

The histology and behavioural analysis was validated by the Spearman's rank Correlation Coefficient, which demonstrated a statistically significant data correlation, *$p<0.05$ with $\rho=0.5$ (Figure 6.f30).

CHAPTER 7

7.1 DISCUSSION

Neurogenesis occurs in physiological as well as pathological conditions and it has been demonstrated in rodents and mammals (Bovetti, Gribaudo et al.; Wang, Zhang et al.; Lennington, Yang et al. 2003; Yamashita, Ninomiya et al. 2006). Although in physiological conditions the role of neurogenesis has mostly been clarified (Whitman and Greer 2009; Shruster, Melamed et al. 2010; Yoshizaki and Osumi 2010), in pathological conditions, for example after stroke, it is still not completely understood.

Neurogenesis occurs post ischemia, but the newly-generated neurons tend to die during the first two weeks after injury (Lindvall and Kokaia 2004). Moreover, the production of glial cell types from SVZ progenitors is also possible (Voigt 1989; Zhang, Zhang et al. 2004; Menn, Garcia-Verdugo et al. 2006)

Determining the role of neurogenesis in the SVZ would allow a better understanding of the brain's functions and help to guide possible therapeutic strategies to improve stroke patients' conditions. Motivated by these reasons this project intended to compare the effect of positive and negative modulation of SVZ neurogenesis on the outcome following focal brain ischemia.

The first achievement of this study was the production of an efficient cell cycle inhibitor system based on LVs, which was designed to be used in vivo to block proliferation of the SVZ progenitors. The system was centred on the inactivation of the Cyclin D1 protein, which is a vital participant in G1 phase of the cell cycle; the inhibition of the Cyclin D1 activity is responsible for to the cell cycle arrest (Fu, Wang et al. 2004; Lange and Yee 2011).

The first method tested was a dominant negative isoform of Cyclin D1 that was cloned into a third generation Lentiviral backbone, and packed into LVs. This strategy was not successful, possibly due to two unexpected extra mutations in the dominant negative Cyclin D1. The results from the in vitro studies did not show any convincing effect of the LV_dnCyclinD1 on the NIH3t3 cell, evaluated by Western Blot and MTT cell viability assay.

The second strategy adopted was based on a shRNA directed against the Cyclin D1 mRNA, originally cloned into a second generation Lentiviral backbone by Thermo Scientific and packed in LVs. This G1 blocking system was validated in vitro by Western Blot analysis and MTT cell viability assay. Both investigations in agreement showed down regulation of the target protein and an efficient effect on cell proliferation and apoptosis.

The mouse MCAo model was evaluated by different occlusion times in order to achieve an optimal ischemic model for long-term study. These experiments were important to allow the best model selection and to optimize post-operative care strategies. As described by Modo et al. (2000), animal care after the ischemia is crucial for the achievement of a successful experiment (Modo, Stroemer et al. 2000); MCAo is a very invasive procedure that needs some careful post-operative care in order to maximize life expectancy. On the other hand the analysis of the occlusion time was pivotal to establish which model was the best in terms of high survival rate with sufficient ischemic damage.

The MCAo is a very well established model, and has been in use since 1975 (Robinson, Shoemaker et al. 1975). One of the major issues with the model is the reproducibility of the infarct incidence and the lesion severity (Bederson, Pitts et al. 1986). There have been many studies focused on developing tools to recognize the source of variability, and in turn modify

the experimental procedure to improve the model. In 1986 Bederson et al. tried to address the problem by looking at variation of cannula insertion in relation to the damage produced. They recognized that uniform severe infarction only occurred when the MCA was occluded from its origin to the junction with the inferior cerebral vein. When the occlusion started at 2 mm proximal to the MCA origin, the uniformity of the damage in the group was already compromised (Bederson, Pitts et al. 1986). The Middle cerebral artery in the rodent is located on the surface of the olfactory tract; from this first tract multiple branches originate and diverge to supply blood to different brain regions. For example, the medial perforating and the leticulo-striate originate between the beginning of the MCA and the lateral edge of the olfactory tract; these branches provide blood to the posterior part of the caudate-putamen complex. Conversely the anterior part of the caudate-putamen complex receives blood from the lateral striated branches originating from the MCA and from the Hubner's arteries that originate from the anterior cerebral artery (ACA) (Tamura, Graham et al. 1981).

Considering the entry site for the cannula at the carotid artery level, the surgery is considered performed once the cannula reaches the beginning of the MCA at the level of the olfactory tract; a proper blockage at this point ensures that all branches are blocked as well. Although all surgeries are performed in the same way, and the cannula is held in place by a suture on the main carotid artery (close to the entry site), movements are still possible (for example due to a convulsion or animal rotation) and these can be responsible for sliding the cannula down from the original site.

Although the two models investigated, the pMCAo and the tMCAo, are both considered highly variable, in the temporary occlusion the restoration of blood flow is responsible for augmenting the cerebral damage and introducing variability. The cerebral flux restoration or reperfusion, can produce physical (due to the effect of the restored flux high pressure on the cerebral tissue) and chemical (oxidative stress, ROS production from

mitochondria) damage (Jung, Kim et al. 2010). Each tMCAo animal can experience a completely different damage induced by reperfusion; this can be dependent on the pressure of the restored flux as well as the oxidative stress and the amount of the ROS can vary. These parameters are subject-specific and are very likely responsible for the increased variability observed in the temporary occlusion model (Heiss 1987; Badruddin, Taqi et al. 2011)

In this study the major concern regarding the permanent occlusion was the extremely high incidence of death observed during the first 36 hours. In addition, a proper recovery was not observed for the surviving subjects. Since this project originated with the intention of understanding the possible relationship between SVZ neurogenesis and recovery, we concluded that the temporary occlusion model (1 hour of occlusion) was the most suitable in terms of ischemic phenotype, long-term survival and recovery capability.

The neurogenesis augmentation systems were based on IDLV encoding for a precursor GDNF or a TTC cassette. In previous experiments Dr. Ahmed, who produced these transfer plasmids, demonstrated the *in vitro* effectiveness for both systems.

The use of the IDLVs to deliver either the GDNF or the TTC cassette, was driven by the needs to assess the effect of the SVZ neurogenesis rather than the effect of the growth factors on the ischemic areas. Since the IDLV does not integrate into the host genome, in mitotically active populations, such as the SVZ neurogenic islands, the vector should be diluted out through sequential cell divisions (Wanisch and Yanez-Munoz 2009). In addition, the progenitor cells that originate in the SVZ leave the neurogenic area to reach the ischemic boundaries. In such circumstances the IDLVs containing the growth factors GDNF or TTC should remained localized, and are supposed to promote proliferation only surrounding the

injection site. The LV carrying the eGFP cassette was co-injected with the IDLVs, integrates the viral DNA into the host genome and is retained through cellular proliferation. For this reason eGFP is detectable not just surrounding the injection sites, but also in the migrated population found in the ischemic regions and the OBs.

In order to prove the effect of the neurogenesis modulator systems based on LVs and IDLVs *in vivo,* normal c57/bl6 mice were injected at the beginning of the RMS. Three weeks later the animals were killed to detect and quantify NPCs migrated at OBs level; technique reported by Goncalves et al. 2007.

Many laboratories have attested that GDNF improves post-ischemic recovery; it was widely applied to improve stem cell transplantation (Chen, Gao et al. 2009; Lee, Park et al. 2009; Shen, Li et al. 2010), to stimulate SVZ neurogenesis by intra-cerebral infusion (Dempsey, Sailor et al. 2003; Kobayashi, Ahlenius et al. 2006), and to reduce edema and infarct size (Abe 2003). All these studies proved an effect of the GNDF in ischemic condition, although a direct action on the NPCs multiplication was not yet proved. The treatment in absence of stroke demonstrated a direct effect of GDNF on the NPCs multiplication in ependymal layer, for which $*p<0.05$ was assigned (comparison to the control), analysis by the Student's t test.

The TTC fragment has been described as a factor involved in the relocation of exogenous GDNF and IGF-1 (mature isoform) to the extracellular space after translation, with the effect of improving survival of degenerating neurons in rodents (Larsen, Benn et al. 2006; Roux, Saint Clement et al. 2006; Chian, Li et al. 2009; Li, Chian et al. 2009; Moreno-Igoa, Calvo et al. 2012). In addition, it has been reported in an ALS mouse model to reduce the decline in hindlimb muscle innervation and in turn to delay the disease onset (Moreno-Igoa, Calvo et al. 2010). The purpose of

this study was to understand the possible applicability of the TTC fragment to stroke therapy. Although, due to the high variability it is not possible to completely exclude an augmentation of the SVZ neurogenesis after the TTC treatment and in absence of stroke, a significant effect was not statistically demonstrated. On the other hand, at least some of the subjects treated with the IDLV_TTC had a strong boost of the SVZ proliferation.

The purpose of this study was to understand the importance of the endogenous neurogenesis occurring in stroke by inhibition of the NPCs cell cycle. Although some studies already attempted a similar investigation by localized irradiation of the SVZ cells (Lazarini, Mouthon et al. 2009; Achanta, Capilla-Gonzalez et al. 2012), this project has the merit to be the first achieved the sub-ependymal layer cell cycle inhibition by lentiviral vector. The advantage of this system is the specificity of the target by which only NPCs are affected by the treatment; only mitotic cells transcribed and transduce Cyclin D1 for the cell cycle regulation, ensuring no effect for the post-mitotic cells in the surrounding area. The injection at RMS level proved the strength of the cell cycle regulation by Cyclin D1; for instance the mRNA inhibition was able to almost completely inhibit NPCs multiplication, estimated by quantification of the migrated cells at OBs level, (***$p<0.001$, Student's t test).

The neurogenesis modulation systems were used to assess the role of the SVZ proliferation on stroke recovery. In this study the vectors were co-injected at SVZ level and the MCAo was performed fourteen days later. The animals' behaviour was observed for one month to detect the influence of the treatments on recovery, and then an histological evaluation was performed in order to assess ischemia, and to detect in this area the neural progenitor cells SVZ derived.

The SVZ derived eGFP+ cells were found in the aci, aca, GrO, CPu, sensorimotor cortex, SVZ and corpus callosum. The maximum distance

from the SVZ, where the migrated eGFP expressing cells were found, was in the cortex, 1.87 mm away; this long migration was in agreement with preceding publications (Yamashita, Ninomiya et al. 2006; Zhang, LeTourneau et al. 2007; Kreuzberg, Kanov et al. 2010; Young, Brooks et al. 2011).

In accordance with the literature, we recurrently found eGFP positive cells toward the aca (Gotts and Chesselet 2005). Moreover as shown in Figure 6.f9, the DCX positive cells migrating from the ependymal layer at the bottom of the third ventricle, to the aca ventrally localized, suggest a possible migratory pathway induced after ischemia. In agreement with previous publications, we hypothesized that at least some of the cells utilized the aca for migration, similarly with the migration occurring through the corpus callosum in the same conditions (Imitola, Raddassi et al. 2004; Gotts and Chesselet 2005).

As described before, we found migrated cells in the cortex and striatum; moreover eGFP positive cells were localized across the corpus callosum and anterior commissure. It might be possible in addition to the radial migration; the NPCs use the commissure and the corpus callosum as "free way" to drive into the neuronal tissue and reach the ischemic environment.

As Yamashita et al reported previously, some of the cells migrated from the SVZ were found in the ischemic cortex and striatum were spread through the tissue, while others were grouped-like neurogenic islands (Yamashita, Ninomiya et al. 2006).

In agreement with previous *in vivo* and *in vitro* experiments, the LVs and IDLVs efficiently affected the SVZ progenitors multiplication; this was estimated based on the number of the eGFP positive cells migrated in the ischemic environment after ischemia. The animals pre-treated with LV_shRNA_CyclinD1 presented an extremely reduced number of eGFP

positive cells in the ischemic regions, for which **p<0.01was assigned. Conversely, a statistically significant increase of eGFP positive cells was estimated for the animals treated with IDLV_GDNF, *p<0.05. The IDLV_TTC, as already reported in the previous *in vivo* experiment, showed an extremely high variability; in addition the low number of survivors (n=10, 5 survivors) did not allow any reliable estimation of the treatment effect. For these reasons and although the increased variability within the survival fraction, it was not possible to evaluate the effect of the treatment. These analyses were performed by the Student's t test.

In the IDLV_GDNF treated group the number of eGFP+ cells migrated into the ischemic regions after stroke was positively correlated with the damage volume, *p<0.05 with R=0.68, by linear regression analysis. Moreover, a further analysis between the eGFP+ cells and each specific component of the ischemic environment, revealed a strong correlation exclusively with the neurodegeneration fraction (core region), ***p<0.001 and R=0.92, but not with the glial scar or the microglia covered volume. From the literature, it is known that SVZ proliferation is highly regulated by factors and compounds acting over long distances. This regulation occurs lifelong in physiological conditions; for example, the OBs induce multiplication and migration of the SVZ progenitors toward the RMS (Kazanis 2009). In a very similar way and in pathological conditions, for example after stroke or a traumatic brain injury (TBI), the SVZ progenitors are induced to multiply and migrate toward the lesion area (Kernie and Parent 2010; Luzzati, De Marchis et al. 2011). It is also well known that the ischemic environment produces factors involved in controlling SVZ proliferation and migration (Salazar-Colocho, Lanciego et al. 2008; Whitney, Eidem et al. 2009; Yoneyama, Shiba et al. 2011). Since diverse cellular populations compose the ischemic environment, the data presented in this study support the hypothesis of a tight regulation of SVZ proliferation dependent on the core region (neurodegenerative area). It might be possible that, analogue to the activated astrocytes that produce

chemokine like SDS-1 to induce migration of the NPCs, the core region acts long distance on the ependymal cells proliferation (Hill, Hess et al. 2004; Jaerve and Muller 2012; Wang, Huang et al. 2012).

The pre-treatment of the SVZ with the IDLV_GDNF increase the survival rate while LV_shRNA_Cyclin D1 reduced it; the survival curves in these two groups were statistically different. Moreover, the life expectancy, defined as the ability to survive with a defined ischemic status, was increased when subjects were treated with IDLV_GDNF, as well as it decreased when the treatment was LV_shRNA_CyclinD1.

Take in consideration the limited investigation power allowed by the selected behavioral test (0-28 focal deficit test), the groups were analyzed and compared using non-parametric statistic. MCAo animals previously injected with the LV_shRNA_CyclinD1 were compared to the control group for the sensorimotor phenotype. The analysis demonstrated a significant increase in the ischemic phenotype and delay of recovery evaluated by the Mann-Whitney rank sum test, $*p<0.05$. This analysis was performed on the fraction of survivors.

MCAo animals previously injected with the IDLV_GDNF or IDLV_TTC and survived for thirty days after the ischemia were initially evaluated for the sensorimotor impoverishment. From this preliminary investigation, the groups treated with the growth factor and TTC had a significant reduction in the sensory-motor performance when compared to the control ($**p<0.01$ for IDLV_GDNF and $***p<0.001$ for IDLV_TTC). Considering the survival rate (70% in the GDNF and 55% in the TTC versus 40% in the control) and the improvement of the life expectancy, but conversely the reduced post-operative body weight and the significant increase in inflammation volume, we hypothesize a selection agent affected the survival fraction in these groups. Despite the longer survival, these subjects were still highly ischemic, while the same sub-population in

the control group was already dead after the first week post MCAo. In these conditions the comparison between groups was highly unbalanced because attempted to compare subjects with different brain damage severity (and different location), which may have significantly skewed the results. Following on this, the animals that survived at least until day 5 after ischemia were analysed for the sensorimotor behaviour. Under these circumstances, is our belief that both groups included a more heterogenic ischemic population with similar characteristics (as at this stage the intermediate severity subjects in the control group were still alive). The sensory-motor recovery for the survivors of the GDNF treated group that were alive up to day five, although did not prove a statistically significant improvement in comparison to the control group, showed a clear trend to recovery.

Although IDLV_GDNF improved animal healing, a complete recovery was not observed for all surviving subjects, especially the ones with severe ischemic damage. However, the rate of sensorimotor recovery varied, being proportional to the initial damage, and faster in IDLV_GDNF treated subjects. From the animals' observation, it looks reasonable to postulate that the modulation of the SVZ affected mostly the ability to survive more than the motor recovery. In addition, and in agreement with the literature, the pre-treatment with GDNF reduced the severity of the ischemia within the group, highlighting a protective effect from ischemia onset and progression (Yu, Liu et al. 2007; Chu, Wang et al. 2008).

The histological analysis did not show any sign of tissue re-building, which taken together with the disperse location of the migrated cells seems to suggest a different role of the NPCs in stroke. The data from the survival proportion, life expectancy and sensorimotor behaviour suggest the SVZ is an important factor involved in recovery. In addition the number of eGFP positive cells estimated in the ischemic boundaries was not big enough to justify such a large effect on animal survival. For these

reasons we cannot exclude a role of these cells on the animal healing process; it seems reasonable to postulate an indirect influence of the SVZ progenitors on the ischemic lesion. It might be the case that these cells are involved in brain restoration by producing growth factors in turn responsible to improve neuronal survival, and branching in the penumbra area.

Many studies are currently focused on brain repair by stem cells transplantation or improvement of the endogenous neurogenesis by growth factors therapy. Although some of them involving human and animal models demonstrated neurological improvement, the efficiency and potentiality of the treatment as well as the mechanism of action is still not clarified (Dibajnia and Morshead 2012; Maucksch, Vazey et al. 2012; Oliveira, Pillat et al. 2012; Sakata, Narasimhan et al. 2012; Song, Mohamad et al. 2012). One of the major issue of stem cells transplantation, is the engrafted cells survival, between 5 and 10% of the originally transplanted cells; this makes even more difficult to comprehend how the treatment could have any effect on the neurological outcome (Fainstein, Cohen et al. 2012; Mora-Lee, Sirerol-Piquer et al. 2012; Wang, Forsythe et al. 2012). Many of these researches failed to prove a proficient tissue re-building, leaving open the doubt of a real effect of the treatment over the sometime weak proves for the neurological enhancement. Something to keep in mind and suggested from this thesis, is the possibility of a different action of the endogenous neurogenesis in the healing process. In addition, the functionality of the NPCs (endogenous and exogenous) might go over the "simple" tissue formation, and we might need to start looking at the phenomena under different light and prospective.

The ability to repair by replacement is not necessary the only way for recovery, and if it is very efficient for the majority of the organs healing process, it might not applicable for the Nervous System. The Nervous System is matter of memories and connections built up in a lifetime,

repairing by replacement might not be the most efficient way to heal. The neurological significance of a neuron is not just the ability to receive input and release output, but the specificity of the connections and excitability is like a code that reflects the organism regulation. It is very possible that the system receives more benefit by enhancing plasticity rather than replacing dead neurons. Under this light an improvement of this study with a bigger number of subjects and a proper selection of the behavioural tests would better clarify the brain healing potentiality and open new strategies for brain restoration.

7.2 TROUBLESHOOTING

During the project development a number of issues rose up; in this session I will describe some of the problems met and trouble shutting.

The analysis *in vitro* of the LV_dnCyclinD1 did not clarify the effectiveness of the mutant. Although the cell cycle analysis was performed at different time points after transduction, the efficacy of the mutant was not proved or clarified. The major issue with the experimental design used, was the absence of an inducible promoter to drive the dnCyclinD1 expression, combined with an antibiotic resistance gene for selection. These two modifications on the transfer plasmid would make possible the selection of an uniform population that is efficiently transduced, in addition to a better control of the transgene transcription at the desired time point. The predicted effect would be to reduce issues related on selection agents on the non-transduced fraction, over the portion that activates the mutant and reduce or block the cell cycle. The non-transduced fraction will always have a faster or active cell cycle leading a time dependent amplification (the NIH3t3 doubling time is 2 days), in turn affecting protein and viability analysis of the whole system (transduced and non-transduced fraction).

In vivo behavioural examination was limited by a not exhaustive test, only able to detect a portion of the damage produced by 1h_MCAo. The analysis of the sensorimotor phenotype was assessed based on the 0-28 focal deficit test, which allows evaluation of damage located in the sensorimotor cortex and striatum. Because the lesion of many subjects extended to the hippocampus, the behavioural analysis performed was not sufficient to evaluate the whole effect of the ischemia, and perform a proper comparison. Although the MCAo model is known to induce damage to the striatum and sensorimotor cortex, as the literature reported, the most severe ischemic subjects can show damage extended also to the hippocampal formation and hypothalamus (Liu, Solway et al. 1998; Gerriets, Stolz et al. 2003; Nikonenko, Radenovic et al. 2009; Li, Pang et al. 2012). For a proper evaluation of the model, subject selection based on damage severity and location, in addition to proper behavioral tests is strongly recommended. Alternatively, the use of an heterogenic battery of tests needs to be performed. Considering these factors, the model could have been more exhaustively analyzed with further tests like the Morris water maze, the 8 arms radial maze or the t-maze (Hodges 1996; Sharma, Rakoczy et al. 2010; Nikbakht, Zarei et al. 2012).

Ultimately, the statistic power was very small due to the reduced size groups performed. The number of subjects used in an experiment depends on the survival fraction expected at the end of the treatment. In an animal study (especially when the behavior is evaluated) a minimum of 10-15 subjects (survivors) is recommended. On the light of the survival fraction estimated by this project a minimum number of 30-32 animals per group would have been advisable (especially for the SVZ inhibition group).

BIBLIOGRAPHY

Abe, K. (2003). "[Gene therapy and neuroprotection for cerebral infarction]." Rinsho shinkeigaku = Clinical neurology **43**(11): 894-6.

Achanta, P., V. Capilla-Gonzalez, et al. (2012). "Subventricular zone localized irradiation affects the generation of proliferating neural precursor cells and the migration of neuroblasts." Stem cells **30**(11): 2548-60.

Adcock, I. M., P. Ford, et al. (2006). "Epigenetics and airways disease." Respir Res **7**: 21.

Aloe, L. (2004). "Rita Levi-Montalcini: the discovery of nerve growth factor and modern neurobiology." Trends in cell biology **14**(7): 395-9.

Altman, J. and G. D. Das (1965). "Autoradiographic and histological evidence of postnatal hippocampal neurogenesis in rats." J Comp Neurol **124**(3): 319-35.

Alvarez-Buylla, A. and D. A. Lim (2004). "For the long run: maintaining germinal niches in the adult brain." Neuron **41**(5): 683-6.

Arvidsson, A., T. Collin, et al. (2002). "Neuronal replacement from endogenous precursors in the adult brain after stroke." Nat Med **8**(9): 963-70.

Arvidsson, A., Z. Kokaia, et al. (2001). "Stroke induces widespread changes of gene expression for glial cell line-derived neurotrophic factor family receptors in the adult rat brain." Neuroscience **106**(1): 27-41.

Ashioti, M., J. S. Beech, et al. (2007). "Multi-modal characterisation of the neocortical clip model of focal cerebral ischaemia by MRI, behaviour and immunohistochemistry." Brain Res **1145**: 177-89.

Badruddin, A., M. A. Taqi, et al. (2011). "Neurocritical care of a reperfused brain." Current neurology and neuroscience reports **11**(1): 104-10.

Bederson, J. B., L. H. Pitts, et al. (1986). "Evaluation of 2,3,5-triphenyltetrazolium chloride as a stain for detection and quantification of experimental cerebral infarction in rats." Stroke **17**(6): 1304-8.

Bederson, J. B., L. H. Pitts, et al. (1986). "Rat middle cerebral artery occlusion: evaluation of the model and development of a neurologic examination." Stroke; a journal of cerebral circulation **17**(3): 472-6.

Belluzzi, O., M. Benedusi, et al. (2003). "Electrophysiological differentiation of new neurons in the olfactory bulb." J Neurosci **23**(32): 10411-8.

Benn, S. C., I. Ay, et al. (2005). "Tetanus toxin fragment C fusion facilitates protein delivery to CNS neurons from cerebrospinal fluid in mice." J Neurochem **95**(4): 1118-31.

Bovetti, S., S. Gribaudo, et al. "From progenitors to integrated neurons: role of neurotransmitters in adult olfactory neurogenesis." J Chem Neuroanat **42**(4): 304-16.

Brehm, A., E. A. Miska, et al. (1998). "Retinoblastoma protein recruits histone deacetylase to repress transcription." Nature **391**(6667): 597-601.

Brinton, R. D., R. F. Thompson, et al. (2008). "Progesterone receptors: form and function in brain." Frontiers in neuroendocrinology **29**(2): 313-39.

Buchschacher, G. L., Jr. and A. T. Panganiban (1992). "Human immunodeficiency virus vectors for inducible expression of foreign genes." J Virol **66**(5): 2731-9.

Burch, P. M. and N. H. Heintz (2005). "Redox regulation of cell-cycle re-entry: cyclin D1 as a primary target for the mitogenic effects of reactive oxygen and nitrogen species." Antioxidants & redox signaling **7**(5-6): 741-51.

Caleo, M. and G. Schiavo (2009). "Central effects of tetanus and botulinum neurotoxins." Toxicon : official journal of the International Society on Toxinology **54**(5): 593-9.

Chen, B., X. Q. Gao, et al. (2009). "Neuroprotective effect of grafting GDNF gene-modified neural stem cells on cerebral ischemia in rats." Brain research **1284**: 1-11.

Chiamulera, C., A. Terron, et al. (1993). "Qualitative and quantitative analysis of the progressive cerebral damage after middle cerebral artery occlusion in mice." Brain Res **606**(2): 251-8.

Chian, R. J., J. Li, et al. (2009). "IGF-1:tetanus toxin fragment C fusion protein improves delivery of IGF-1 to spinal cord but fails to prolong survival of ALS mice." Brain research **1287**: 1-19.

Chu, L. F., W. T. Wang, et al. (2008). "Ischemic brain cell-derived conditioned medium protects astrocytes against ischemia through GDNF/ERK/NF-kB signaling pathway." Brain research **1239**: 24-35.

Clark, W., L. Gunion-Rinker, et al. (1998). "Citicoline treatment for experimental intracerebral hemorrhage in mice." Stroke **29**(10): 2136-40.

Cockrell, A. S. and T. Kafri (2003). "HIV-1 vectors: fulfillment of expectations, further advancements, and still a way to go." Current HIV research **1**(4): 419-39.

Cockrell, A. S. and T. Kafri (2007). "Gene delivery by lentivirus vectors." Molecular biotechnology **36**(3): 184-204.

Coqueret, O. (2002). "Linking cyclins to transcriptional control." Gene **299**(1-2): 35-55.

Corotto, F. S., J. A. Henegar, et al. (1993). "Neurogenesis persists in the subependymal layer of the adult mouse brain." Neurosci Lett **149**(2): 111-4.

Curtis, M. A., M. Kam, et al. (2007). "Human neuroblasts migrate to the olfactory bulb via a lateral ventricular extension." Science **315**(5816): 1243-9.

Deierborg, T., D. Soulet, et al. (2008). "Emerging restorative treatments for Parkinson's disease." Prog Neurobiol **85**(4): 407-32.

Dempsey, R. J. and H. S. Kalluri (2007). "Ischemia-induced neurogenesis: role of growth factors." Neurosurg Clin N Am **18**(1): 183-90, xi.

Dempsey, R. J., K. A. Sailor, et al. (2003). "Stroke-induced progenitor cell proliferation in adult spontaneously hypertensive rat brain: effect of exogenous IGF-1 and GDNF." J Neurochem **87**(3): 586-97.

Dempsey, R. J., K. A. Sailor, et al. (2003). "Stroke-induced progenitor cell proliferation in adult spontaneously hypertensive rat brain: effect of exogenous IGF-1 and GDNF." Journal of neurochemistry **87**(3): 586-97.

Dibajnia, P. and C. M. Morshead (2012). "Role of neural precursor cells in promoting repair following stroke." Acta pharmacologica Sinica.

Diehl, J. A. and C. J. Sherr (1997). "A dominant-negative cyclin D1 mutant prevents nuclear import of cyclin-dependent kinase 4 (CDK4) and its phosphorylation by CDK-activating kinase." Mol Cell Biol **17**(12): 7362-74.

Doetsch, F., J. M. Garcia-Verdugo, et al. (1997). "Cellular composition and three-dimensional organization of the subventricular germinal zone in the adult mammalian brain." J Neurosci **17**(13): 5046-61.

Dowdy, S. F., P. W. Hinds, et al. (1993). "Physical interaction of the retinoblastoma protein with human D cyclins." Cell **73**(3): 499-511.

Etgen, A. M., T. Jover-Mengual, et al. "Neuroprotective actions of estradiol and novel estrogen analogs in ischemia: translational implications." Front Neuroendocrinol **32**(3): 336-52.

Ewen, M. E., H. K. Sluss, et al. (1993). "Functional interactions of the retinoblastoma protein with mammalian D-type cyclins." Cell **73**(3): 487-97.

Fainstein, N., M. E. Cohen, et al. (2012). "Time associated decline in neurotrophic properties of neural stem cell grafts render them dependent on brain region-specific environmental support." Neurobiology of disease **49C**: 41-48.

Fouchier, R. A. and M. H. Malim (1999). "Nuclear import of human immunodeficiency virus type-1 preintegration complexes." Advances in virus research **52**: 275-99.

Frankel, A. D. and J. A. Young (1998). "HIV-1: fifteen proteins and an RNA." Annu Rev Biochem **67**: 1-25.

Frankle, R. T. (1976). "Nutrition education in the medical school curriculum: a proposal for action: a curriculum design." The American journal of clinical nutrition **29**(1): 105-9.

Fu, M., C. Wang, et al. (2004). "Minireview: Cyclin D1: normal and abnormal functions." Endocrinology **145**(12): 5439-47.

Fujii, M., H. Hara, et al. (1997). "Strain-related differences in susceptibility to transient forebrain ischemia in SV-129 and C57black/6 mice." Stroke **28**(9): 1805-10; discussion 1811.

Galea, L. A., M. D. Spritzer, et al. (2006). "Gonadal hormone modulation of hippocampal neurogenesis in the adult." Hippocampus **16**(3): 225-32.

Gerriets, T., E. Stolz, et al. (2003). "Neuroprotective effects of MK-801 in different rat stroke models for permanent middle cerebral artery occlusion: adverse effects of hypothalamic damage and strategies for its avoidance." Stroke; a journal of cerebral circulation **34**(9): 2234-9.

Gibson, C. L. and S. P. Murphy (2004). "Progesterone enhances functional recovery after middle cerebral artery occlusion in male mice." Journal of cerebral blood flow and metabolism : official journal of the International Society of Cerebral Blood Flow and Metabolism **24**(7): 805-13.

Goncalves, M. B., P. Suetterlin, et al. (2008). "A diacylglycerol lipase-CB2 cannabinoid pathway regulates adult subventricular zone neurogenesis in an age-dependent manner." Mol Cell Neurosci **38**(4): 526-36.

Gotts, J. E. and M. F. Chesselet (2005). "Mechanisms of subventricular zone expansion after focal cortical ischemic injury." J Comp Neurol **488**(2): 201-14.

Gotts, J. E. and M. F. Chesselet (2005). "Migration and fate of newly born cells after focal cortical ischemia in adult rats." J Neurosci Res **80**(2): 160-71.

Gotts, J. E. and M. F. Chesselet (2005). "Migration and fate of newly born cells after focal cortical ischemia in adult rats." Journal of neuroscience research **80**(2): 160-71.

Gould, E., A. Beylin, et al. (1999). "Learning enhances adult neurogenesis in the hippocampal formation." Nat Neurosci **2**(3): 260-5.

Gritti, A., P. Frolichsthal-Schoeller, et al. (1999). "Epidermal and fibroblast growth factors behave as mitogenic regulators for a single multipotent stem cell-like population from the subventricular region of the adult mouse forebrain." J Neurosci **19**(9): 3287-97.

Gu, W., T. Brannstrom, et al. (2000). "Cortical neurogenesis in adult rats after reversible photothrombotic stroke." J Cereb Blood Flow Metab **20**(8): 1166-73.

Hamburger, V. (1993). "The history of the discovery of the nerve growth factor." Journal of neurobiology **24**(7): 893-7.

Han, E. K., S. C. Ng, et al. (1999). "Roles of cyclin D1 and related genes in growth inhibition, senescence and apoptosis." Apoptosis **4**(3): 213-9.

Heiss, W. D. (1987). "[Therapy of cerebral ischemia]." Zeitschrift fur Kardiologie **76 Suppl 4**: 87-98.

Hill, W. D., D. C. Hess, et al. (2004). "SDF-1 (CXCL12) is upregulated in the ischemic penumbra following stroke: association with bone marrow cell homing to injury." Journal of neuropathology and experimental neurology **63**(1): 84-96.

Hodges, H. (1996). "Maze procedures: the radial-arm and water maze compared." Brain research. Cognitive brain research **3**(3-4): 167-81.

Imayoshi, I., M. Sakamoto, et al. (2009). "Continuous neurogenesis in the adult brain." Development, growth & differentiation **51**(3): 379-86.

Imitola, J., K. Raddassi, et al. (2004). "Directed migration of neural stem cells to sites of CNS injury by the stromal cell-derived factor 1alpha/CXC chemokine receptor 4 pathway." Proceedings of the National Academy of Sciences of the United States of America **101**(52): 18117-22.

Ino, H. and T. Chiba (2001). "Cyclin-dependent kinase 4 and cyclin D1 are required for excitotoxin-induced neuronal cell death in vivo." J Neurosci **21**(16): 6086-94.

Isayama, K., L. H. Pitts, et al. (1991). "Evaluation of 2,3,5-triphenyltetrazolium chloride staining to delineate rat brain infarcts." Stroke **22**(11): 1394-8.

Jaerve, A. and H. W. Muller (2012). "Chemokines in CNS injury and repair." Cell and tissue research **349**(1): 229-48.

Janssen, R. S., M. E. St Louis, et al. (1992). "HIV infection among patients in U.S. acute care hospitals. Strategies for the counseling and testing of the hospital patients. The Hospital HIV Surveillance Group." The New England journal of medicine **327**(7): 445-52.

Jin, K., M. Minami, et al. (2001). "Neurogenesis in dentate subgranular zone and rostral subventricular zone after focal cerebral ischemia in the rat." Proc Natl Acad Sci U S A **98**(8): 4710-5.

Jung, J. E., G. S. Kim, et al. (2010). "Reperfusion and neurovascular dysfunction in stroke: from basic mechanisms to potential strategies for neuroprotection." Molecular neurobiology **41**(2-3): 172-9.

Kalluri, H. S., R. Vemuganti, et al. (2007). "Mechanism of insulin-like growth factor I-mediated proliferation of adult neural progenitor cells: role of Akt." Eur J Neurosci **25**(4): 1041-8.

Kazanis, I. (2009). "The subependymal zone neurogenic niche: a beating heart in the centre of the brain: how plastic is adult neurogenesis? Opportunities for therapy and questions to be addressed." Brain : a journal of neurology **132**(Pt 11): 2909-21.

Kernie, S. G. and J. M. Parent (2010). "Forebrain neurogenesis after focal Ischemic and traumatic brain injury." Neurobiology of disease **37**(2): 267-74.

Kobayashi, T., H. Ahlenius, et al. (2006). "Intracerebral infusion of glial cell line-derived neurotrophic factor promotes striatal neurogenesis after stroke in adult rats." Stroke; a journal of cerebral circulation **37**(9): 2361-7.

Kobayashi, T., H. Ahlenius, et al. (2006). "Intracerebral infusion of glial cell line-derived neurotrophic factor promotes striatal neurogenesis after stroke in adult rats." Stroke **37**(9): 2361-7.

Kornmann, M., N. Arber, et al. (1998). "Inhibition of basal and mitogen-stimulated pancreatic cancer cell growth by cyclin D1 antisense is associated with loss of tumorigenicity and potentiation of cytotoxicity to cisplatinum." J Clin Invest **101**(2): 344-52.

Kreuzberg, M., E. Kanov, et al. (2010). "Increased subventricular zone-derived cortical neurogenesis after ischemic lesion." Experimental neurology **226**(1): 90-9.

Kuhn, H. G., J. Winkler, et al. (1997). "Epidermal growth factor and fibroblast growth factor-2 have different effects on neural progenitors in the adult rat brain." J Neurosci **17**(15): 5820-9.

Lange, C. A. and D. Yee (2011). "Killing the second messenger: targeting loss of cell cycle control in endocrine-resistant breast cancer." Endocrine-related cancer **18**(4): C19-24.

Larsen, K. E., S. C. Benn, et al. (2006). "A glial cell line-derived neurotrophic factor (GDNF):tetanus toxin fragment C protein conjugate improves delivery of GDNF to spinal cord motor neurons in mice." Brain research **1120**(1): 1-12.

Larsen, K. E., S. C. Benn, et al. (2006). "A glial cell line-derived neurotrophic factor (GDNF):tetanus toxin fragment C protein conjugate improves delivery of GDNF to spinal cord motor neurons in mice." Brain Res **1120**(1): 1-12.

Lazarini, F., M. A. Mouthon, et al. (2009). "Cellular and behavioral effects of cranial irradiation of the subventricular zone in adult mice." PloS one **4**(9): e7017.

Le Magueresse, C., J. Alfonso, et al. "Subventricular Zone-Derived Neuroblasts Use Vasculature as a Scaffold to Migrate Radially to the Cortex in Neonatal Mice." Cereb Cortex.

Leavitt, A. D., G. Robles, et al. (1996). "Human immunodeficiency virus type 1 integrase mutants retain in vitro integrase activity yet fail to integrate viral DNA efficiently during infection." J Virol **70**(2): 721-8.

Lee, H. J., I. H. Park, et al. (2009). "Human neural stem cells overexpressing glial cell line-derived neurotrophic factor in experimental cerebral hemorrhage." Gene therapy **16**(9): 1066-76.

Lennington, J. B., Z. Yang, et al. (2003). "Neural stem cells and the regulation of adult neurogenesis." Reprod Biol Endocrinol **1**: 99.

Leventhal, C., S. Rafii, et al. (1999). "Endothelial trophic support of neuronal production and recruitment from the adult mammalian subependyma." Mol Cell Neurosci **13**(6): 450-64.

Levison, S. W., S. K. Druckman, et al. (2003). "Neural stem cells in the subventricular zone are a source of astrocytes and oligodendrocytes, but not microglia." Dev Neurosci **25**(2-4): 184-96.

Lewis, P., M. Hensel, et al. (1992). "Human immunodeficiency virus infection of cells arrested in the cell cycle." EMBO J **11**(8): 3053-8.

Li, J., R. J. Chian, et al. (2009). "Insect GDNF:TTC fusion protein improves delivery of GDNF to mouse CNS." Biochem Biophys Res Commun **390**(3): 947-51.

Li, J., R. J. Chian, et al. (2009). "Insect GDNF:TTC fusion protein improves delivery of GDNF to mouse CNS." Biochemical and biophysical research communications **390**(3): 947-51.

Li, Z., L. Pang, et al. (2012). "Resveratrol attenuates brain damage in a rat model of focal cerebral ischemia via up-regulation of hippocampal Bcl-2." Brain research **1450**: 116-24.

Lin, T. N., Y. Y. He, et al. (1993). "Effect of brain edema on infarct volume in a focal cerebral ischemia model in rats." Stroke **24**(1): 117-21.

Lindvall, O. and Z. Kokaia (2004). "Recovery and rehabilitation in stroke: stem cells." Stroke **35**(11 Suppl 1): 2691-4.

Lippoldt, A., A. Reichel, et al. (2005). "Progress in the identification of stroke-related genes: emerging new possibilities to develop concepts in stroke therapy." CNS Drugs **19**(10): 821-32.

Liu, J., K. Solway, et al. (1998). "Increased neurogenesis in the dentate gyrus after transient global ischemia in gerbils." The Journal of neuroscience : the official journal of the Society for Neuroscience **18**(19): 7768-78.

Liu, J. J., J. R. Chao, et al. (1995). "Ras transformation results in an elevated level of cyclin D1 and acceleration of G1 progression in NIH 3T3 cells." Mol Cell Biol **15**(7): 3654-63.

Louissaint, A., Jr., S. Rao, et al. (2002). "Coordinated interaction of neurogenesis and angiogenesis in the adult songbird brain." Neuron **34**(6): 945-60.

Luo, R. X., A. A. Postigo, et al. (1998). "Rb interacts with histone deacetylase to repress transcription." Cell **92**(4): 463-73.

Luskin, M. B. (1993). "Restricted proliferation and migration of postnatally generated neurons derived from the forebrain subventricular zone." Neuron **11**(1): 173-89.
Luzzati, F., S. De Marchis, et al. (2011). "New striatal neurons in a mouse model of progressive striatal degeneration are generated in both the subventricular zone and the striatal parenchyma." PloS one **6**(9): e25088.
Maeda, K. and H. Mitsuya (2007). "Development of therapeutics for AIDS: structure-based molecular targeting." Tuberculosis **87 Suppl 1**: S31-4.
Magnaghi-Jaulin, L., R. Groisman, et al. (1998). "Retinoblastoma protein represses transcription by recruiting a histone deacetylase." Nature **391**(6667): 601-5.
Mahmood ur, R., I. Ali, et al. (2008). "RNA interference: the story of gene silencing in plants and humans." Biotechnol Adv **26**(3): 202-9.
Maric, D., I. Maric, et al. (2003). "Prospective cell sorting of embryonic rat neural stem cells and neuronal and glial progenitors reveals selective effects of basic fibroblast growth factor and epidermal growth factor on self-renewal and differentiation." J Neurosci **23**(1): 240-51.
Maucksch, C., E. M. Vazey, et al. (2012). "Stem cell-based therapy for Huntington's disease." Journal of cellular biochemistry.
McIntyre, G. J. and G. C. Fanning (2006). "Design and cloning strategies for constructing shRNA expression vectors." BMC Biotechnol **6**: 1.
Menn, B., J. M. Garcia-Verdugo, et al. (2006). "Origin of oligodendrocytes in the subventricular zone of the adult brain." The Journal of neuroscience : the official journal of the Society for Neuroscience **26**(30): 7907-18.
Menzies, S. A., J. T. Hoff, et al. (1992). "Middle cerebral artery occlusion in rats: a neurological and pathological evaluation of a reproducible model." Neurosurgery **31**(1): 100-6; discussion 106-7.
Ming, G. L. and H. Song (2011). "Adult neurogenesis in the mammalian brain: significant answers and significant questions." Neuron **70**(4): 687-702.
Modo, M., R. P. Stroemer, et al. (2000). "Neurological sequelae and long-term behavioural assessment of rats with transient middle cerebral artery occlusion." J Neurosci Methods **104**(1): 99-109.
Mora-Lee, S., M. S. Sirerol-Piquer, et al. (2012). "Therapeutic effects of hMAPC and hMSC transplantation after stroke in mice." PloS one **7**(8): e43683.
Moreno-Igoa, M., A. C. Calvo, et al. (2012). "Non-viral gene delivery of the GDNF, either alone or fused to the C-fragment of tetanus toxin protein, prolongs survival in a mouse ALS model." Restorative neurology and neuroscience **30**(1): 69-80.
Moreno-Igoa, M., A. C. Calvo, et al. (2010). "Fragment C of tetanus toxin, more than a carrier. Novel perspectives in non-viral ALS gene therapy." Journal of molecular medicine **88**(3): 297-308.
Naldini, L. (1998). "Lentiviruses as gene transfer agents for delivery to non-dividing cells." Curr Opin Biotechnol **9**(5): 457-63.
Naldini, L., U. Blomer, et al. (1996). "Efficient transfer, integration, and sustained long-term expression of the transgene in adult rat brains

injected with a lentiviral vector." Proc Natl Acad Sci U S A **93**(21): 11382-8.
Naldini, L., U. Blomer, et al. (1996). "In vivo gene delivery and stable transduction of nondividing cells by a lentiviral vector." Science **272**(5259): 263-7.
Nguyen, D. H. and D. Taub (2002). "CXCR4 function requires membrane cholesterol: implications for HIV infection." Journal of immunology **168**(8): 4121-6.
Nielsen, M. H., F. S. Pedersen, et al. (2005). "Molecular strategies to inhibit HIV-1 replication." Retrovirology **2**: 10.
Nielsen, S. J., R. Schneider, et al. (2001). "Rb targets histone H3 methylation and HP1 to promoters." Nature **412**(6846): 561-5.
Nikbakht, N., B. Zarei, et al. (2012). "Experience-dependent expression of rat hippocampal Arc and Homer 1a after spatial learning on 8-arm and 12-arm radial mazes." Neuroscience **218**: 49-55.
Nikonenko, A. G., L. Radenovic, et al. (2009). "Structural features of ischemic damage in the hippocampus." Anatomical record **292**(12): 1914-21.
Nisole, S. and A. Saib (2004). "Early steps of retrovirus replicative cycle." Retrovirology **1**: 9.
Ohab, J. J., S. Fleming, et al. (2006). "A neurovascular niche for neurogenesis after stroke." J Neurosci **26**(50): 13007-16.
Ohira, K., T. Furuta, et al. "Ischemia-induced neurogenesis of neocortical layer 1 progenitor cells." Nat Neurosci **13**(2): 173-9.
Ohira, K., T. Furuta, et al. (2010). "Ischemia-induced neurogenesis of neocortical layer 1 progenitor cells." Nature neuroscience **13**(2): 173-9.
Okuno, S., H. Nakase, et al. (2001). "Comparative study of 2,3,5-triphenyltetrazolium chloride (TTC) and hematoxylin-eosin staining for quantification of early brain ischemic injury in cats." Neurol Res **23**(6): 657-61.
Oliveira, S. L., M. M. Pillat, et al. (2012). "Functions of neurotrophins and growth factors in neurogenesis and brain repair." Cytometry. Part A : the journal of the International Society for Analytical Cytology.
Orts Llorca, F. (1988). "[Nerve growth factor and the history of its discovery]." Anales de la Real Academia Nacional de Medicina **105**(4): 483-8.
Owen, S. M. (2012). "Testing for acute HIV infection: implications for treatment as prevention." Current opinion in HIV and AIDS **7**(2): 125-30.
Pardon, M. C. (2010). "Role of neurotrophic factors in behavioral processes: implications for the treatment of psychiatric and neurodegenerative disorders." Vitamins and hormones **82**: 185-200.
Parent, J. M., Z. S. Vexler, et al. (2002). "Rat forebrain neurogenesis and striatal neuron replacement after focal stroke." Ann Neurol **52**(6): 802-13.
Popp, A., N. Jaenisch, et al. (2009). "Identification of ischemic regions in a rat model of stroke." PLoS One **4**(3): e4764.
Poznansky, M., A. Lever, et al. (1991). "Gene transfer into human lymphocytes by a defective human immunodeficiency virus type 1 vector." J Virol **65**(1): 532-6.

Reynolds, B. A. and S. Weiss (1992). "Generation of neurons and astrocytes from isolated cells of the adult mammalian central nervous system." Science **255**(5052): 1707-10.

Riquelme, P. A., E. Drapeau, et al. (2008). "Brain micro-ecologies: neural stem cell niches in the adult mammalian brain." Philos Trans R Soc Lond B Biol Sci **363**(1489): 123-37.

Robinson, R. G., W. J. Shoemaker, et al. (1975). "Effect of experimental cerebral infarction in rat brain on catecholamines and behaviour." Nature **255**(5506): 332-4.

Roux, S., C. Saint Cloment, et al. (2005). "[C-terminal fragment of tetanus toxin: its use in neuronal network analysis and its potential as non-viral vector]." Journal de la Societe de biologie **199**(1): 35-44.

Roux, S., C. Saint Cloment, et al. (2006). "Brain-derived neurotrophic factor facilitates in vivo internalization of tetanus neurotoxin C-terminal fragment fusion proteins in mature mouse motor nerve terminals." The European journal of neuroscience **24**(6): 1546-54.

Sakata, H., P. Narasimhan, et al. (2012). "Interleukin 6-preconditioned neural stem cells reduce ischaemic injury in stroke mice." Brain : a journal of neurology **135**(Pt 11): 3298-310.

Sakuma, T., M. A. Barry, et al. (2012). "Lentiviral vectors: basic to translational." The Biochemical journal **443**(3): 603-18.

Salazar-Colocho, P., J. L. Lanciego, et al. (2008). "Ischemia induces cell proliferation and neurogenesis in the gerbil hippocampus in response to neuronal death." Neuroscience research **61**(1): 27-37.

Sanai, N., M. S. Berger, et al. (2007). "Comment on "Human neuroblasts migrate to the olfactory bulb via a lateral ventricular extension"." Science **318**(5849): 393; author reply 393.

Schoenfeld, T. J. and E. Gould (2012). "Stress, stress hormones, and adult neurogenesis." Experimental neurology **233**(1): 12-21.

Sharma, S., S. Rakoczy, et al. (2010). "Assessment of spatial memory in mice." Life sciences **87**(17-18): 521-36.

Shen, L. H., Y. Li, et al. (2010). "Astrocytic endogenous glial cell derived neurotrophic factor production is enhanced by bone marrow stromal cell transplantation in the ischemic boundary zone after stroke in adult rats." Glia **58**(9): 1074-81.

Shruster, A., E. Melamed, et al. (2010). "Neurogenesis in the aged and neurodegenerative brain." Apoptosis : an international journal on programmed cell death **15**(11): 1415-21.

Small, D. L. and A. M. Buchan (2000). "Animal models." Br Med Bull **56**(2): 307-17.

Smith, E. J., R. P. Stroemer, et al. "Implantation Site and Lesion Topology Determine Efficacy of a Human Neural Stem Cell Line in a Rat Model of Chronic Stroke." Stem Cells.

Song, M., O. Mohamad, et al. (2012). "Restoration of Intracortical and Thalamocortical Circuits after Transplantation of Bone Marrow Mesenchymal Stem Cells into the Ischemic Brain of Mice." Cell transplantation.

Sugiura, S., K. Kitagawa, et al. (2005). "Adenovirus-mediated gene transfer of heparin-binding epidermal growth factor-like growth factor enhances neurogenesis and angiogenesis after focal cerebral ischemia in rats." Stroke **36**(4): 859-64.

Sullivan, T. J., P. Patel, et al. (2011). "Evaluation of pooling strategies for acute HIV-1 infection screening using nucleic acid amplification testing." Journal of clinical microbiology **49**(10): 3667-8.

Tamura, A., D. I. Graham, et al. (1981). "Focal cerebral ischaemia in the rat: 1. Description of technique and early neuropathological consequences following middle cerebral artery occlusion." Journal of cerebral blood flow and metabolism : official journal of the International Society of Cerebral Blood Flow and Metabolism **1**(1): 53-60.

Taupin, P. and F. H. Gage (2002). "Adult neurogenesis and neural stem cells of the central nervous system in mammals." J Neurosci Res **69**(6): 745-9.

Thored, P., A. Arvidsson, et al. (2006). "Persistent production of neurons from adult brain stem cells during recovery after stroke." Stem Cells **24**(3): 739-47.

Traystman, R. J. (2003). "Animal models of focal and global cerebral ischemia." ILAR J **44**(2): 85-95.

Tropepe, V., M. Sibilia, et al. (1999). "Distinct neural stem cells proliferate in response to EGF and FGF in the developing mouse telencephalon." Dev Biol **208**(1): 166-88.

Voigt, T. (1989). "Development of glial cells in the cerebral wall of ferrets: direct tracing of their transformation from radial glia into astrocytes." The Journal of comparative neurology **289**(1): 74-88.

Wang, C., M. Zhang, et al. "Sustained increase in adult neurogenesis in the rat hippocampal dentate gyrus after transient brain ischemia." Neurosci Lett **488**(1): 70-5.

Wang, T. Y., J. S. Forsythe, et al. (2012). "Promoting engraftment of transplanted neural stem cells/progenitors using biofunctionalised electrospun scaffolds." Biomaterials **33**(36): 9188-97.

Wang, Y., J. Huang, et al. (2012). "Roles of chemokine CXCL12 and its receptors in ischemic stroke." Current drug targets **13**(2): 166-72.

Wanisch, K. and R. J. Yanez-Munoz (2009). "Integration-deficient lentiviral vectors: a slow coming of age." Molecular therapy : the journal of the American Society of Gene Therapy **17**(8): 1316-32.

Weinberg, J. B., T. J. Matthews, et al. (1991). "Productive human immunodeficiency virus type 1 (HIV-1) infection of nonproliferating human monocytes." J Exp Med **174**(6): 1477-82.

Whitman, M. C. and C. A. Greer (2009). "Adult neurogenesis and the olfactory system." Progress in neurobiology **89**(2): 162-75.

Whitney, N. P., T. M. Eidem, et al. (2009). "Inflammation mediates varying effects in neurogenesis: relevance to the pathogenesis of brain injury and neurodegenerative disorders." Journal of neurochemistry **108**(6): 1343-59.

Wurmser, A. E., T. D. Palmer, et al. (2004). "Neuroscience. Cellular interactions in the stem cell niche." Science **304**(5675): 1253-5.

Yamashita, T., M. Ninomiya, et al. (2006). "Subventricular zone-derived neuroblasts migrate and differentiate into mature neurons in the post-stroke adult striatum." J Neurosci **26**(24): 6627-36.

Yamashita, T., M. Ninomiya, et al. (2006). "Subventricular zone-derived neuroblasts migrate and differentiate into mature neurons in the post-stroke adult striatum." The Journal of neuroscience : the official journal of the Society for Neuroscience **26**(24): 6627-36.

Yan, Y. P., K. A. Sailor, et al. (2006). "Insulin-like growth factor-1 is an endogenous mediator of focal ischemia-induced neural progenitor proliferation." Eur J Neurosci **24**(1): 45-54.

Yanez-Munoz, R. J., K. S. Balaggan, et al. (2006). "Effective gene therapy with nonintegrating lentiviral vectors." Nat Med **12**(3): 348-53.

Yang, G., K. Kitagawa, et al. (1997). "C57BL/6 strain is most susceptible to cerebral ischemia following bilateral common carotid occlusion among seven mouse strains: selective neuronal death in the murine transient forebrain ischemia." Brain Res **752**(1-2): 209-18.

Yao, J., Y. Mu, et al. (2012). "Neural stem cells: mechanisms and modeling." Protein & cell **3**(4): 251-61.

Yoneyama, M., T. Shiba, et al. (2011). "Adult neurogenesis is regulated by endogenous factors produced during neurodegeneration." Journal of pharmacological sciences **115**(4): 425-32.

Yoshikawa, T., Y. Akiyoshi, et al. (2008). "Ginsenoside Rb1 reduces neurodegeneration in the peri-infarct area of a thromboembolic stroke model in non-human primates." J Pharmacol Sci **107**(1): 32-40.

Yoshizaki, K. and N. Osumi (2010). "[Molecular mechanism and mental function of postnatal neurogenesis]." Brain and nerve = Shinkei kenkyu no shinpo **62**(12): 1315-22.

Young, C. C., K. J. Brooks, et al. (2011). "Cellular and molecular determinants of stroke-induced changes in subventricular zone cell migration." Antioxidants & redox signaling **14**(10): 1877-88.

Yu, A. C., R. Y. Liu, et al. (2007). "Glial cell line-derived neurotrophic factor protects astrocytes from staurosporine- and ischemia- induced apoptosis." Journal of neuroscience research **85**(15): 3457-64.

Zhang, R., Z. Zhang, et al. (2004). "Stroke transiently increases subventricular zone cell division from asymmetric to symmetric and increases neuronal differentiation in the adult rat." The Journal of neuroscience : the official journal of the Society for Neuroscience **24**(25): 5810-5.

Zhang, R. L., Y. LeTourneau, et al. (2007). "Neuroblast division during migration toward the ischemic striatum: a study of dynamic migratory and proliferative characteristics of neuroblasts from the subventricular zone." The Journal of neuroscience : the official journal of the Society for Neuroscience **27**(12): 3157-62.

Zhang, R. L., Z. G. Zhang, et al. (2001). "Proliferation and differentiation of progenitor cells in the cortex and the subventricular zone in the adult rat after focal cerebral ischemia." Neuroscience **105**(1): 33-41.